Fatigue Estimation of Drill-string and Drill-pipe Threaded Connection Subjected to Random Loadings

by

©Jiahao Zheng

A thesis submitted to the School of Graduate Studies in partial fulfillment of the requirements for the degree of

Master of Engineering

Department of Engineering and Applied Science

Memorial University of Newfoundland

Feb 2015

St. John's Newfoundland

AUTHOR'S DECLARATION

I hereby declare that I am the sole author of this thesis. This is a true copy of the thesis, including any required final revisions, as accepted by my examiners. I understand that my thesis may be made electronically available to the public.

Abstract

Drill-strings are slender structures used to drill the oil-well in searching for oil and gas. Failures of drill-strings cause the loss of time and money and therefore predicting fatigue damage induced by vibrations is of benefit. In this thesis, fatigue calculation of drill-strings is conducted in both time domain and frequency domain, considering axial and torsional vibrations.

In time domain analysis, the stress time histories at any specific location of the drill-string are obtained from a finite element model. Both deterministic and random excitations are taken into account. Then using a rainflow counting method, the damaging stress cycles are extracted. Based on the linear cumulative damage law, fatigue damage is then calculated and fatigue life of the drill-string is therefore predicted. Results under both deterministic and random excitations are compared against each other.

Time domain fatigue analysis gives accurate predictions at the cost of long calculating time. For the sake of time-saving, a method in frequency domain is developed. The drill-string vibration model is built using continuous parameter method. Power spectral densities (PSD) of the random excitation are assumed. In the process to gain expected damage, equivalent stress spectra are calculated based on Mocha's random

fatigue failure criterion. Then the expected fatigue damage and predicted life are estimated by a spectral method: Dirlik's method.

Further, the drill-pipe threaded connection, which is used to connect numerous drill-pipes/collars to form a drill-string, is investigated. With the help of ANSYS workbench 15.0, a standard 4.5" API line pipe threaded connection model is built. Random excitation is considered mainly due to the unevenness of rock formation being drilled. Firstly, a static stress analysis is conducted considering "make-up" and "tensile load" steps. Then modal analysis and random vibration analysis are conducted, assuming acceleration PSD as input. Finally, based on three-band technique, the fatigue damage is caluclated.

Computer simulations are run and results are given by the above three fatigue damage calculation methods. Results show the critical positions of both the drill-string and the threaded connection, where attention should be paid to by the manufacters and the drilling operators.

Although some limitations exist, this thesis proposed two ways to evaluate fatigue damage of a drill-string. The threaded pipe connection, which is a complex structure, is also analyzed. Further research work will aim at the validation of the simulations.

Keywords: Drill-sting fatigue, Rainflow counting method, Spectral method, Random excitation, Threaded pipe connection

Acknowledgements

The author would like to show appreciation to people who had given advice and suggestion to this research work.

First, the author would like to express his gratefulness to his supervisor, Dr. James Yang, for his professional supervision, critical comments and immeasurable advice and guidances during the author's two years' research work. Without his advices and ideas, this work cannot be completed with quality and efficiency. The author enjoyed the time spent with him during the last two years' work.

Secondly, the author would like to thank his family for their supports. Without their spiritual encouragements and frequent concerns, the author cannot devote himself in this research work.

Then, the author would like to thank his friends in Memorial University of Newfoundland. With their accompanies, the feeling of homesick and the academic pressure was relieved. It is the friendship that brought me happiness and offered warmly help when necessary.

Finally, the author would like to express his sincere gratitude to the faculty, staff, and

students of the Faculty of Engineering and Applied Science for making his study and research at Memorial University of Newfoundland such a great experience.

Notes on Units

The drilling industry normally uses imperial units to report the relative parameters while International System of Units (SI) is employed in some research. In this thesis, SI units are mainly used and other units will be converted. Table 1 shows the conversion between Centimetre–Gram–Second unit system (CGS) and SI unit system for some quantities related in this reasearch.

Table 1: Conversion between Imperial units and SI units in Mechanics

Quantity	Symbol	Impeial units	Equivalent in SI units
Length/Position	L/x	25.4 $inch$	$10^{-3}m$
Area	A	645.2 $inch^2$	mm^2
Mass	m	0.4536 $pound$	Kg
Force	F	9.807 kg	N
Pressure	P	0.2491 inches of water	KPa

List of Symbols, Nomenclature and their data

For Chapter 3

$l_e = 50$ For drill-pipe

$l_e = 20$ For drill-collar

$J = 1.754 \times 10^{-5}\ m^4$ For drill-pipe

$J = 2.648 \times 10^{-4}\ m^4$ For drill-collar

$g = 9.84\ m/s^2$ Gravity Acceleration

$G = 7.6923{\times}10^{10}\ N/m^2$ Drill-string shear modulus

$E = 210\ Gpa$ Drill-string elastic modulus

$\rho = 7850\ kg/m^3$ Drill-sting density

$E_0 = 4 \times 10^{10}\ N/m^2$ Rock elastic modulus

$\nu = 0.25$ Poisson ratio

$G_0 = 1.6 \times 10^{10}\ N/m^2$ Rock shear modulus

$r_0 = 0.2$ Foundation diameter

$\rho_0 = 2100\ kg/m^3$ Rock density

$k_c = 4.27 \times 10^9\ N/m$ Rock stiffness

$c = 1.05 \times 10^6$ Rock damping coefficient

$m = 500\ kg$ Stabilizer mass

$k = 10\ MN/m$ Stabilizer stiffness

$r = 0.03\ m$ Eccentric distance of stabilizer mass

w Average bit speed

$r_b = 0.22$ Bit radius

$L = 0.005\ H$ Motor inductance

$R_m = 0.01\ \Omega$ Armature resistance

$K_m = 6\ V/s$ Motor constant

$n = 7.2$ Gear ratio of the gearbox

$\alpha = 0.01$

$\beta = 0.01$

$c_1 = 1.35 \times 10^{-8}$

$c_2 = -1.9 \times 10^{-4}$

$\xi_0 = 1$

$\alpha_1 = 2$

$\alpha_2 = 1$

$\nu = 0.01$

For Chapter 4

$O.D. = 0.1651m$ For drill-collar

$O.D. = 0.1140m$ For drill-pipe

$I.D. = 0.0572m$ For drill-collar

$I.D. = 0.0972m$ For drill-pipe

$A_1 = 0.0188m^2$ For drill-collar

$A_2 = 0.0028m^2$ For drill-pipe

$L_1 = 200m$ Drill-collar length

$L = 2500m$ Whole drill-string length

$\rho = 7850\ kg/m^3$ Drill-sting density

$\rho_{mud} = 7850\ kg/m^3$ Drill-mud density

$F_h = 7 \times 10^5 N$ Hook load

$W_s = 1 \times 10^5 N$ Static weight on bit

$g = 9.81 m/s^2$ Gravity acceleration

$\omega_+ = 1000 Hz$ Upper bound of white noise

$E = 207 GPa$ Drill-string elastic modulus

$\gamma_1 = 239.4 Ns/m$ Drill-collar damping

$\gamma_2 = 33.5 Ns/m$ Drill-pipe damping

$K_d = 9.34 \times 10^6 N/m$ Stiffness of derrick

$M_d = 9070 kg/m$ Mass of traveling block

$U_0 = 0.003 m$ Amplitude of drill-bit displacement

$G = 8.28 \times 10^{10}\ Nm$ Drill-string shear modulus

$\gamma_{T1} = 2.22 Ns/m^2$ Torsional drill-collar damping

$\gamma_{T2} = 0.311 Ns/m^2$ Torsional drill-pipe damping

$K_T = 678 N/m$ Torsional stiffness of derrick

$M_T = 210.7 kgm^2$ Torsional mass of traveling block

$\theta_0 = 0.1745\ rad$ Amplitude of torsional displacement

$R_0 = 0.0825\ m$ Outer radius of drill-pipe

Table of Contents

List of Tables

List of Figures

Chapter 1

Introduction

In recent decades, demands for natural resources such as oil and gas have been increasing rapidly. Development of modern society requires safe and efficient exploitation of resources. This drives the industry to develop technology and conduct research on oil and gas drilling, in order to improve the drilling performance.

Over the recent years, dramatic changes in drilling technology has been witnessed [1]. Drilling operations are performed more and more efficiently due to the advanced drilling tools and drilling methods. However, the rate of the occurence of drill-string failures remains high, which causes significant loss of money and time. Fatigue problem, which is induced by cyclic loadings, is reported as the major cause of drill-string failures. Therefore, it is of necessity and importance to develop a way of calculating fatigue damage on drill-strings, which is the focus of this thesis.

In this chapter, a brief overview of the drilling rig system is given. Modes of the vibration while drilling and the harmful phenomena induced by them are introduced. Then a description of fatigue problem and its inspections and improvements will also be given.

1.1 Overview of a Rotary Drill Rig System

Normally, a drill rig system contains four major components: rotating equipment, circulating system, hoisting system and power generation system. Figure 1.1 shows the basic components of a drill rig system.

1.1.1 Drill-string

Drill-string is the major component of a drilling system. Usually, it is made up of drill-pipes, drill-collars, stabilizers and a drill-bit. It transports the torque generated by the rotary table or top drive to the drill-bit to realize the drilling operation. And it also serves as a conduit for drilling fluid [3]. During drilling operation, the drill-string is subjected to various loads, such as hook load at the top, rotary system driven torque, weight on bit (WOB), torque on bit (TOB), drilling fluid buoyant force and its self-weight. The hoisting system can support the drill-string weight.

The drill-pipe section is normally the longest part of the drill-string and it is normally in tension. Drill-collars are extra heavy steel pipes providing necessary WOB to assist the bit to cut the rock formation, which are placed right above the drill-bit and below the drill-pipe section. The significant strength of drill-collars helps stabilize the down-hole assembly, facilitate straight drilling and protect itself from excessive fatigue or wear.

1.1.2 Drill-bit

Another important component of a drilling system is the drill-bit. Its main task is to fracture and penetrate into the rock formation at down-hole. Two main kinds of drill-bits are commonly used: roller-cone bits (RC) and polycrystalline diamond compact bits (PDC). The property of the formation (soft or hard) determines which type of

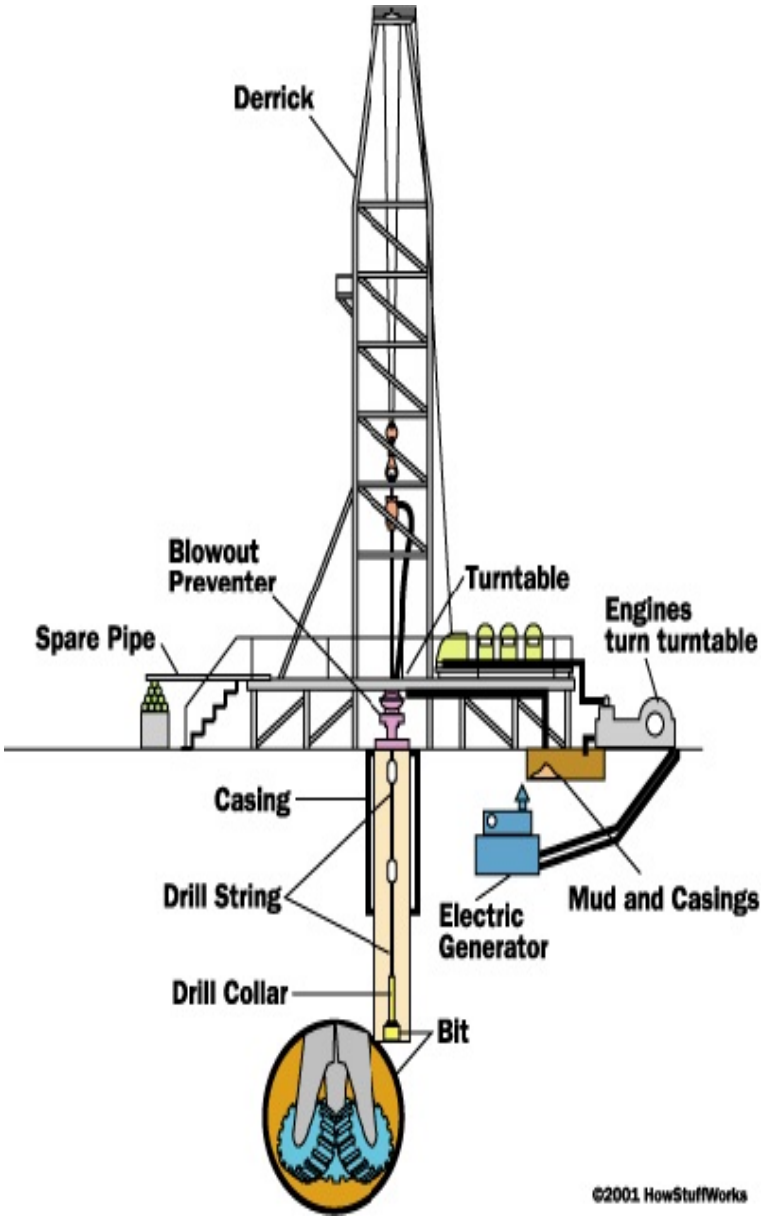

Figure 1.1: Basic Elements of a Drill Rig System [2]

the drill-bit to be selected. Figure 1.2 and Figure 1.3 show a tri-cone bit and a PDC bit, respectively.

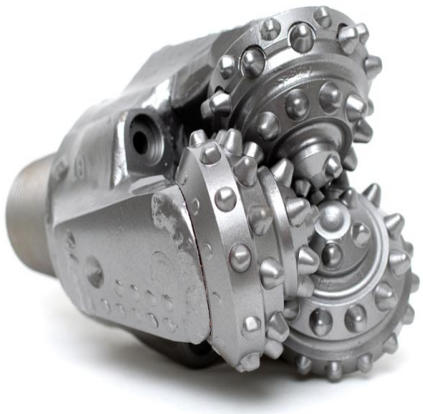

Figure 1.2: A tricone bit [4]

Figure 1.3: A PDC bit [5]

1.1.3 Threaded connection

A drill-string is made up of numerous drill-collars and drill-pipes. Threaded pipe connection serves as a connector between the adjacent drill-pipes or drill-collars to

form a great length of drill-string. Three types of thin-walled pipe threaded connection are shown in Figure 1.4. They are usually used for drill casing, which is normally placed and cemented after drilling.

Among them, threaded and coupled connection (T&C) is the most commonly used type. In this thesis, this kind of connection is analyzed. It includes three parts: two pins serve as master parts and one box serves as slave part of the coupling pair (See Figure 1.4 (a)).

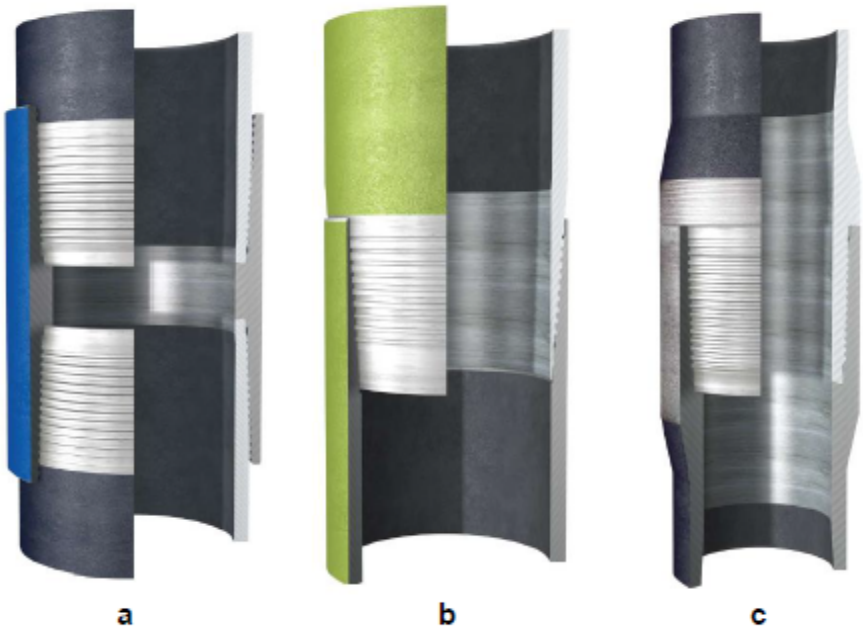

Figure 1.4: Three types of threaded connection a) Threaded and Coupled, b) Integral Flush, c)Integral Upset Connection [6]

1.1.4 Drilling fluid

The circulating system serves as a maintenance for well bore stability and drilling pressure balance. During drilling process, drilling fluid (also called drilling mud) runs in the circulating system. The pressure it produces can prevent the formation fluids

from overflowing to the surface. Further, by circulating down the drilling mud and ejecting the rock cuttings from the bit nozzle, the down-hole is cleaned. Unexpected failure caused by unclean down-hole environment can be effectively avoided.

1.1.5 Hoisting system

The hoisting system enables the installation of a great length of drill-string, making it possible to extend a great length of drill-string to reach the deep oil-well bottom, as well as to replace a drill-bit when necessary.

The hoisting system is made up of crown block, derrick, traveling block, drilling line and draw-works. A hoisting system is depicted in Figure 1.5.

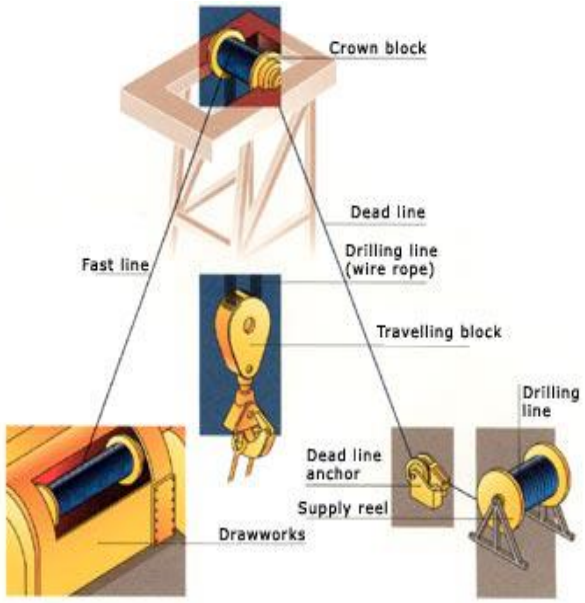

Figure 1.5: Hoisting system [7]

1.1.6 Power generation system

The power supplied for the drill rig system is either generated at the rig site using internal-combustion diesel engines or taken as electric power supply from existing power lines [8].

1.1.7 Well blowout preventer

Blowout preventers (BOPs) are the safety equipment to prevent a blowout. BOPs and associated valves are installed on the top of the casing head before drilling ahead after rigging up. These high-pressure safety valves and associated equipments are designed to shut off the well hole and prevent the escape of the underground fluids or gases when blowout is to occur.

1.1.8 Measurement while drilling equipment

Measurement while drilling (MWD) can provide the directional drillers with the accurate and qualified data to keep the oil-well on the planned trajectory. The inclination and azimuth of the well-bore at certain locations are measured using accelerometers and magnetometers. Furthermore, MWD tools can also provide useful information about the drill-string such as the rotational speed, WOB and TOB, type and severity of down-hole vibrations, and mud flow volume. These information is useful for both the operator and researchers.

1.2 Drill-string Fatigue

1.2.1 Field reports

Failure due to fatigue is a time-consuming and costly problem in oil and gas industry. Even though many researches have been conducted to deal with this problem, the fatigue failures still occur frequently.

It is reported that drill-string failure occurs on 14% of all drill-rig systems, and costs approximately 106,000 US dollars each time the system experiences failure [9].

In Hill's report [10], 76 drill-string failures occurred from 1987 to 1990 on three continents were investigated. Fatigue was estimated as the major cause of 65% of these failures and had a vital impact on 12% of them. The other factors such as excessive tension and torque, low toughness of the material were minor causes to failures compared to fatigue.

1.2.2 Causes of fatigue failure

1.2.2.1 Dog-legs

In drilling operation, the drill-string will inevitably be bent when the drilling well path is not vertical. This bending can occur intentionally due to the designed directional well. It may also happen unintentionally since the minor changes of the well direction are unpredictable. The bent part of a drill-string is called dog-leg, which is illustrated in Figure 1.6.

As the drill-string rotates, a cyclic bending stress will occur within the drill-string. If this bending stress is large enough, the drill-string can be damaged by each rotation. Based on the Miner's damage accumulative law, as the damage comes to an certain extent, fatigue failure will occur.

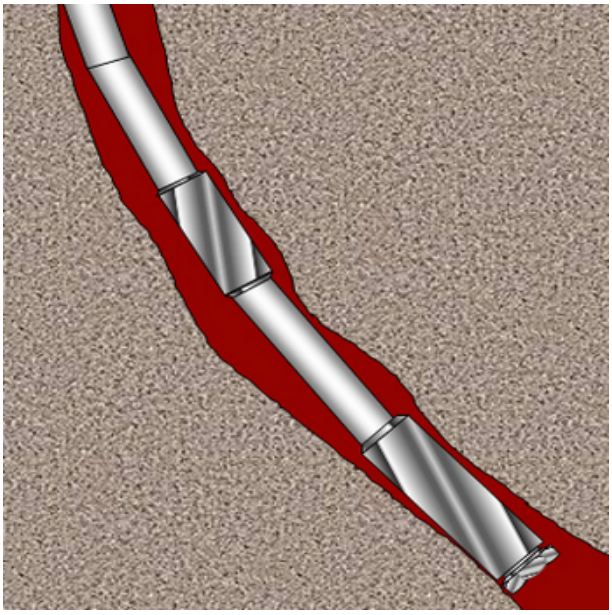

Figure 1.6: Dog-leg of a drill-string

1.2.2.2 Mechanical vibrations

Mechanical vibrations, as mentioned in the previous sections, are not negligible factors in fatigue study. These vibrations can occur in axial, torsional and lateral directions or in a combination of two or three of them, as depicted in Figure 1.7. They are affected not only by the drill-string's properties such as inertia, stiffness but also induced by external excitations from bit-rock interaction, well-bore contact, and drilling fluid's friction. As a result of vibrations, cyclic stresses in the three vibratory modes can produce fatigue damage to the drill-string, as dog-legs do [11].

Drill-string vibrations can decrease rate of penetration (ROP), interfere with MWD tools and even cause premature fatigue of the components.

Firstly, as can be seen in Figure 1.7, the drill-string's axial vibration results in the longitudinal motion of its components. The bit-formation interaction is the main cause for axial vibration. One of the negative effects induced by axial vibration is bit bounce. It means the bit repeatedly lifts off the bottom and impacts the rock

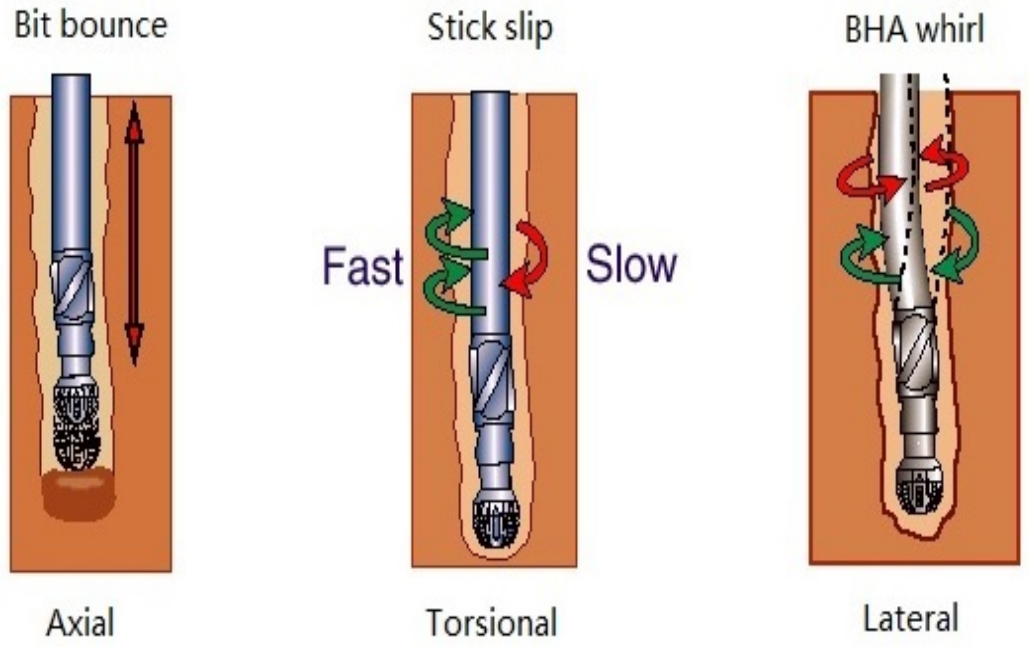

Figure 1.7: Modes of vibration in drill-string [12]

formation. Severe bit bounce may lead to premature bit and bottom hole assembly (BHA) failure and ROP reduction.

Secondly, it is found by down-hole measurements that applying a constant rotary speed at the surface does not necessarily lead to a steady rotational motion of the drill-bit. In fact, during a significant fraction of the drilling time, the down-hole torsional speed may experience large amplitude fluctuations due to the torsional flexibility of the drilling assembly [13, 14].

The most common damaging phenomenon caused by torsional vibration is stick-slip. Stick-slip can stop the drill-string from rotating (stick) and can lead to a sudden increase of rotary speed (slip). This phenomenon can produce unstable torque and bit-velocity, which can induce harmful friction, impact and wear of the drill-string.

Finally, lateral vibration can also cause drill-string failure, stabilizer wear and bore-hole wall enlargement. However, lateral vibration is difficult to detect at the surface because it barely travels beyond the neutral point [13]. Normally, the BHA will be in compression when the drill-string operates. This situation causes the whirling phenomenon of the drill-string. The BHA whirl can be qualified as forward or backward whirl as can be seen in Figure 1.8.

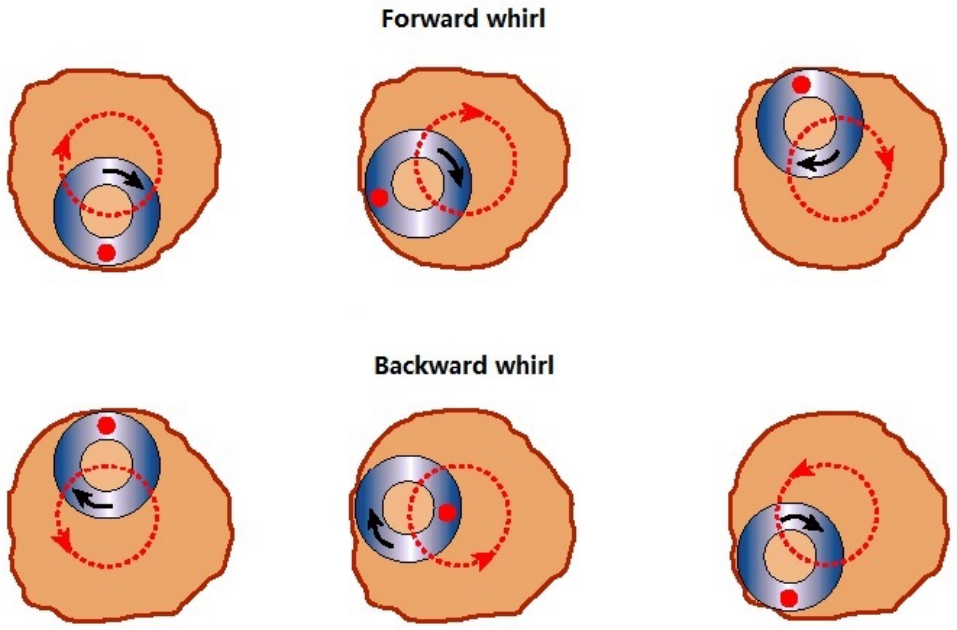

Figure 1.8: BHA whirl phenomenons [12]

Further, coupled vibrations are common during drilling operation, when the above mentioned two or three vibration modes occur simultaneously. In other words, the harmful phenomena: bit-bounce, stick-slip and whirl phenomena can also happen at the same time.

Firstly, initial curvature of the BHA can result in the coupling between the axial and lateral vibrations. Bit bounce can be sometimes triggered by the large lateral

vibrations of the BHA. Secondly, the drill-bit also plays an important role in coupling drill-sting axial and torsional vibrations as it relates the WOB to the TOB. Thirdly, the high rotary speed which the drill-string experiences during the stick-slip can lead to BHA whirl phenomenon. This couples the lateral and torsional vibrations.
Although the down-hole vibrations are usually coupled, analyzing axial, torsional and lateral vibrations separately is crucial for securing physical integrity and minimizing risks of formulation errors [16].

1.2.2.3 Casing while drilling

Casing while drilling (CWD) is an emerging technology that by its definition, it is a process for simultaneously drilling and casing a well where: 1. the well is used for the drill-string; 2. the casing is rotated as needed to drill; 3. the casing is cemented in well. Rather than conventional drill-string, in CWD the drilling is done along with the casing to reduce overall drilling time [15].
However, this comes up with a number of challenges, one of which is the appropriate design and evaluation of the threaded casing connections so that they can withstand the rigours of drilling. As can be seen in Figure 1.4, the three types of thin walled pipe threaded connections typically used to connect drill casing are the weakest spots in casing drilling systems. Fatigue problems can occur in these connections due to random vibrations. Chapter 5 will give elaborate investigation on this topic.

1.2.2.4 Environmental effect

Environmental effect, mainly the corrosion, plays an important role in drill-string fatigue failures. Hill [10] pointed out that corrosion can accelerate the drill-string crack initiation as well as the crack growth rate. The corrosion mainly comes from the drilling mud, which is affected by various factors: dissolved oxygen, carbon dioxide,

pH level, H_2S level and temperature [17].

Moreover, Grondin and Kulak [18] also recognized the importance of environmental effect. Fatigue experiments on full-sized drill-pipes carried out by them included the condition in air and the condition in corrosive 3.5 percent NaCl solution. S-N curves were constructed and results were compared for both conditions. It was concluded that corrosion has a detrimental effect on the fatigue life of drill-pipes. And the corrosive environment affected fatigue life more significantly at lower stress ranges, since the exposing time is longer at low stress ranges than large ones.

1.2.3 Fatigue failure inspection

Inspection of a drill-string should follow the specifications and methods, which are developed for different parts of drill-string. For example, API Specification 5D should be adopted for tubes and upset definition, API-RP-7G for drill-collar and tool-joints and API-RP-5A5 for inspection procedure.

Hill [19] summarized the available inspection methods and their characteristics, shown in Figure 1.9. Among them, visual inspection should always be performed for all inspections while the others may require special equipments and follow specific procedures. Gross fatigue crack, thread damage, surface and coating wears and other external damage of the drill-string can be detected by visual inspection.

1.2.4 Improvements of the drill-string

Noticing the harmfulness of the fatigue, plenty of new designs have been presented to improve drill-strings. Vaisberg et al.[17] divided these improvements into five parts as: improvements for drill-pipe, drill-collar, heavy weight drill-pipe, connections and steel properties. Belows are brief descriptions of drill-pipe, drill-collar and threaded connection improvements.

Drillpipe tube bodies	Electromagnetic inspection Ultrasonic wall thickness OD(1) gauging Visual Dry magnetic particle inspection (MPI(2)) of end areas Electronic end area inspection	Fatigue cracks, corrosion pits, mechanical damage Wall reduction OD(1) wear, crushing, necking, swell Mechanical damage Fatigue cracks in end areas Fatigue cracks, corrosion pits, mechanical damage in end areas
Drillpipe tool-joints	Visual Dimensional Wet magnetic particle inspection (MPI(2))	Mechanical damage, weight/grade identification Mechanical damage, wear Fatigue cracks in threads
Rotary shouldered connections on drill collars and BHA(3) components	Visual Dimensional Wet magnetic particle inspection (MPI(2)) Ultrasonic inspection	Mechanical damage Mechanical damage, wear, inadequate BSR(4) Fatigue cracks in threads Fatigue cracks in threads
Floor safety valves inside BOP's(5)	Disassembly and visual Hydrotest Wet MPI internal threads	Improper components, worn or damaged components Leaks Fatigue cracks

(1) OD is outside diameter.
(2) MPI is magnetic particle inspection.
(3) BHA is bottom hole assembly.
(4) BSR is bending strength ratio.
(5) BOP is blow out preventer.

Figure 1.9: Common inspection methods for used drill-pipe and $BHA^{(3)}$ components [19]

Firstly, the areas to improve drill-pipe are mainly the upset area, where the welding area locates. Figure 1.10 shows the critical drill-pipe fatigue areas and three typical upset designs are dipicted in Figure 1.11.

Secondly, the focus of drill-collar improvement lies on: 1. Coldworking, which produces residual compressive stresses to increase the resistance to fatigue cracks initiation. 2. Gall resistant coating, which is to relieve damage from friction.

Thirdly, the improvements of threaded connections are important since the threads are the most vulnerable areas of the whole drill-string. Redesigns of the threaded connection geometries are made mainly to reduce stress concentration. These designs can be made at the pin, the box, the thread areas. An example of stress relief groove designed on the pin and the box by Weiner [20], is shown in Figure 1.12.

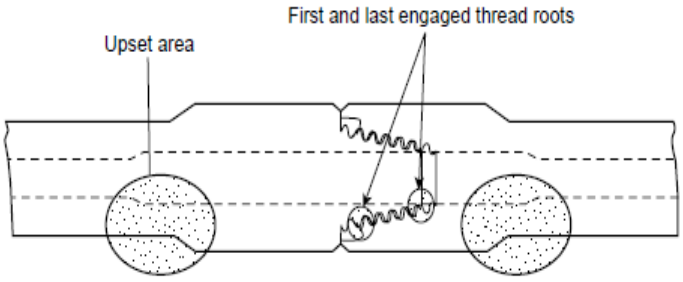

Figure 1.10: Drill-pipe fatigue critical areas [17]

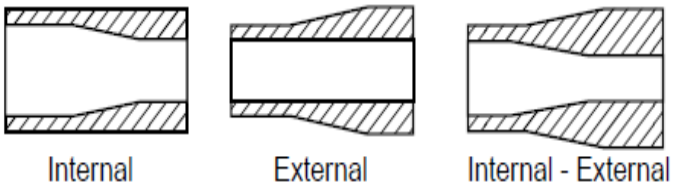

Figure 1.11: Typical upsets [17]

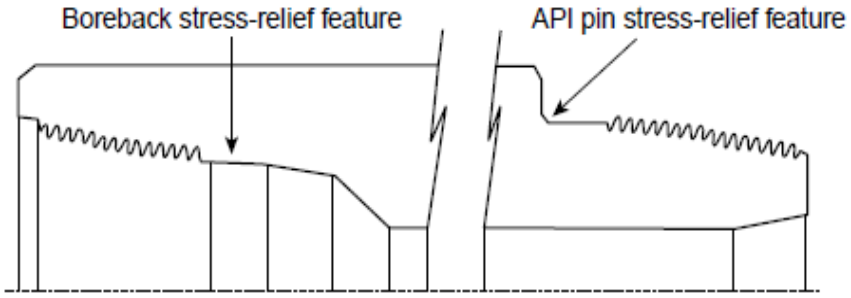

Figure 1.12: Box and pin stress relief design[20]

1.3 Conclusion

This chapter introduced the major components of a rotary drilling rig system. Mechanical vibrations, considered as the major cause of drill-string fatigue, are described explicitly. Then other causes of the fatigue problem, drill-string inspections and improvements are reviewed.

Chapter 2

Literature Review

2.1 Drill-string Fatigue Analysis

Many researchers have conducted various fatigue analysis on drill-strings. The common purpose of these researches is to predict the critical position as well as the life time of a drill-string. These researches can be divided into two categories: Experimental tests and theoretical works. The former focuses on developing experiments to demonstrate the similar condition in which the drill-string operates. While the latter concentrates on modeling and simulation of the drill-string with the aid of computer software.

2.1.1 Experimental tests

Experimental researches on drill-strings in the laboratory are aiming at demonstrating the situation in which the drill-string is excited by cyclic loadings. The obtained results can be used to construct a S-N curve of a certain type of drill-pipe, which can then serve as reference and validation of the theoretical works.

Among the various experiments, the followings are most representative: Bachman [21]

investigated fatigue of full-size drill-pipes. In his tests, the drill-pipes were clamped as cantilevered beams and subjected to rotational bending. A limitation is that his experiments did not consider axial load to the drill-pipes, and the test was conducted only in the condition of air.

Morgan and Robin [22] reported testing results from small-scale coupons cut from as-produced seamless hot-rolled drill pipes. Axial load was applied to the specimens in their work to gain realistic data.

In 1991, Grondin and Kulak [18] conducted experiments using full-size drill pipes. Their tests provided the most comprehensive data for drill-string fatigue in which full-size drill pipes were subjected to axial load, fluctuating bending and rotating bending in both air and corrosive media. One of their experiment setups, rotating bending setup, is depicted in Figure 2.1.

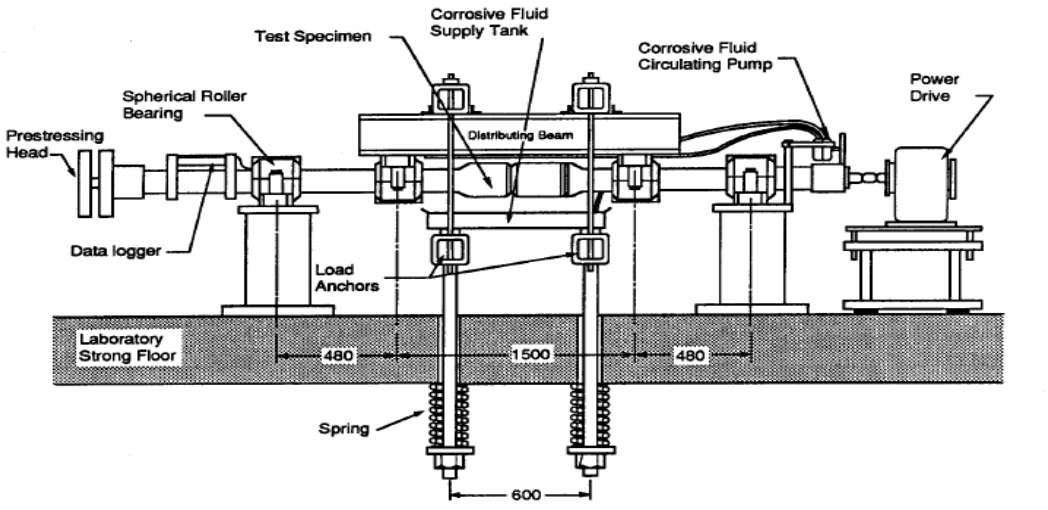

Figure 2.1: Rotating bending setup for drill-pipe fatigue experiments conducted by Grondin and Kulak [18]

2.1.2 Theoretical works

Besides the experimental researches, theoretical works on drill-string fatigue can predict fatigue damage of the drill-string. These researches are mainly conducted along two lines.

One is based on fracture mechanics theory [23]. This theory assumes micro cracks exist in the drill-string materials. As the drill-string is under cyclic loadings, these micro cracks tend to grow in certain direction. When the cracks grow to a certain extent, fractures will ultimately occur within the drill-string, which induce fatigue failures [17].

The other way of theoretical research combines fatigue S-N relationship with the linear damage cumulative law (Miner's Rule). Based on this, the fatigue damage caused by loadings with different amplitudes is calculated and then summed to form an equivalent total damage. This kind of fatigue calculating method was initiated by Lubinski [24]. In his work, maximum permissible changes of well hole angle (i.e. dog-leg) were specified.

Hansford and Lubinski [25] considered that the drill-pipe is bent due to intentional well path design or unintentional well direction changes. Cyclic bending stress inside the drill-pipe is formed as the drill-pipe rotates, which results in fatigue damage accumulation. The work calculated fatigue damage for drill-pipe under conditions of different materials and dog-leg severities.

J. Wu [26] developed an analytical solution for calculating drill-pipe bending stress. Different from Hansford and Lubinski's research, his work considered that a rotary drill-string in a horizontal well is under axial compressive load, which induces larger bending and deflection in the dog-leg interval. Cycles to fatigue failure was calculated by referring to the drill-pipe S-N curve. However, a limitation of this work is that the consideration of the mean stress was excluded.

To improve theoretical damage predictions, many researchers have made modifications to the S-N relationships and the stress analysis of the drill-string.

In addition, vibrations are also noticed as a major cause of the cyclic stress inside the drill-string. Patel and Vaz [11] are pioneers of the research on drill-string fatigue caused by vibrations. In their work, an analytical model was developed for three independent vibratory directions, in order to obtain stresses. Comparisons of the fatigue damage caused by vibrations and dog-legs showed that vibrations have even larger effects on fatigue damage than those due to dog-legs. Suggestions were made that tuning the rotary speed to avoid resonant excitations and the use of shock-subs could reduce fatigue damage induced by vibrations. Limitations of this work are: 1. the stress in each direction is treated independently without calculating an equivalent stress; 2. random vibration, which is common in practice, is not mentioned.

2.2 Threaded Connection Fatigue Analysis

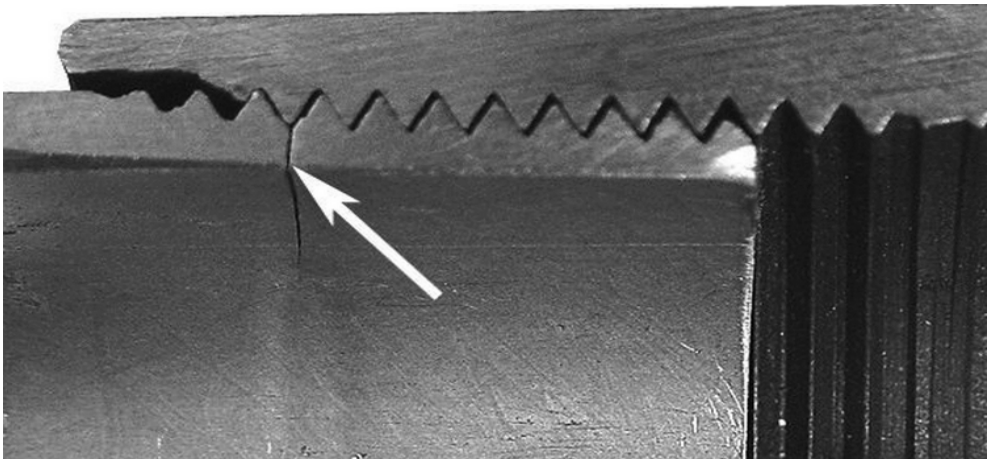

Figure 2.2: Fatigue failure at a threaded connection [27]

Threaded connections are widely used in drilling system to combine adjacent drill-

pipes or drill-collars. Due to the special geometries of the threads, stress concentration may occur in specific location where fatigue damage can happen. An example of fatigue failure at threaded connection is shown in Figure 2.2.

2.2.1 Experimental tests

Many fatigue tests are done on different types of threaded connections in different settings. These experiments can be categorized into three types based on how the load is applied on the specimen.

The first type of experimental setup is axial tension setup, in which the threaded connection is subjected to a fluctuating axial tension load. An example of this type is shown in Figure 2.3(a). Brennan [28] tested 6.5" drill-pipe samples with this type of setup. The main disadvantage is that it requires extremely high forces which consume considerable amount of power.

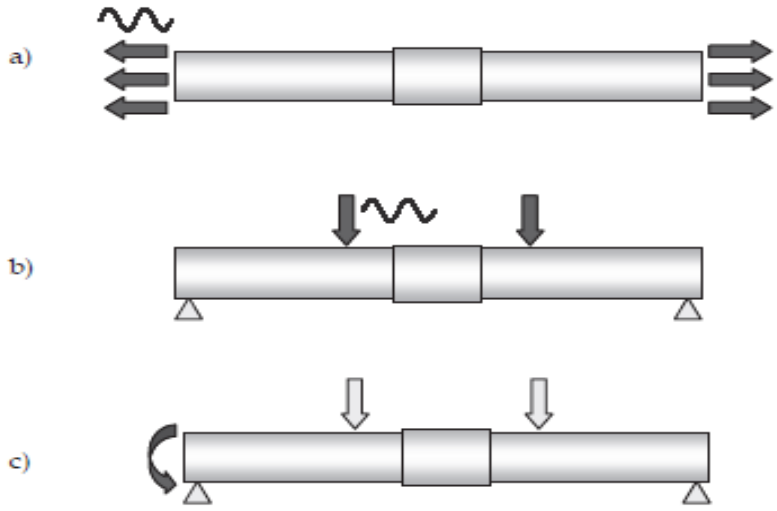

Figure 2.3: Three types of fatigue experiments (a) axial tension (b) 4-point bending (c) rotating bending

The second type of experimental setup is four point bending setup. An example of

this type is shown in Figure 2.3(b). It requires smaller load than axial tension setup. It applies fluctuating forces at two points in the vertical direction in order to form bending stresses within the drill-pipe threaded connection. Lourencco [29] conducted this type of experiment on small scale drill-pipe samples considering internal pressure. A limitation of this type is that the frequency of loading is quite low as between 0.1 to 5 Hz, which results in long testing time.

The third type of experimental setup is the rotating bending setup. An example of this type is shown in Figure 2.3(c). In this type of setup, a constant bending moment is applied while the drill-pipe rotates. Additional axial force can be loaded during the fatigue tests.

The results from the above setups are analyzed by many authors to obtain S-N curves on different types of threaded connections. A comprehensive summary of the test data is listed in reference [30].

2.2.2 Theoretical works

Researchers [31, 32, 33, 34] have developed their models for different types of threaded connections, using 2-D axisymmetric modeling method.

Tafreshi and Dover [34] conducted stress analysis on the drill-string threaded connections under axial, bending and torsion loadings. For axial loading, 2-D axisymmetric model was used, while a full 3-D model was investigated for bending and torsion loading. Results were given as stress concentration factor (SCF) at the critical thread roots. It was found that maximum SCF is at the root of the last engaged thread (LET). However, no fatigue analysis was made in this work.

Macdonald and Deans [33] made improvements of stress analysis by taking into account elastic-plastic material and preload from make-up in their 2-D axisymmetric model. It was concluded that preload affects the static stress distribution within the

threaded connection and the peak mean stress levels. They also predicted that the expected critical site for fatigue is the box LET, though no further fatigue calculation was done.

Further development of the rainflow counting method for this thesis is given in Section 3.2.1.

Among the many researches, Van Wittenberghe's work [30] is the most comprehensive one for threaded connection stress and fatigue analysis. In his work, not only the previous experimental test results were summarized to acquire S-N curves, but also numerical simulations using the Abaqus software were carried out. And the effect from software error - meshing, was investigated by assigning coarse meshes to fine meshes. 2-D and 3-D modeling were compared to validate accuracy of the 2-D model. Furthermore, the validity of the 2-D model was shown experimentally by comparisons between the strain values from simulations and strain gauge measurements during experimental tests. Fatigue due to cyclic axial tension load was also included in his work.

However, random vibration effects are not included in the existing literatures. Improvement of threaded connection fatigue can be made by accounting for random excitation, since the vibrations during drilling operations are often random in nature.

2.3 Fatigue Analysis techniques

Fatigue damage can be predicted with the time domain method and the frequency domain method, depending on which domain the measured data is in.

2.3.1 Time domain method

In the time domain method, based on the solution of finite element model, stress time histories of interested positions can be obtained, under both deterministic and random excitations. The time histories resulting from random excitations usually have an irregular form, which consist of a great number of small stress cycles with various stress range and mean stress. (Figure 2.4).

In fatigue study, it is important to take into account all these stress cycles. Hence, rainflow counting method [35], which is regarded as an efficient cycle counting method, is introduced to address the stress time histories.

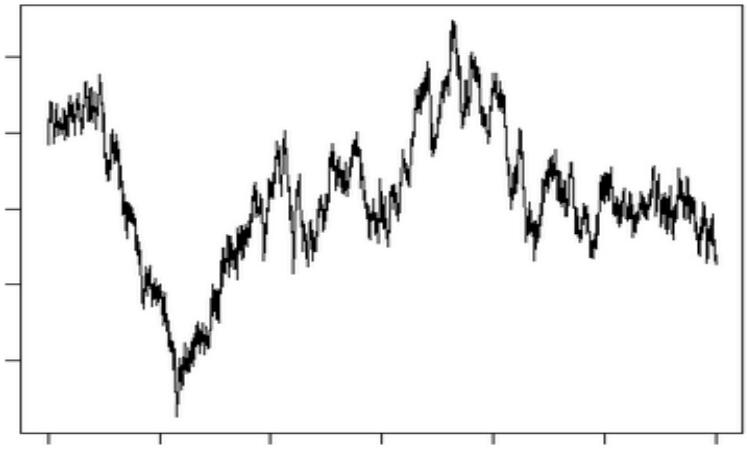

Figure 2.4: An example of irregular time history

The rainflow counting method is used to extract the cycles important for fatigue calculation, which are called "rainflow cycles". The rainflow counting algorithm consists of three steps (see also Figure 2.5) [35]:

1. Pick a local maximum M_k

2. For each M_k, before it reaches the same level again, find the minimum m_k^-, m_k^+ from the left and the right.

3. The rainflow cycle's minimum is the one which has the smaller deviation. Here is m_k^-.

Then, the k_{th} rainflow cycle is constructed as: (m_k^-, M_k).

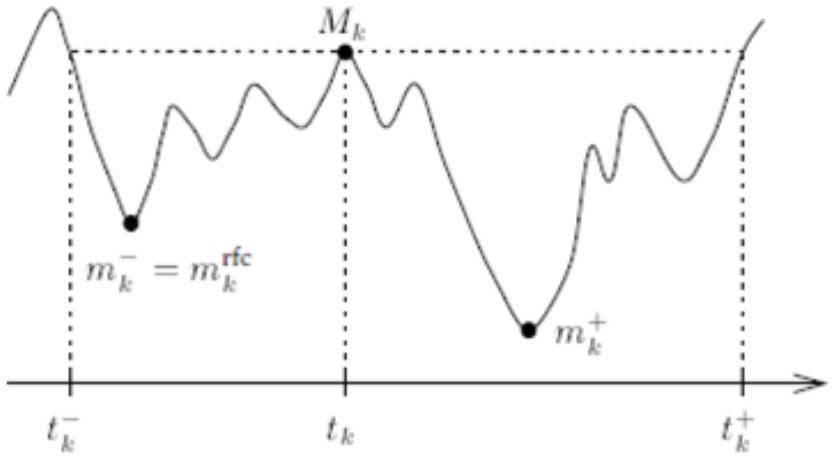

Figure 2.5: Definition of rainflow counting

Rainflow cycles are then stored in a two column matrix, in which the first column records rainflow minimum and the second column records maximum. These cycles are then ready for the use of fatigue calculation.

Fatigue calculation in time domain is straightforward. It follows the conventional fatigue calculation method: firstly refer to S-N curve and then sum up the damage based on Miner's Rule. Generally, S-N relationship can be expressed as:

$$N(s) = \begin{cases} K^{-1}s^{-\beta}, s > s_\infty \\ \infty, s < s_\infty \end{cases} \tag{2.1}$$

where s, N denotes the stress range and the cycles to failure, K, β are constants, s_∞ represents the fatigue limit of the material. Then the total damage are calculated by

the accumulation of each cycle's damage:

$$D = \sum_{1}^{i} \frac{1}{N(s_i)} \tag{2.2}$$

where s_i denotes the i_{th} stress range, $N(s_i)$ represents the cycles to failure under this stress range. Noted that the structure is likely to fail when total damage $D > 1$.

2.3.2 Frequency domain method

In engineering practice, the measured stress time histories are often random in nature. In other words, it can consist of a great number of stress cycles with different stress ranges and means. For this type of irregular time histories, time domain method has the drawback of time-consuming. This is because accurate fatigue damage results can only be obtained from long enough time history samples. However, frequency domain method can avoid this problem as well as giving accurate results.

In frequency domain, spectral methods have been developed for fatigue problems, under different kinds of random loadings such as Gaussian/ non-Gaussian, narrow-band/ broad-band or bi-modal random loadings. Examples of narrow-band and wide-band stress power spectral densities (PSDs), together with their time-histories are illustrated in Figure 2.6.

Generally, frequency domain method only requires the stress PSD as its input. Then expected damage and predicted life can be derived explicitly.

For narrow-band random processes, conventional narrow-band spectral method originally proposed by Miles [36] can be adopted. For broad-band Gaussian random processes, several methods have been proposed to estimate fatigue damage: Benasciutti [37] presented analogies and differences for seven spectral methods for broad-band

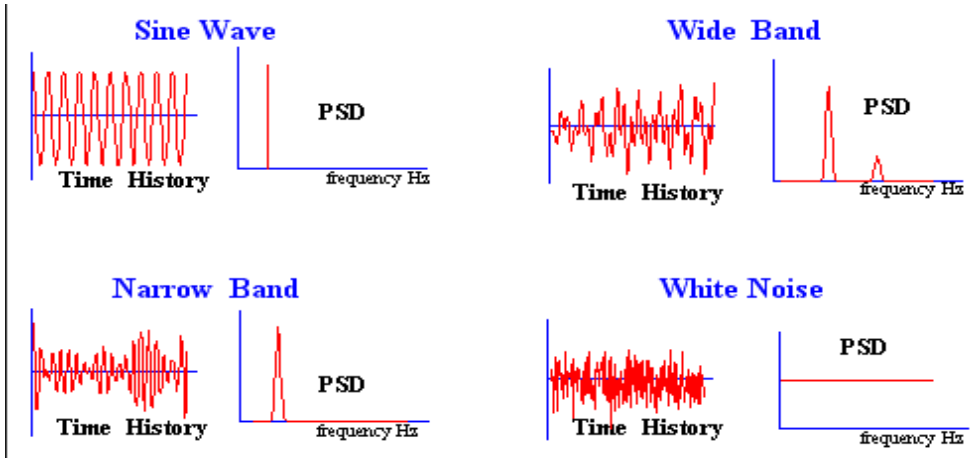

Figure 2.6: Narrow-band and wide-band process

fatigue analysis. Numerical simulations were conducted to find the accuracy of these methods in estimating fatigue damage in Gaussian broad-band processes under a damage cumulative law. Comparisons between results by the seven spectral methods indicated that the Dirlik method [38], the Tovo-Benasciutti method [39] and the Zhao-Baker method [40] tend to give most accurate fatigue damage estimation among all the methods.

2.4 Drill-string Modeling Method

In recent decades, theoretical models have been built to simulate drill-string dynamics. These models can be divided into three dominant categories: finte-element-method (FEM) [41, 42, 43], lumped parameter method [44, 45] and continuous parameter method [46, 47, 48, 14]. In this section, existing drill-string models using finite element method and continuous parameter method as well as the modeling technique for threaded connection are reviewed.

2.4.1 Finite element method

Regarded as one of the most powerful numerical tools, the finite element method (FEM) is adopted by many researchers in drill-string dynamic analysis. This method is adopted for developing models in Chapter 3. The following is a brief review of this modeling method.

Trindade et al. [49] studied drill-string vibrations simulating the drill-string as a vertical slender beam. The considered loading was gravity force and geometric softening effect of its lower portion was included in their model. The results showed that micro-impacts and reaction forces at both ends are well presented only when using the non-linear axial-bending coupling model.

Khulief and Al-Naser [50] employed an Euler-Bernoulli beam model to represent the whole elastic drill-string including both drill-pipes and drill-collars (bottom hole assembly). In their paper, the model has six degrees of freedom per node and accounted for the gyroscopic effect, the torsional-bending inertia coupling and gravity force effect. The method developed is proved to furnish a basic building block for further research of more comprehensive drilling assembly models considering wellbore/ drill-pipe contact, drill-string/mud flow interaction, and stick-slip at the bit.

Sampaio et al. [43] employed a geometrically non-linear model to study the coupling of axial-torsional vibrations on a drill-string. The geometrical stiffening was discussed in the paper using a non-linear finite element approximation, which accounted for large rotations and non-linear strain-displacements. The result of the paper showed that the responses of the linear and non-linear models, drill-bit rotary speed and the predicted forces, after the first periods of stick-slip, were considerably different.

Pivovan and Sampaio [51] presented a finite element model considering the coupling of axial, torsional and lateral vibrations on a rotating drill-string. The drill-string model was discretized using a finite element with 12 degrees of freedom. In the simulation,

the model was subjected to distributed loads due to gravity force, impacts between the drill-string and well-bore and perturbation moments at the lower end. The results showed that the influence of the geometric non-linearities in the dynamic response of the drill-strings is crucial.

2.4.2 Continuous parameter method

Continuous parameter method is also a widely used modeling method which can give results of any interested position in a model. This method is adopted in developing model in Chapter 4. The following is a brief review of this modeling method.

Khan [47] first developed an analytical and numerical model for drill-string, considering linear longitudinal and torsional vibration directions. Dynamic results were given as natural frequencies and mode shapes under different boundary conditions. The excitations included were fluctuating weight on bit and torque generated by rotary table.

Li [48] also built a longitudinal and torsional model by means of continuous parameter method. Both longitudinal and torsional displacement, velocity and acceleration results were obtained and compared to the downhole data during field tests and lab experiments. Sources of excitation were considered as combination of four factors: bit displacement due to drill-bit geometry, due to penetration depth, due to three-lobed pattern of rock formation and due to static weight on bit.

Sengupta [52] investigated lift-off phenomenon of the drill-bit due to the weight on bit variation and the changing of rock formation surface. Analytical dynamic results were solved via continuous system and it was concluded that rotary speeds are critical factor affecting the axial resonant frequencies and fluctuations of weight on bit.

Dareing and Livesay [53] considered periodic bit motions as excitation of longitudinal and angular vibrations along the drill-string. Friction which acts along the length of

the drill-string was included as a damping term in the continuous model. Effects of rotary speed, friction and shock sub were discussed in their paper.

2.4.3 Threaded connection modeling method

In the recent decades, with the development of computer, finite element method becomes popular in modeling complex geometry, such as the threaded connection. With the powerful calculation software, a variety of finite element models can be investigated relatively faster than conducting experimental tests.

Two dimensional (2-D) axisymmetric model is widely accepted for modeling threaded connections, because it has the advantage of time-saving, and it can give accurate results as three dimensional (3-D) model does. This is concluded by Zhong [54], who compared the resulting stresses and simulation time between 2-D and 3-D models.

In 2-D axisymmetric model, several simplifications should be noted [30]. First, the thread helix angle is neglected. Secondly, thread run-in and run-out regions are not modeled. It is assumed that these two simplifications have little effect on the resulting stress distribution.

2.5 Brief Introduction of the Thesis

2.5.1 Scope of the thesis

This research work is to calculate drill-string fatigue damage in both time domain and frequency domain. The considered vibration includes axial and torsional directions. In the drill-string model, both deterministic and random excitations are taken into account.

Further, threaded connection fatigue damage due to axial random excitation is also investigated.

2.5.2 Objective and significance

Noticing limitations still exist in the available literatures, 3 major improvements will be made in this thesis. Firstly, all research works on drill-string except Patel and Vaz's work [11] considered only the fatigue caused by cyclic loadings in dog-leg and/or drill-string buckling, without accounting for drill-string vibrations. Secondly, research on fatigue life estimation of a drill-string under random loadings is still not studied. Finally, random vibration also has not been included in the available literatures on threaded connections study.

Therefore, the main objective of this thesis is to predict the drill-string fatigue damage caused by random vibration. Also, this thesis will develop a way of fatigue analysis on the whole drill-string and the local structure - threaded pipe connection. The fatigue calculating methods in this thesis can be used for fatigue damage calculation in other similar structure.

2.5.3 Organization of the thesis

The drill-string model in Chapter 3 is built by FEM in both axial and torsional directions. Random excitation is assumed as the interaction between the drill-bit and the rock at the well bottom. Fatigue damage calculation is based on rainflow counting method, which is to address the dynamic stress time history resulting from the dynamic model. Then Miner's Rule is applied to gain damage results along the drill-string.

In Chapter 4 the drill-string model is developed by continuous parameter method in both axial and torsional vibration. This will result in a fatigue problem under a stress state of uni-axial tension-compression with torsion. Instead of simply summing up the fatigue damage caused by each vibratory direction, an equivalent stress is required

to determine the expected fatigue damage. This is obtained by adopting a multiaxial random fatigue criterion. According to the equivalent stress PSD, specific spectral method is then employed to calculate expected fatigue damage along the drill-string. In Chapter 5, the threaded connection is modeled by FEM with the help of ANSYS workbench 15.0. Different from the previous researches where only a half model was developed, in this paper a full threaded connection with three parts: upper pin, box and lower pin is generated. The boundary conditions are assumed as two equivalent springs attached to the two ends. Apart from a deterministic tensile load, random loading due to the uncertainties of the down-hole interaction is included by assigning power spectral density (PSD) in the model. Then three-band technique is used to give damage predictions.

2.5.4 Limitations

The study of drill-string fatigue is limited to axial and torsional vibration directions, excluding lateral direction. And the random excitations are chosen as ideal white noise since no spectral data is recorded by previous researches.

Chapter 3

Fatigue Estimation of drill-string in Time Domain

3.1 Dynamic Model

This chapter introduces a fatigue damage calculation method for drill-strings, in time domain. It focuses on damage caused by axial and torsional vibrations. Lateral vibration is not included in this thesis because of the complicated coupled vibrations.

3.1.1 Finite Element Method

A typical rotary drilling system commonly seen in the oil and gas industry is illustrated in Fig. 3.1.The drill-string is discretized with finite element method based on Euler-Bernoulli beam theory. Using Lagrange linear shape function with axial and torsional displacements, the axial displacement u and twisting angle θ_u of an element can be presented as:

$$u = N_u q, \quad \theta_u = N_\theta q \tag{3.1}$$

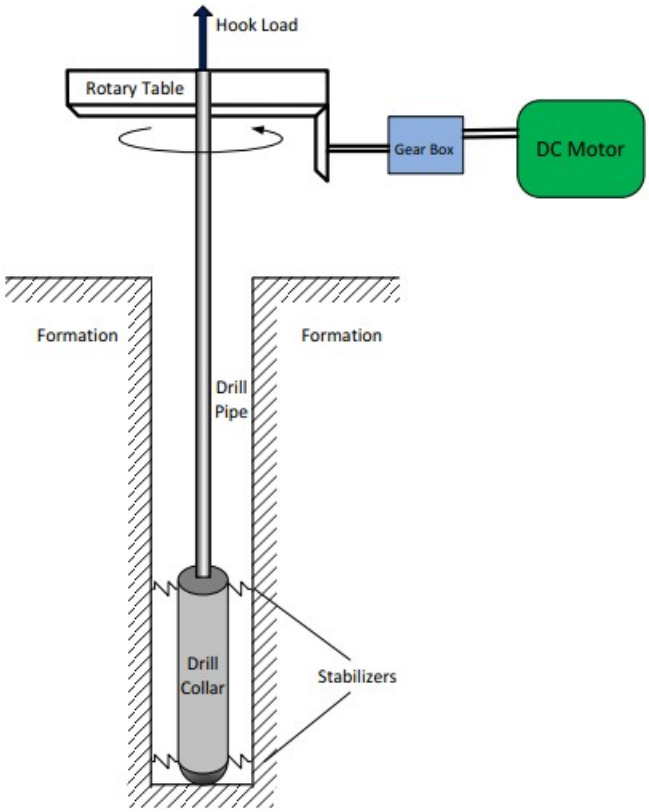

Figure 3.1: The simplified model of the system

where N_u, and N_θ are shape function matrices, and q is the vector of nodal coordinates of the two-node finite element as shown in Fig. 3.2, which is defined by:

$$q = \{u_1 \quad \theta_{u_1} \quad u_2 \quad \theta_{u_2}\}^T \tag{3.2}$$

where u, represents $u-$ translational degree of freedom (DOF), while θ_u represents the rotational DOF around the axial $u-$ axis.

By defining the element length l_e and the non-dimensional element variable $\xi = x/l_e$,

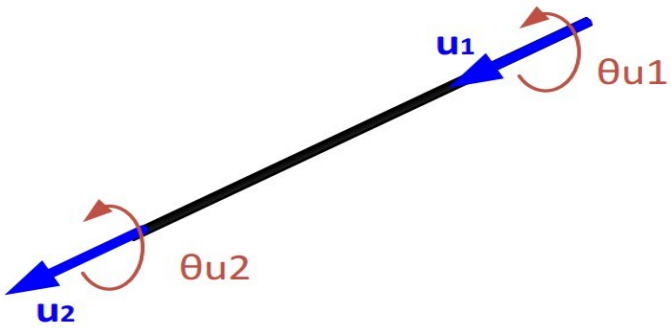

Figure 3.2: Degrees of freedom of an element

the shape function matrices are given as:

$$N_1 = 1 - \xi \tag{3.3}$$

$$N_2 = \xi \tag{3.4}$$

$$N_u = \{N_1, 0, N_2, 0\} \tag{3.5}$$

$$N_\theta = \{0, N_1, 0, N_2\} \tag{3.6}$$

The expression for the linear stiffness K_e is:

$$K_e = \int_0^1 [\frac{EA}{l_e} N_u'^T N_u' + \frac{GJ}{l_e} N_\theta'^T N_\theta'] d\xi \tag{3.7}$$

where N_u and N_θ are for axial and torsional respectively. The expression for the mass matrix M_e is:

$$M_e = \int_0^1 [\rho A l_e N_u^T N_u + \rho J l_e N_\theta^T N_\theta] d\xi \tag{3.8}$$

Substituting Eqn. 3.3 through 3.6 into Eqn. 3.7 and 3.8, the linear stiffness K_e and

mass M_e are obtained:

$$K_e = \begin{bmatrix} \frac{EA}{le} & 0 & -\frac{EA}{le} & 0 \\ 0 & \frac{GJ}{le} & 0 & -\frac{GJ}{le} \\ -\frac{EA}{le} & 0 & \frac{EA}{le} & 0 \\ 0 & -\frac{GJ}{le} & 0 & \frac{GJ}{le} \end{bmatrix} \tag{3.9}$$

$$M_e = \begin{bmatrix} \frac{\rho A l_e}{3} & 0 & \frac{\rho A l_e}{6} & 0 \\ 0 & \frac{\rho J l_e}{3} & 0 & \frac{\rho J l_e}{6} \\ \frac{\rho A l_e}{6} & 0 & \frac{\rho A l_e}{3} & 0 \\ 0 & \frac{\rho J l_e}{6} & 0 & \frac{\rho J l_e}{3} \end{bmatrix} \tag{3.10}$$

By assembling the local stiffness and mass matrices, the system's global mass and stiffness matrices can be obtained.

After certain mathematical manipulations and taking the mass of the stabilizer into account, the equations of motion for the system can be represented in a compact matrix form as:

$$M\ddot{q}(t) + C\dot{q}(t) + Kq(t) = F(x, \dot{x}, \phi, \dot{\phi}, F_c, I) \tag{3.11}$$

$$M = M' + Am \tag{3.12}$$

where M', C and K are system global mass, damping and stiffness matrices, respectively. $q(t)$ is the displacement vector, $F(x, \dot{x}, \phi, \dot{\phi}, F_c, I)$ is the excitation vector which is random in nature, including WOB, TOB, gravity force F_g, hook load F_h and torque from rotory table T_{rb}. Expressions of these excitations will be given in the following section. A is the corresponding transformation matrices, while m is the mass of the stabilizer.

The downhole damping C is assumed to be a linear combination of K and M as

below:

$$C = \alpha M + \beta K \tag{3.13}$$

where α and β are constants to be selected. In this chapter the system is assumed as underdamped which is common in engineering application.

3.1.2 Deterministic Excitations

Due to the bit-rock interaction at the bottom of the bore-hole, the drill- string system is subjected to weight on bit (WOB) and torque on bit (TOB). WOB is represented as:

$$WOB = \begin{cases} k_c(x-s) + c(\dot{x}-\dot{s}) & x \geq s \\ 0 & x < s \end{cases} \tag{3.14}$$

where x is the axial displacement of the bit, k_c is the formation contact stiffness, c is the rock damping coefficient and s is the elevation of the formation surface. k_c , c and s are given by reference [55, 45]

$$G_0 = \frac{E_0}{2(1+\nu)} \tag{3.15}$$

$$k_c = \frac{G_0 r_0}{1-\nu} \tag{3.16}$$

$$c = \frac{3.4 r_0^2 \sqrt{G_0 \rho_0}}{1-\nu} \tag{3.17}$$

$$s = s_0 sin(\phi) \tag{3.18}$$

where E_0, G_0, ν, ρ_0 are determined by the property of the rock, r_0 is the foundation diameter, ϕ is bit torsional displacement.

The TOB is related with WOB and cutting conditions [45], which can be calculated by:

$$TOB = WOB r_b(\mu(\dot{\phi}) + \xi_0 \sqrt{\frac{\delta_c}{r_b}}\ ) \tag{3.19}$$

where r_b is the radius of the bit and δ_c is the depth of cut per circle:

$$\delta_c = \frac{2\pi ROP}{w} \tag{3.20}$$

where w is the average bit speed. ROP, representing the average ROP, is given as [45]:

$$ROP = c_1 F_0 \sqrt{w} + c_2 \tag{3.21}$$

where F_0 is the difference between the total weight and the hook load. $\mu(\dot{\phi})$ is modeled as a continuous function [45]:

$$\mu(\dot{\phi}) = \mu_0(tanh\ \dot{\phi} + \frac{\alpha_1 \dot{\phi}}{1 + \alpha_2 \dot{\phi}^2} + \nu\dot{\phi}) \tag{3.22}$$

F_g is the elementary load vector resulting from the gravity field:

$$F_g = \int_0^1 \rho g A l_e N_u^T d\xi + Cmg \tag{3.23}$$

where C is the corresponding transformation matrix.

F_h is the hook load given as:

$$F_h = r_c W_r \tag{3.24}$$

where r_c is a constant, W_r is the total weight of the drilling system.

T_{rb} is the torque given by the rotary table. It is assumed that the rotary table is

driven by a DC motor through a gear box and T_{rb} is given as [45]:

$$L\dot{I} + R_m I + K_m n\dot{\phi}_{rt} = V_c \tag{3.25}$$

$$V_c = K_m n w_d \tag{3.26}$$

$$T_{rb} = K_m n I \tag{3.27}$$

where I is the motor current and $\dot{\phi}_{rt}$ is the speed of the rotary table. w_d is assumed to be the desired table speed.

3.1.3 Random Components

Considering the randomness of the downhole excitation, two stationary Gaussian white noise excitation $W_1(t)$ and $W_2(t)$ are introduced into the bit axial and torsional directions as the random components. The continuous time white noise excitation needs to be discretized in the simulation. It is achieved by using [56]:

$$W(t_i) = \sqrt{\frac{2\pi S_0}{\Delta t}} U_i \tag{3.28}$$

where random variables U_i are normal distributed with zero mean and unit standard deviation. S_0 denotes the white noise power spectral density and time step Δt depends on the maximum natural frequency ω_n of the system. Δt is determined by the following equation:

$$\Delta t < \frac{2\pi}{\omega_n} \times \frac{1}{10} \tag{3.29}$$

Therefore, the equation of motion for the system is renewed as:

$$M\ddot{q}(t) + C\dot{q}(t) + Kq(t) = F(x, \dot{x}, \phi, \dot{\phi}, F_c, I) + T_1 \cdot W_1(t) + T_2 \cdot W_2(t) \tag{3.30}$$

where T_1 and T_2 are transformation matrices, which will put $W_1(t)$ and $W_2(t)$ into bit axial and torsional directions respectively.

3.1.4 Solution for dynamic stresses

From the above section, the equation of motion for the system is given as:

$$M\ddot{q}(t) + C\dot{q}(t) + Kq(t) = F \tag{3.31}$$

where F is the excitation vector including deterministic and random components which are shown in the right-hand-side of Eqn. 3.30. Eqn. 3.31 is valid for any given time instant. Using the central difference method, the acceleration and velocity vectors at time t_i can be written as [57]:

$$\dot{q}_i = \frac{1}{2\Delta t}(q_{i+1} - q_{i-1}) \tag{3.32}$$

$$\ddot{q}_i = \frac{1}{\Delta t^2}(q_{i+1} - 2q_i + q_{i-1}) \tag{3.33}$$

By substituting Eqns. (3.32) and (3.33) into Eqn. 3.31, and rearranging the terms one has[57]:

$$q_{i+1} = \Delta t^2 N_1 F_i + N_2 q_i + N_3 q_{i-1} \tag{3.34}$$

with

$$N_1 = [M + \frac{1}{2}\Delta t C]^{-1} \tag{3.35}$$

$$N_2 = N_1[2M - \Delta t^2 K] \tag{3.36}$$

$$N_3 = N_1[\frac{1}{2}\Delta t C - M] \tag{3.37}$$

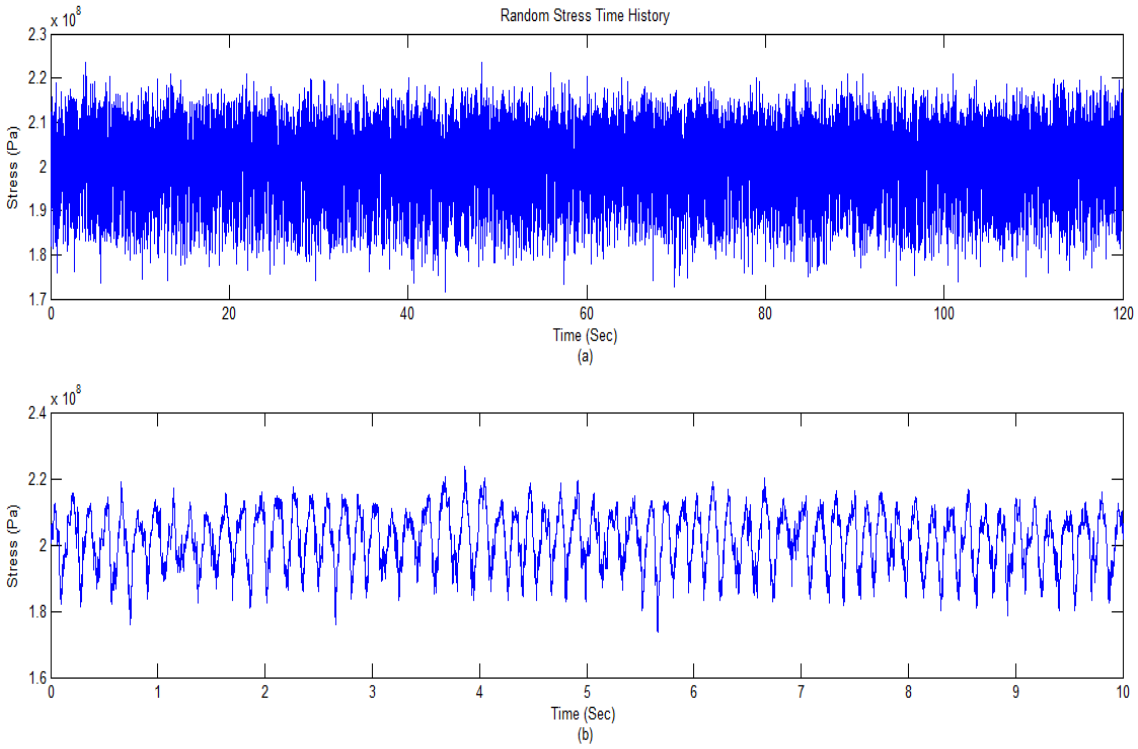

Figure 3.3: Random stress time history of the bottom (30_{th} element) of the drill-string (time interval: 120s, 10s respectively)

M, K, C are all constants at each time step. However, Eqn. 3.32 can not be used directly here to calculate $\dot{q}_i$ because the value of q_{i+1} is unknown. To solve this problem, velocity vectors at time t_i are calculated in terms of:

$$\dot{q}_i = \dot{q}_{i-1} + \ddot{q}_{i-1}\Delta t \tag{3.38}$$

with

$$\ddot{q}_{i-1} = M^{-1}[F_{i-1} - C\dot{q}_{i-1} - Kq_{i-1}] \tag{3.39}$$

Additionally, the torque given by the DC motor (Eqn. 3.27) is given as:

$$T_{rb_i} = K_m n I_i \tag{3.40}$$

$$I_i = \frac{1}{L} \times (2\Delta t V_c - 2\Delta t n K_m \dot{\phi}_{i-1} - 2R_m I_{i-1} \Delta t + L I_{i-2}) \tag{3.41}$$

Once the displacement vector at each time step is obtained, the axial stress σ_u and torsional stress σ_τ for each element are computed as:

$$\sigma_u = E\frac{\Delta u}{l_e} \tag{3.42}$$

$$\sigma_\tau = G\frac{D\Delta\theta}{2l_e} \tag{3.43}$$

where E and G are elasticity and shear modulus of the drill-string, Δu and $\Delta\theta$ are the axial and torsional relative displacements between the two nodes of each element. It should be noted that D is the outer diameter, since the largest torsional shear stress σ_τ is at the outer surface of the drill-string.

For fatigue calculation, a critical equivalent stress is required which combines the axial and torsional stresses. Due to the fact that only axial and torsional directions are considered, the stress state at any location of the drill-string is given by:

$$\begin{bmatrix} \sigma_u & \sigma_\tau & 0 \\ \sigma_\tau & 0 & 0 \\ 0 & 0 & 0 \end{bmatrix} \tag{3.44}$$

The eigenvalues of matrix 3.44 are the principal stresses. Then the critical equivalent stress for fatigue is calculated by the maximum absolute value of these principal

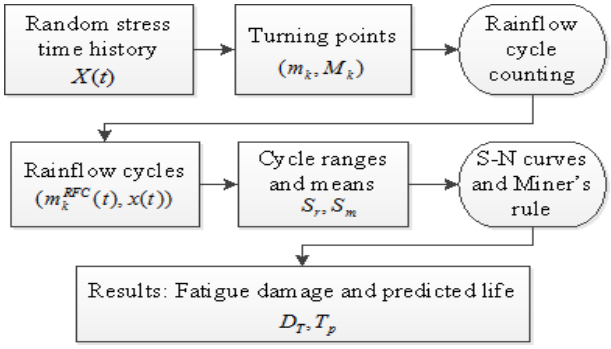

Figure 3.4: Flowchart of fatigue damage calculation

stresses:

$$\begin{bmatrix} \sigma_{p_1} \\ \sigma_{p_2} \\ \sigma_{p_3} \end{bmatrix} = eigenvalues\ of \left\{ \begin{bmatrix} \sigma_u & \sigma_\tau & 0 \\ \sigma_\tau & 0 & 0 \\ 0 & 0 & 0 \end{bmatrix} \right\} \tag{3.45}$$

$$\sigma_{critical} = max(\left|\sigma_{p_1}\right|, \left|\sigma_{p_2}\right|, \left|\sigma_{p_3}\right|) \tag{3.46}$$

By far, the displacements along with the stress values within any position of the drill-string can be obtained under specific excitations. An example of the critical equivalent stress time history of the 30_{th} element (at the bottom of the drill-string) is shown in Fig. 3.1.4, under the condition of rotary speed $\omega = 15 rad/s$ as well as white noise intensity S_0 equal to 4000.

Then the stress data $X(t)$ is saved in an $[n \times 2]$ matrix in which the first column represents the discretized time instants and the second represents the corresponding stress values. This stress matrix will be the basis of fatigue calculations in the following section.

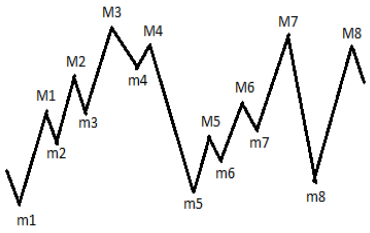

Figure 3.5: Sequence of turning points

3.2 Fatigue calculation

3.2.1 Rainflow Counting Method

In fatigue analysis, the turning points are of great significance, while the curve connecting two adjacent turning points is of no importance [35]. The sequence of turning points in a time history $X(t)$ (an example of turning points is shown in Fig. 3.5) are found out to form a cycle matrix $[n \times 2]$, where the first column records minimums and the second records maximums.

Stress time history in this thesis can also be represented by a sequence of turning points:

$$X(t) = \{m_1, M_1, m_2, M_2, m_3, M_3 \cdots m_k, M_k\}$$

where m_k are minimums and M_k are maximums.

In rainflow counting, for each local maximum M_k, when trying to reach above the same level in the backward (left) and forward (right) directions with an as small downward route as possible, the minimums, m_{k-} and m_{k+} on both sides, are identified (See Fig. 3.6). Then the minimum which has a smaller deviation from the maximum M_k is defined as the corresponding rainflow minimum m_k^{RFC}. This is how the rainflow maximum and minimum are paired. Mathematically, in a stress time history $X(t)$ with finite extremes occurring at a certain time interval $(t_k^+ - t_k^-)$, for the k_{th} maximum

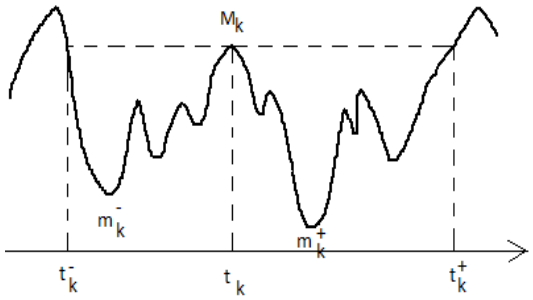

Figure 3.6: Definition of a rainflow cycle (m_k^{RFC}, M_k)

M_k at time t_k, the minimums to the left and the right are [58]:

$$m_k^- = inf\left\{X(t) : t_k^- < t < t_k\right\} \tag{3.47}$$

$$m_k^+ = inf\left\{X(t) : t_k < t < t_k^+\right\} \tag{3.48}$$

where

$$t_k^- = \begin{cases} sup\left\{t \in [0, t_k) : X(t) > X(t_k)\right\}, & if \;\; X(t) > X(t_k) for\ some\ t \in [0, t_k) \\ 0\ , & otherwise \end{cases} \tag{3.49}$$

$$t_k^+ = \begin{cases} sup\left\{t \in (t_k, T] : X(t) > X(t_k)\right\}, & if\ X(t) > X(t_k)\ for\ some\ t \in (t_k, T] \\ T\ , & otherwise \end{cases} \tag{3.50}$$

where T is the length of stress time history $X(t)$. Then, the k_{th} rainflow cycle is defined as (m_k^{RFC}, M_k), where:

$$m_k^{RFC} = \begin{cases} max(m_k^-, m_k^+) & ,if \;\; t_k^+ < T, \\ m_k^- & ,if\ t_k^+ = T. \end{cases} \tag{3.51}$$

The rainflow cycles are obtained by the counting program and saved in a matrix of $[n \times 2]$, denoted by M^{RFC}, where the first column $M^{RFC}(:, 1)$ records RFC minimums

and the second column $M^{RFC}(:,2)$ records RFC maximums. The stress range S_r and mean stress S_m for each rainflow cycle are calculated by:

$$S_r = \left| M^{RFC}(:,1) - M^{RFC}(:,2) \right| \tag{3.52}$$

$$S_m = \left| M^{RFC}(:,1) + M^{RFC}(:,2) \right| /2 \tag{3.53}$$

Given the fact that extremely small cycles have no significant impact on fatigue damage but cause great inconvenience for cycle counting, the stress time history need to be filtered. In Ref. [35, 59] a predetermined threshold h is set to extract all rainflow cycles $(m^{RFC}(t),\ x(t))$ such that $x(t) - m^{RFC}(t) > h$, while the cycles with ranges smaller than h are all removed.

In this thesis, h is set to be 0.02 times of the largest range of $X(t)$: $X_{max}(t) - X_{min}(t)$. This h value is chosen for reducing the calculating time while not affecting the accuracy of the results.

A comparison between an original stress time history and its counterpart after rainflow cycle counting is given in Fig. 3.7. This stress time history is obtained from the bottom (30_{th} position) of the drill-string. It can be found that the extremely small oscillations in the original data are removed.

To better illustrate the effect of rainflow cycle counting, histograms of the stress ranges before and after the counting are given in Fig. 3.8, where the x-axis stands for stress range levels and the y-axis stands for the number of cycles counted. It is clearly seen from part (a), that cycles with small stress ranges are dominant. The cycles with ranges larger than $1 \times 10^7\ Pa$ are much fewer than cycles with ranges smaller than $1 \times 10^7\ Pa$. However, in part (b) where the small oscillations have been removed, the larger cycles stand out.

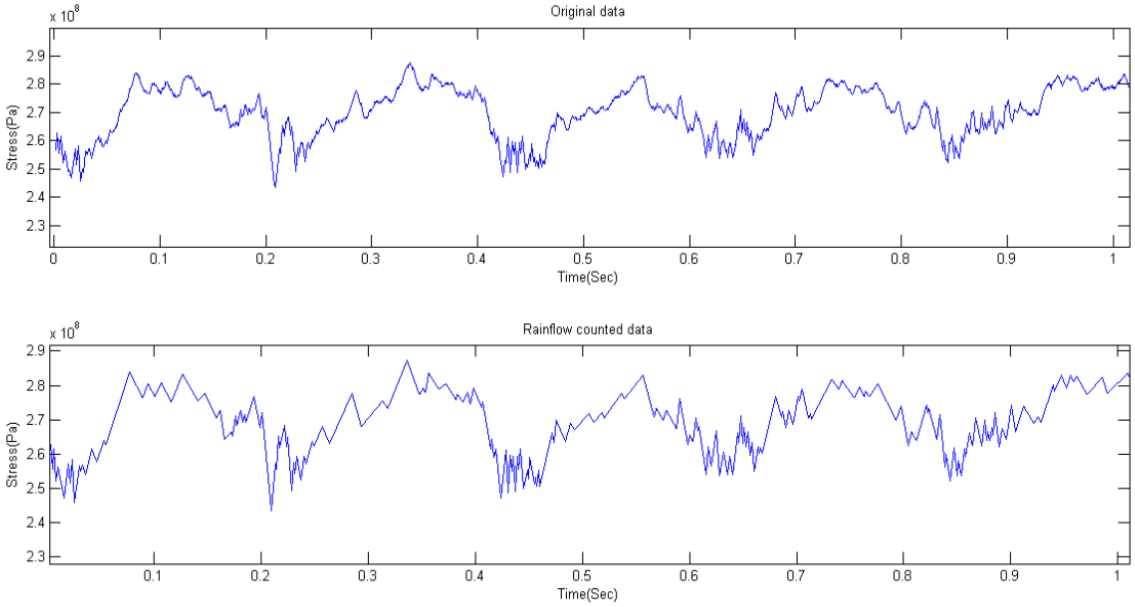

Figure 3.7: Original data and data after rainflow cycle counting

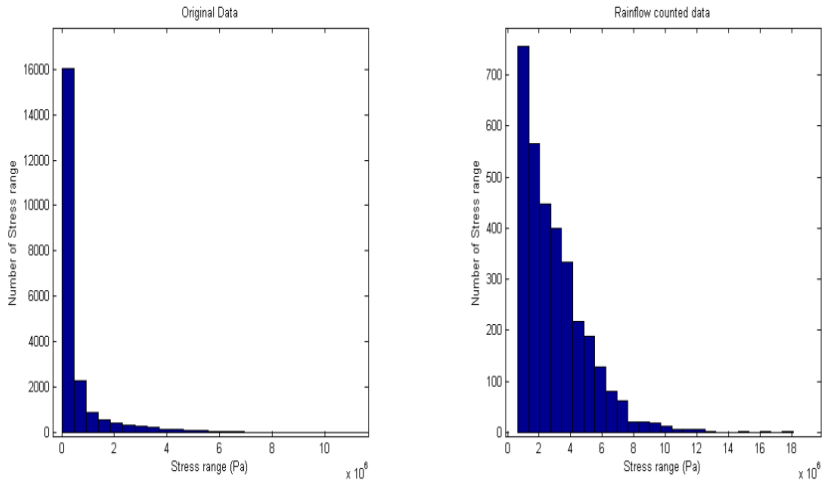

Figure 3.8: Comparison between original data and filtered data

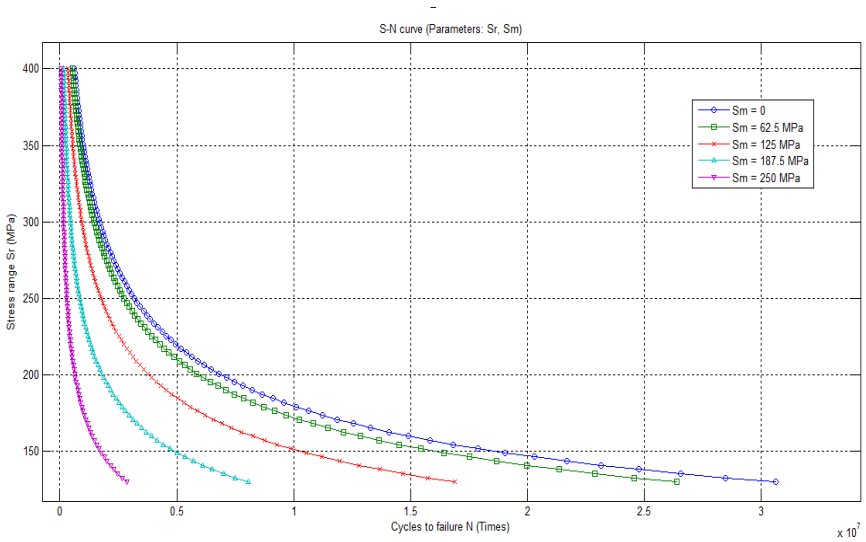

Figure 3.9: S-N model (Parameters: Sr, Sm)

3.2.2 S-N Model

The S-N curve model from Grondin and Kulak[18]'s work is used to estimate drill-pipe fatigue. It is obtained from experimental test accounting for the mean stress effect, which is given by:

$$log_{10}[N(S_r, S_m)] = a + b_1 \times log_{10}(S_r) + b_2 \times (S_m)^2 \tag{3.54}$$

where a, b_1 and b_2 are constants. According to the tests conducted in Grondin and Kulak[18]'s work, they are taking the following values, for full-scale steel drill-pipe: $a = 14.8$, $b_1 = -3.46$, $b_2 = -1.65 \times 10^{-5}$. Several curves with different mean stresses are shown in Fig. 3.9.

3.2.3 Miner's Rule

The Palmgren-Miner linear damage hypothesis is employed to sum up the damage caused by a specific stress cycle. The total damage D_T is given by:

$$D_T = \sum_{i=1}^{k} \frac{1}{N_i} \tag{3.55}$$

where k is the total number of cycles counted from the stress time history and N_i is the number of cycles to failure of the i_{th} cycle. Then the predicted life T_p can be expressed by:

$$T_p = \frac{1}{D_\beta} \tag{3.56}$$

where D_β is the damage intensity, i.e. how much damage is accumulated per unit time:

$$D_\beta = \frac{D_T}{T} \tag{3.57}$$

and T is the length of the stress time history being analyzed.

3.3 Results Analysis

3.3.1 Fatigue Analysis Under Deterministic Excitation

The data used in this chapter are all included in List of Symbols, at the beginning of this thesis. By setting the random component of the excitations to zero, the fatigue under deterministic excitations can be examined. Fig. 3.10 shows the predicted life of the drill-string from the top (Element No.1) to the bottom (Element No.30), under

deterministic excitations. Simulation results with the rotary speed $\omega = 15\ rad/s$, $\omega = 30\ rad/s$ and $\omega = 45\ rad/s$, are given in three sub-plots.

One observation made on those figures is that the fatigue damage at $\omega = 15\ rad/s$ is much bigger than that at $\omega = 30\ rad/s$ and $\omega = 45\ rad/s$. This seems contradictory with common sense. However, the existence of stick-slip phenomenon makes this reasonable. The examination of the dynamic response, which is given in Fig. 3.11 and Fig. 3.12, shows that at low rotary speed $\omega = 15\ rad/s$, stick-slip does happen to the system. When rotary speed increases to $\omega = 30\ rad/s$, the phenomenon disappears.

Therefore, the damage to the fatigue is much severe in the case of slower rotary speed, since stick-slip induces stronger impact on the drill-string. While the rotation speeds up, the drill-string tends to operate more smoothly, with stick-slip reduced. This is verified with that at $\omega = 45\ rad/s$ the life prediction values are generally larger than the counterpart at $\omega = 30\ rad/s$ except several positions.

Another observation is that the drill-string has different fatigue damage at different positions. This is resulted from the diverse values of stress ranges and mean stress at different positions. From Fig. 3.10, it can be seen that the variation of fatigue damage along the drill-string is not monotonous. In order to find the reason for this, the stress time histories for 30 positions with the same rotary speed $\omega = 30\ rad/s$ are examined and depicted in Fig. 3.13. It can be seen that with increase of depth, the stress ranges become larger. However, at deeper position the mean stress level is smaller than that near the top. A lower mean stress level near the bottom is reasonable because the drill-collar part is usually in compression with mean stress level negative. While in the drill-pipe part, mean stress level is positive because of it being

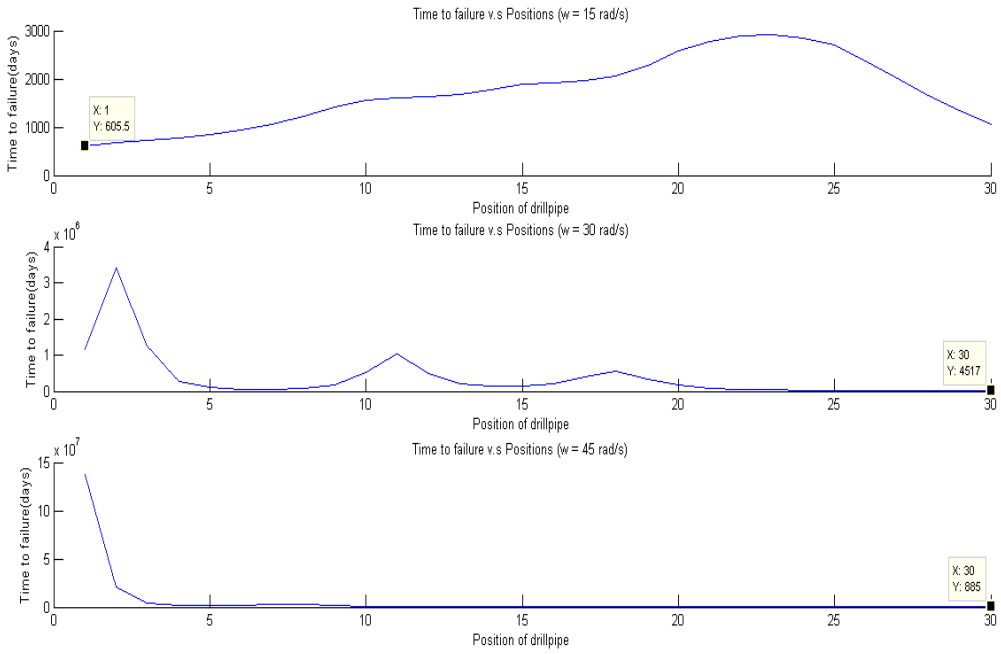

Figure 3.10: Predicted life of the drill-string (Under deterministic excitations)

in tension. The mean stress changes its sign at the neutral point, a position where internal and external forces are balanced, between element No. 23 and 24.

Therefore, a conclusion can be drawn that the fatigue damage comes from two conflicting factors: mean stress and stress range, which results in the fact that the critical point of a drill-string varies at different rotary speed.

3.3.2 Fatigue Analysis of Random Results

By assuming the intensity of $W(t)$ as 4000, the effects of random excitations are examined. The predicted life in this case at $\omega = 15,\ 30,\ 45\ rad/s$ are presented in Fig. 3.14 along with the same deterministic loadings in the previous section. Changes of life prediction values can be observed between Fig. 3.10 and 3.14 while the general

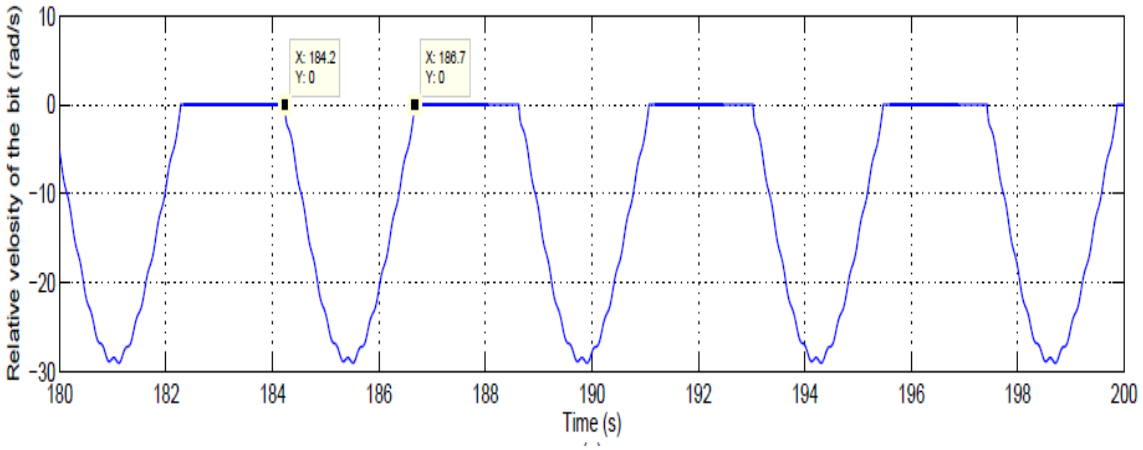

Figure 3.11: Stick-slip phenomenon occurs at low rotary speed $\omega = 15 rad/s$

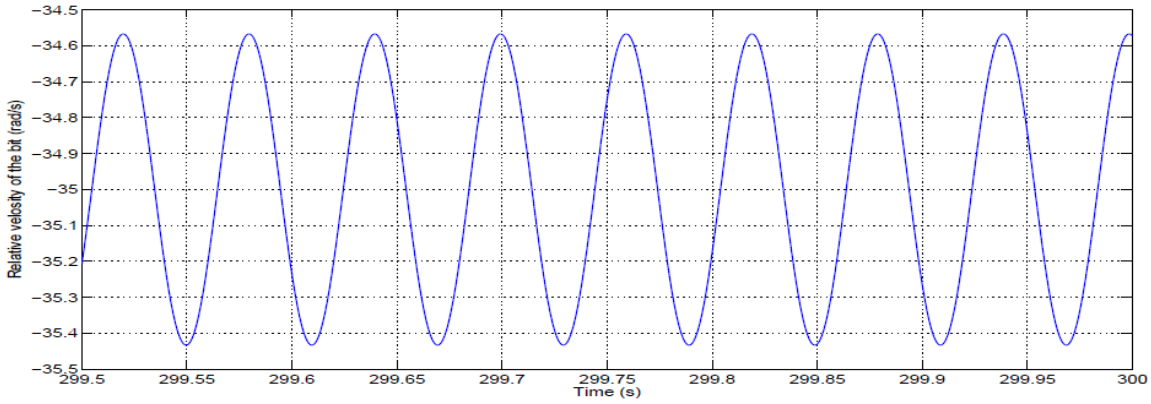

Figure 3.12: Stick-slip phenomenon disappears at rotary speed $\omega = 30 rad/s$

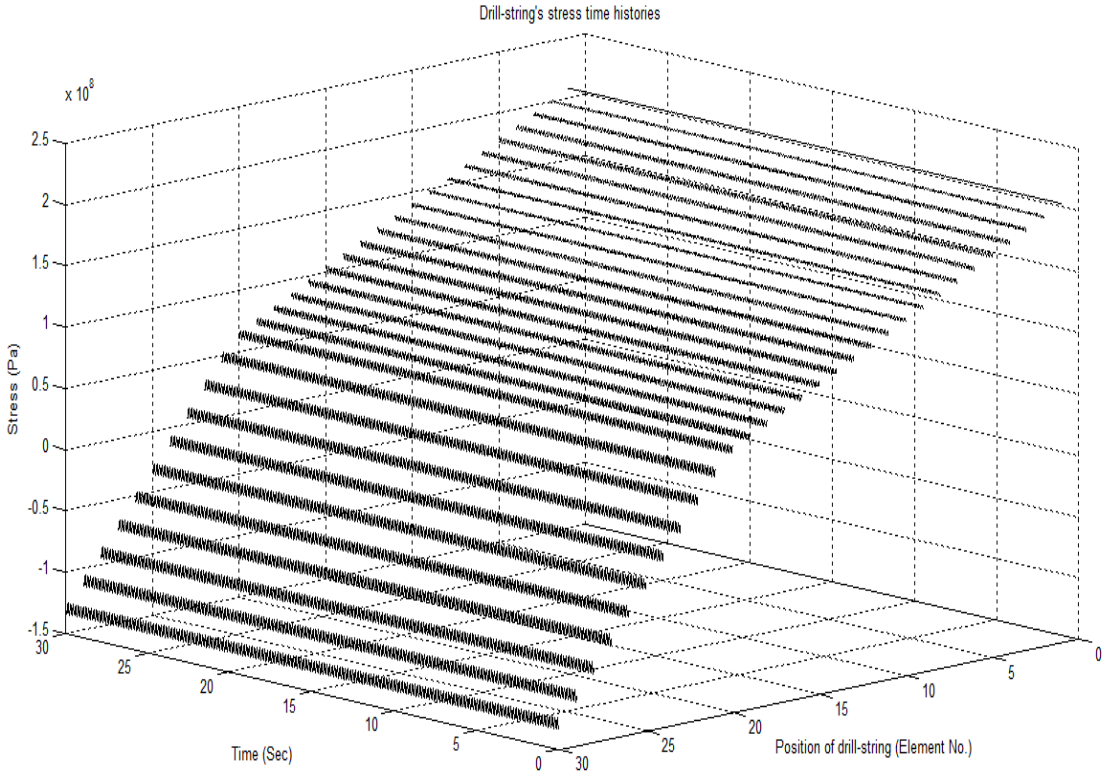

Figure 3.13: Stress time histories of drill-string when $w_d = 30\ rad/s$

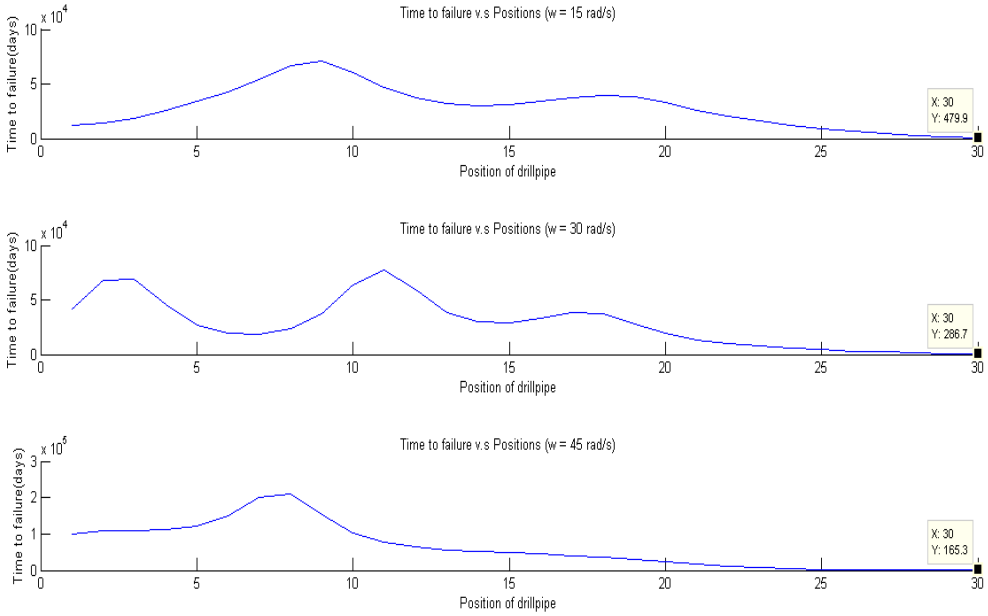

Figure 3.14: Predicted life of the drill-string (Under random excitations)

shapes of the curves do not change. This indicates that random components have no effect on the critical position of a drill-string. However, with random components considered, more severe damage is witnessed, which is believed to be more realistic since in actual drilling operations random loadings are common.

Due to the lack of knowledge of the measurement of the random loadings, no further work is done at this point for this random effect. However, with more knowledge of the random part, there will be no theoretical difficulty in digging deeper into this topic.

3.4 Conclusion

This chapter develops a fatigue life prediction methodology for drill-strings based on linear damage accumulation law and rainflow cycle counting method. The dynamic model accounts for the stress caused by drill-string vibrations, including both deterministic vibration and random vibration. The resulting dynamic stress at different position of the drill-string is obtained by solving the FEM dynamic model. The following conclusions are drawn from this chapter:

1. For analysis under deterministic loadings, stick-slip phenomenon has more severe negative effect on the fatigue life of drill-string, therefore it should be avoided in drilling operation.

2. For analysis under deterministic loadings, the fatigue life increases with the increase of rotary speed. This is because the drill-string tends to operate more smoothly with a larger rotary speed, while stick-slip phenomenon occurs at lower rotary speed.

3. The different life predictions at different position of the drill-string are affected by two factors: mean stress and stress range. Depending on different operational conditions, different critical point of the drill-string may be found.

4. The random excitations have obvious effect on the fatigue life of drill-string. The amount of the effect depends on the intensity and the characteristic of the random excitations.

Chapter 4

Fatigue of Drill-string in the Frequency Domain

4.1 Vibration model

This chapter introduces a fatigue damage calculation method for drill-strings, in the frequency domain. It focuses on damage caused by axial and torsional vibrations. Lateral vibration is again not included because of the complicated coupled vibrations.

4.1.1 Equation of motion

In this chapter, drill-string vibrations are modeled by means of continuous parameter method [60]. Due to the similarity of axial and torsional models, only axial vibration is described explicitly.

According to the continuous modeling method, it is assumed that the drill-string is a straight elastic bar as shown in Fig. 4.1. It accounts for traveling block mass M_d and stiffness of elastic cable and derrick K_d at the surface of the drilling well.

Let x denotes the axial position, and $x = 0$ is set to be at the bottom of the drill-

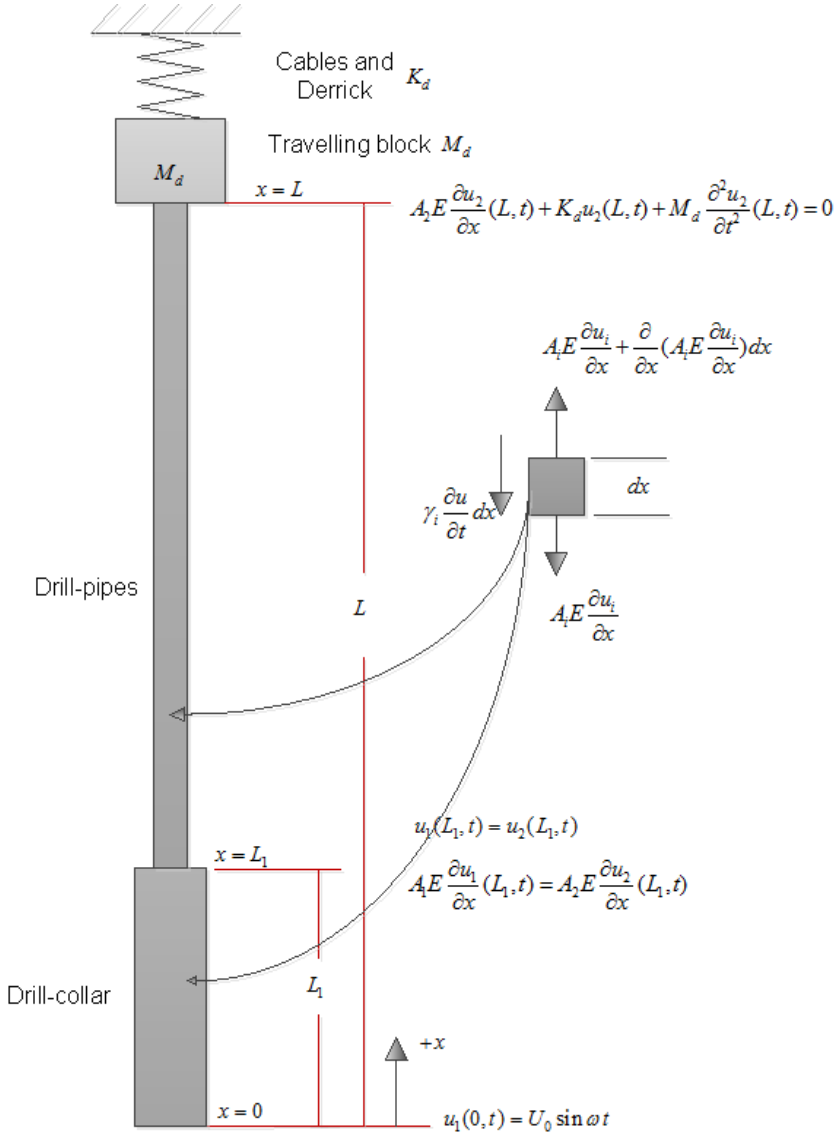

Figure 4.1: Axial vibration model of drill-string

string. According to Newton's second law of motion, the axial equation of motion can be derived from an infinitesimal element $d\tilde{x}$ in the drill-string (See Fig. 4.1):

$$A_i E\frac{\partial^2 \tilde{u}_i(x,t)}{\partial x^2} - \gamma_i \frac{\partial \tilde{u}_i(x,t)}{\partial t} - \rho A_i \frac{\partial^2 \tilde{u}_i(x,t)}{\partial t^2} - (\rho - \rho_{mud})gA_i = 0 \tag{4.1}$$

In the above equation, ρ, E are material density and Young's modulus. γ_i denotes axial viscous damping coefficient and A_i represents the cross section area, where $i = 1, 2$ stands for the drill-pipe section and the drill-collar section respectively. $\tilde{u}_i$ denotes the total axial displacement, which includes static and dynamic displacement: $\tilde{u}_i(x,t) = u_{is}(x) + u_i(x,t)$. Substituting this equation into Eqn. 4.1, the terms of the static stress will be cancelled. Then the dynamic equation of motion is expressed as:

$$A_i E\frac{\partial^2 u_i(x,t)}{\partial x^2} - \gamma_i \frac{\partial u_i(x,t)}{\partial t} - \rho A_i \frac{\partial^2 u_i(x,t)}{\partial t^2} = 0 \tag{4.2}$$

In this chapter, the excitation of the system is assumed to be induced by base motion at the bottom of the drill-string. It is applicable to assume that the base motion $u_b(t)$ is in the longitudinal direction, satisfying:

$$u_i(x,t) = v_i(x,t) + u_b(t) \tag{4.3}$$

where $v_i(x,t)$ denotes the axial displacement relative to the base. Further, from Eqn. 4.3 we also have:

$$\frac{\partial u_i}{\partial t} = \frac{\partial v_i}{\partial t} + \frac{\partial u_b}{\partial t} \tag{4.4}$$

$$\frac{\partial^2 u_i}{\partial t^2} = \frac{\partial^2 v_i}{\partial t^2} + \frac{\partial^2 u_b}{\partial t^2} \tag{4.5}$$

substituting the above two equations into Eqn. 4.2, it yields:

$$\rho A_i \frac{\partial^2 v_i}{\partial t^2} + \gamma_i \frac{\partial v_i}{\partial t} - A_i E \frac{\partial^2 v_i}{\partial x^2} = -\gamma_i \frac{\partial u_b}{\partial t} - \rho A_i \frac{\partial^2 u_b}{\partial t^2} \tag{4.6}$$

where the right-hand side of the above equation denotes the equivalent distributed loading induced by the base motion.

In addition, the base motion is assumed as:

$$u_b(t) = p(t) + w(t) \tag{4.7}$$

where $p(t)$ and $w(t)$ represent the deterministic base motion and random base motion, respectively. These will be described in the following sections.

4.1.2 Galerkin Discretization

Solution to the equation of motion (Eqn. 4.6) can be written by two separate variables, using the Galerkin method [61]:

$$v(x,t) = \sum_{n=1}^{R} X_n(x) p_n(t) \tag{4.8}$$

where R stands for the order of discretization of the equivalent lumped parameter system. $p_n(t)$ are the generalized coordinates, and $X_n(x)$ are the appropriate basis functions satisfying specific boundary conditions, which will be derived in the next two subsections.

4.1.3 Boundary conditions

The boundary conditions at the top, interface between drill-pipe and drill-collar and the bottom are presented as (See Fig. 4.1):

$$Top: \qquad A_2E\frac{\partial u_2}{\partial x}(L,t) + K_d u_2(L,t) + M_d\frac{\partial^2 u_2}{\partial t^2}(L,t) = 0 \tag{4.9}$$

$$Interface: \qquad \begin{cases} A_1E\frac{\partial u_1}{\partial x}(L_1,t) = A_2E\frac{\partial u_2}{\partial x}(L_1,t) \\ u_1(L_1,t) = u_2(L_1,t) \end{cases} \tag{4.10}$$

$$Bottom: \qquad u_1(0,t) = 0 \tag{4.11}$$

where $K_d,\ M_d$ are stiffness of the derrick cable and mass of traveling block. L_1 is the drill-collar section length and L is that of the drill-pipe section.

4.1.4 Basis functions

As mentioned above, the basis functions $X_n(x)$ are the ones which satisfy the model's boundary conditions. In other word, the system's mode shape functions, which are derived from the four boundary conditions, can be used as basis functions.
Mode shapes are solved from free vibration equation of motion:

$$A_iE\frac{\partial^2 v_i(x,t)}{\partial x^2} - \rho A_i\frac{\partial^2 v_i(x,t)}{\partial t^2} = 0 \tag{4.12}$$

it can be assumed that the solution of Eqn. 4.12 is:

$$v_i(x,t) = X_i(x)e^{j\omega t} \tag{4.13}$$

by substituting Eqn. 4.13 into Eqn. 4.12, $X_i(x)$ should satisfy:

$$\frac{d^2X_i(x)}{dx^2} + \lambda^2 X_i(x) = 0 \tag{4.14}$$

where the eigenvalue λ is:

$$\lambda^2 = \frac{\omega^2}{c^2} \tag{4.15}$$

where ω denotes the natural frequency of the drill-string.

The solution to Eqn. 4.14 can be expressed as:

$$X_i(x) = B_i cos\lambda x + C_i sin\lambda x \tag{4.16}$$

where $B_i,\ C_i$ are constants that can be determined by substituting Eqn. 4.16 into the four boundary condition equations (Eqn. 4.9 to 4.11):

$$-B_2\lambda sin\lambda L + C_2\lambda cos\lambda L = \frac{K_d}{EA_2}[\frac{M_d\omega^2}{K_d} - 1](B_2 cos\lambda L + C_2 sin\lambda L) \tag{4.17}$$

$$C_1 cos\lambda L_1 = -\frac{A_2}{A_1}(B_2 sin\lambda L_1 - C_2 cos\lambda L_1) \tag{4.18}$$

$$C_1 sin\lambda L_1 = B_2 cos\lambda L_1 + C_2 sin\lambda L_1 \tag{4.19}$$

$$B_1 = 0 \tag{4.20}$$

the above four equation can be rewritten in a matrix form:

$$\begin{bmatrix} a_{11} & a_{12} & a_{13} \\ a_{21} & a_{22} & a_{23} \\ a_{31} & a_{32} & a_{33} \end{bmatrix} \begin{bmatrix} C_1 \\ B_2 \\ C_2 \end{bmatrix} = \begin{bmatrix} 0 \\ 0 \\ 0 \end{bmatrix} \tag{4.21}$$

the expansion of the square matrix is the charateristic equation, whose roots are the eigenvalues: λ's. Also B_i and C_i values for the drill-pipe and the drill-collar section can be determined. Then, explicit expressions of axial vibration mode shape $X_i(x)$ can be obtained.

For torsional vibration, derivation can be conducted by simply replacing the axial parameters by torsional ones. Details of these parameters are given in Appendix A.

4.1.5 Transfer function

In this section, the transfer function for the drill-string vibration system will be derived. It is a function which establish an input-output relationship of a random vibration system [62] . Again, due to the similarity, only the axial transfer function is derived in detail.

Derivation is conducted by substituting Eqns. 4.8 into Eqn. 4.6, then multiplying both sides of the equation by: $\int_0^{L_2} X_k(x)dx$ (k = 1, 2, ..., R). After simplification the resulting ordinary differential equations (ODEs) of axial vibration are expressed in a matrix form:

$$\ddot{\mathbf{p}}(t) + \Xi\dot{\mathbf{p}}(t) + \Omega^2\mathbf{p}(t) = \tau_{\mathbf{1}}\frac{\partial u_b(t)}{\partial t} + \tau_{\mathbf{2}}\frac{\partial^2 u_b(t)}{\partial t^2} \tag{4.22}$$

where $\mathbf{p}(t)$, $\tau_{\mathbf{1}}$ and $\tau_{\mathbf{2}}$ are R_{th} order column vector. And Ξ, Ω are R_{th} order matrices with components:

$$\Xi_{kj} = -\frac{\gamma}{\rho A}\delta_{kj} \tag{4.23}$$

$$\Omega^2_{kj} = -\frac{E}{\rho}b_{kj} \tag{4.24}$$

in which the parameters are:

$$b_{kj} = \frac{I^{(2)}_{kj}}{I^{(1)}_{kk}} \tag{4.25}$$

$$\tau_{1k} = -\frac{\gamma I^{(3)}_k}{\rho A\ I^{(1)}_{kk}} \tag{4.26}$$

$$\tau_{2k} = -\frac{I^{(3)}_k}{I^{(1)}_{kk}} \tag{4.27}$$

$$I^{(1)}_{kk} = \int_0^L X^2_k(x)dx \tag{4.28}$$

$$I^{(2)}_{kj} = \int_0^L X_k(x)X''_j(x)dx \tag{4.29}$$

$$I_k^{(3)} = \int_0^L X_k(x)dx \tag{4.30}$$

in the above equations, $k,\ j = 1, 2, ..., R$. Also noted that Eqn. 4.22 has been derived using the orthogonality of mode shape functions:

$$\int_0^L X_k(x)X_j(x)dx = I_{kk}^{(1)}\delta_{kj}; \tag{4.31}$$

where δ_{kj} is the Kronecker delta function.

Finally, from the derived linear ODEs as Eqn. 4.22, the transfer function for axial displacement as output is then given as an R_{th} order square matrix. The forms depend on the type of input PSD:

$$Input = acceleration: \qquad \alpha_{A1}(f) = [-f^2\mathbf{I} + if\Xi_A + f^2]^{-1} \tag{4.32}$$

$$Input = velocity: \qquad \alpha_{A2}(f) = i \cdot f \cdot [-f^2\mathbf{I} + if\Xi_A + f^2]^{-1} \tag{4.33}$$

$$Input = displacement: \qquad \alpha_{A3}(f) = f^2 \cdot [-f^2\mathbf{I} + if\Xi_A + f^2]^{-1} \tag{4.34}$$

in which $\mathbf{I}$ is an R_{th} order identity matrix.

Similarly, with axial vibration parameters replaced by torsional ones, the torsional transfer function can also be obtained. The torsional parameters are given in Appendix A at the end of this thesis.

4.2 Random fatigue assessment

4.2.1 Excitation PSD

Refering to equation of motion Eqn. 4.22, the PSDs of the velocity and acceleration of the axial base motion $u_b(t)$ should be determined as input. From references [53, 63], it was recorded that the downhole forces are periodic with a frequency of 3 cycles per

revolution of a tri-cone drill-bit. And it was assumed that the bit displacement as a cosine function with a frequency related to the rotary speed N, given as:

$$u_b = u_0 cos w_c t \tag{4.35}$$

$$w_c = 2\pi f_c = 2\pi \frac{3N}{60} \tag{4.36}$$

where u_0 is the bit displacement amplitude. w_c, f_c represents the frequency of the rotary speed in rad and Hz, respectively.

Thus, it is applicable to assume that the base acceleration $\ddot{u}_b(t)$ has a similar form as displacement. Additionally, random effects are included. Then it can be expressed as:

$$\ddot{u}_b(t) = A_d cos(w_c t) + W(t) \tag{4.37}$$

where A_d is the amplitude of the deterministic dynamic acceleration. $W(t)$ denotes the randomness of the acceleration. It can be assumed that $W(t)$ is a stationary white noise process which has the same PSD levels at all frequencies. Hence, the acceleration's one-sided PSD is expressed as:

$$G_{\ddot{u}_b}(f) = \frac{A_d^2}{2}\delta(f - f_c) + \frac{A_w^2}{2}; \qquad f \in [0, +\infty] \tag{4.38}$$

where A_w is the intensity of random dynamic acceleration. And the velocity and displacement's PSDs can be easily obtained by:

$$G_{\dot{u}_b}(f) = \frac{G_{\ddot{u}_b(t)}(f)}{(2\pi f)^2}; \qquad f \in [0, +\infty] \tag{4.39}$$

$$G_{u_b}(f) = \frac{G_{\ddot{u}_b(t)}(f)}{(2\pi f)^4}; \qquad f \in [0, +\infty] \tag{4.40}$$

where f denotes the frequency in units of Hz.

From downhole measurement [63], it is reported that the axial acceleration can range from 0 to 4 times the gravity acceleration G, while the torsional acceleration ranges from 0 to 200 rad/s^2. In this study, five sets of axial/ torsional excitation PSDs are investigated, which are listed in Table 4.1.

4.2.2 Stress PSD

According to linear random vibration theory and referring to Eqn. 4.22, PSD of axial generalized coordinates $\mathbf{G_p}(f)$ can be obtained by the following input-output relationship [62]:

$$\mathbf{G_p}(f) = \alpha_{\mathbf{A2}}(f)\tau_{\mathbf{1}}{\tau_{\mathbf{1}}}^T G_{\ddot{u_b}}(f){\alpha_{\mathbf{A2}}}^{*T}(f) + \alpha_{\mathbf{A1}}(f)\tau_{\mathbf{2}}{\tau_{\mathbf{2}}}^T G_{\ddot{u_b}}(f){\alpha_{\mathbf{A1}}}^{*T}(f) \tag{4.41}$$

where the * means complex conjugate and $\alpha_{\mathbf{A1}}(f)$, $\alpha_{\mathbf{A2}}(f)$ are the matrix of transfer functions for velociy and acceleration, respectively.

The PSD of relative axial displacement $\mathbf{v}(x,t)$ can be expressed in terms of $\mathbf{G_p}(f)$ by using Eqn. 4.8:

$$G_{\mathbf{v}}(f,x) = \mathbf{X}^T(x)\mathbf{G_p}(f)\mathbf{X}(x) \tag{4.42}$$

Since the contribution of the cross-spectral densities of the generalized coordinates, $G_{p_j p_k}(f),\ G_{q_j q_k}(f),\ j \neq k$, are often negligible, then $G_{\mathbf{v}}$ can be simplified as:

$$G_{\mathbf{v}}(f,x) = \sum_{j=1}^{R} X_j^2(x) G_{p_j p_j}(f) \tag{4.43}$$

The PSD of total axial displacement $\mathbf{u}(t)$ is then given as:

$$G_{\mathbf{u}}(f,x) = G_{\mathbf{v}}(f,x) + G_{u_b}(f) \tag{4.44}$$

To proceed the current drill-string fatigue calculation, the axial and maximum shear stress PSDs are of interest. The axial stress and maximum shear stress at the outer surface of the drill-string are given by:

$$\sigma_{axial}(x,t) = E\frac{\partial u(x,t)}{\partial x} \tag{4.45}$$

$$\sigma_{shear}(x,t) = GR_o\frac{\partial \phi(x,t)}{\partial x} \tag{4.46}$$

where R_o is the outer radius of the drill-string, $\phi(x,t)$ represents the torsional displacement at position x. Again referring to Eqn. 4.8 and taking into account the above two equations, the axial and shear stress PSDs are given by:

$$G_{axial}(f,x) = E^2\sum_{j=1}^{R} X_j'^2(x)G_{p_jp_j}(f) \tag{4.47}$$

$$G_{shear}(f,x) = (GR_o)^2\sum_{j=1}^{R} Y_j'^2(x)G_{q_jq_j}(f) \tag{4.48}$$

where $Y(x)$ is the torsional mode shape function.

4.2.3 Equivalent stress PSD

4.2.3.1 Fatigue failure criterion

In general, the stochastic stress tensor at position x of the drill-string is given by (Fig. 4.2(a)):

$$\sigma(x,t) = \begin{bmatrix} \sigma_{xx}(x,t) & \sigma_{xy}(x,t) & \sigma_{xz}(x,t) \\ \sigma_{yx}(x,t) & \sigma_{yy}(x,t) & \sigma_{yz}(x,t) \\ \sigma_{zx}(x,t) & \sigma_{zy}(x,t) & \sigma_{zz}(x,t) \end{bmatrix} \tag{4.49}$$

Since the drill-string material, steel, is isotropic, the above matrix is symmetric consisting of 6 independent components. Therefore, the stochastic stress tensor can be written as a random process vector $\chi(x,t)$:

$$\chi(x,t) = [\chi_1(x,t), \cdots, \chi_6(x,t)] \tag{4.50}$$

where $\chi_k(x,t) = \sigma_{ij}(x,t)$ with (i, j = x, y, z).

It is known that the total damage of a structure is not just the sum of the individual damage caused by each stress component process. Aiming at getting a uni-axial equivalent stress for fatigue calculation, the fatigue failure criterion based on stress state can be applied.

All random fatigue failure criteria theories are developed in dealing with fatigue damage in time domain except Nieslony and Macha's work [64]. They extended the fatigue failure criteria theory to frequency domain, which is a desired tool for spectral fatigue analysis in this paper.

For elastic-plastic material as drill-string, the criterion of maximum shear stress can be employed [65]. Under this criterion, it is assumed that the critical plane is determined by the mean position of one of two planes in which the maximum shear stress occurs. Mathematically, the equivalent stress at position x in terms of stress components and

critical plane position is then given by:

$$\sigma_{eq}(x,t) = a_1\sigma_{xx}(x,t) + a_2\sigma_{yy}(x,t) + a_3\sigma_{zz}(x,t) + a_4\sigma_{xy}(x,t) + a_5\sigma_{xz}(x,t) + a_6\sigma_{yz}(x,t) \tag{4.51}$$

in this equation:

$$a_1 = l_\eta^2 - l_s^2 \tag{4.52}$$

$$a_2 = m_\eta^2 - m_s^2 \tag{4.53}$$

$$a_3 = n_\eta^2 - n_s^2 \tag{4.54}$$

$$a_4 = 2 \cdot (l_\eta m_\eta - l_s m_s) \tag{4.55}$$

$$a_5 = 2 \cdot (l_\eta n_\eta - l_s n_s) \tag{4.56}$$

$$a_6 = 2 \cdot (m_\eta n_\eta - m_s n_s) \tag{4.57}$$

where l_η , m_η , n_η are directional cosines of the vector normal to the critical plane, and l_s , m_s , n_s are those of the vector tangential to it. Fig. 4.2(b) shows components of an example normal vector η. And Fig. 4.2(c) shows an example critical plane with normal vector $\bar{\eta}$ and one of the many possible corresponding tangential vectors $\bar{s}$. Their values will be found by simulation using the variance method [64] introduced in following subsections.

In the frequency domain, the stress state is described by a stress PSD matrix [66]:

$$\mathbf{G}(\omega;x) = \begin{bmatrix} G_{11}(f,x) & \cdots & G_{16}(f,x) \\ \vdots & \ddots & \vdots \\ G_{61}(f,x) & \cdots & G_{66}(f,x) \end{bmatrix} \tag{4.58}$$

Noted that the diagonal components $G_{kk}(f,x)$ are auto-spectral density of the corresponding stochastic stress component $\chi_k(x,t)$, and $G_{kl}(f;x)$ are cross-spectral density

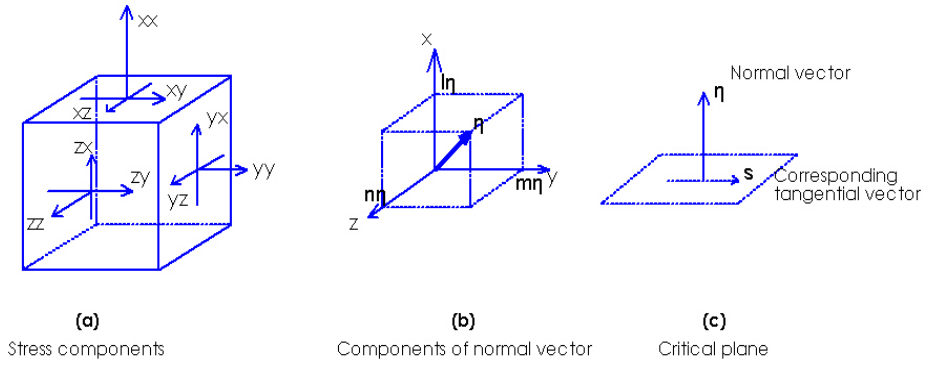

Figure 4.2: Stress components, coordinates and critical plane definition

of $\chi_k(x,t)$ and $\chi_l(x,t)$. Analogically, in spectral analysis the equivalent stress PSD can be determined by taking into account failure criterion Eqn. 4.51. It is given by [64]:

$$G_{\sigma_{eq}}(f,x) = \sum_{k=1}^{6}\sum_{l=1}^{6} a_k a_l G_{kl}(f,x) \tag{4.59}$$

4.2.3.2 Determination of the critical plane position

In this subsection, the variance method is applied to estimate the expected critical plane position. It assumes that the plane in which the equivalent stress' variance reaches its maximum is critical for the material, and the random fatigue failure is expected to occur in this plane. Variance of the equivalent stress is calculated by [64]:

$$\mu_{\sigma_{eq}} = \sum_{k=1}^{6}\sum_{l=1}^{6} a_k a_l \mu_{kl} \tag{4.60}$$

where:

$$\mu_{kl} = Real[\int_0^{\infty} G_{kl}(f,x)df] \tag{4.61}$$

where $G_{kl}(\omega, x)$ are stress component's PSD in Eqn. 4.58. Then a program is made to find the maximum variance using Eqn. 4.60 so that the critical plane is determined.

4.2.3.3 Case study: drill-string

In the current study, only axial and torsional vibrations are considered. As a result, the stress state is uniaxial tension-compression with torsion. The stress tensor (Eqn. 4.49) becomes:

$$\sigma(x,t) = \begin{bmatrix} \sigma_{xx}(x,t) & \sigma_{xy}(x,t) \\ \sigma_{xy}(x,t) & 0 \end{bmatrix} \tag{4.62}$$

According to Eqn. 4.60, the corresponding equivalent stress PSD becomes:

$$G_{\sigma_{eq}}(f,x) = (l_\eta^2 - l_s^2)^2 G_{11}(f,x) + (2 \cdot (l_\eta m_\eta - l_s m_s))^2 G_{44}(f,x) \tag{4.63}$$

where G_{11}, G_{44} are auto-spectral densities of $\chi_1(x,t)$, $\chi_4(x,t)$, which are already obtained by Eqn. 4.47 and Eqn. 4.48. The variance of equivalent stress Eqn. 4.60 becomes:

$$\mu_{\sigma_{eq}} = a_1^2 \mu_{11} + a_4^2 \mu_{44} \tag{4.64}$$

which has established a relationship between stress PSD's variance and the critical plane directional cosines.

In simulation conducted in this thesis, a number of directional cosines of normal vector $(l_\eta,\ m_\eta,\ n_\eta)$ will be generated to describe all possible positions in three-dimensional space as a half sphere. Mathematically, it is restrained by:

$$\sqrt{l_\eta^2 + m_\eta^2 + n_\eta^2} = 1 \tag{4.65}$$

and the tangential vector $\bar{\mathbf{s}}$ $(l_s,\ m_s,\ n_s)$ is restrained by $\bar{\eta} \cdot \bar{\mathbf{s}} = 0$ because of the orthogonality of $\bar{\eta}$ and $\bar{\mathbf{s}}$„ i.e:

$$l_\eta \cdot l_s + m_\eta \cdot m_s + n_\eta \cdot n_s = 0 \tag{4.66}$$

and vector $\bar{\mathbf{s}}$ should also satisfy:

$$\sqrt{l_s^2 + m_s^2 + n_s^2} = 1 \tag{4.67}$$

Under the assumption that $l_\eta \in [0, 1]$ (half of the sphere), the other two directional cosines are given by:

$$m_\eta^2 + n_\eta^2 = 1 - l_\eta^2 \tag{4.68}$$

assuming a single parameter $\theta \in [0, \pi]$, it gives:

$$m_\eta^2 = (sin\theta)^2(1 - l_\eta^2) \tag{4.69}$$

$$n_\eta^2 = (cos\theta)^2(1 - l_\eta^2) \tag{4.70}$$

thus, by setting step length of l_n and θ, all possible positions of normal vector $\bar{\eta}$ can be generated.

For a specific set of (l_η, m_η, n_η), corresponding directional cosines (l_s, m_s, n_s) can be derived combining Eqn. 4.66 and 4.67:

$$\sqrt{[\frac{-(m_\eta m_s + n_\eta n_s)}{l_\eta}]^2 + m_s^2 + n_s^2} = 1 \tag{4.71}$$

assuming $m_s \in [-1, 1]$, all possible (l_s, m_s, n_s) can also be determined.

With the determined critical plane's directional cosines, the resulting equivalent stress PSD ($G_{\sigma_{eq}}$) can be obtained for fatigue calculation use. Fig. 4.7 depicted the equivalent stress PSD under excitation Set No.6 for 9 positions along the drill-string.

4.2.4 Fatigue calculation

The obtained equivalent stress spectra show multiple peaks at different frequencies, as can be seen from Fig. 4.7. The PSD is described by bandwidth parameters. According to the parameter, a spectrum can be qualified as narrow-band or broad-band. Then corresponding spectral method will be chosen to estimate fatigue damage. The below gives the Vanmarcke's bandwidth equation:

$$q = \sqrt{1 - \frac{m_1^2}{m_0 m_2}} \tag{4.72}$$

where spectral moments m_n are defined as:

$$m_n = \int_0^\infty |f|^n \, G_{\sigma_{eq}}(f, x) df \tag{4.73}$$

When bandwidth parameter q approaches 1, the stochastic process can be regarded as broad-band, while it approaches 0 it is regarded as narrow-band.

4.2.4.1 Narrow-band method

However, to investigate the effect of randomness, it is necessary to calculate fatigue life only under deterministic input. For only deterministic excitation, the resulting equivalent stress PSDs are strictly narrow-band, as a pulse function. This kind of stress PSDs are illustrated in Fig. 4.5, under the excitation Set No.1 in Table 4.1. To calculate the fatigue damage caused by narrow-band processes, the narrow-band method [39] can be adopted.

The expected fatigue damage intensity per time unit is given by:

$$E[D^{NB}] = \nu_0 c^{-1} (\sqrt{2m_0})^b \Gamma(1 + b/2) \tag{4.74}$$

where $c,\ b$ are constants of S-N curve which will be given in next subsection. ν_0 is the expected rate of mean up-crossings given by:

$$\nu_0 = \frac{1}{2\pi}\sqrt{\frac{m_2}{m_0}} \tag{4.75}$$

then fatigue life T_F^{NB} is obtained from:

$$T_F^{NB} = \frac{1}{E[D^{NB}]} \tag{4.76}$$

4.2.4.2 Dirlik method

Various spectral methods were proposed to calculate fatigue caused by different random processes. Benasciutti [37] presented analogies and difference of seven different spectral methods for broad-band fatigue. Comparisons of the fatigue damage results showed that Dirlik method [38] and Tovo-Benasciutti method [39] tend to give most accurate fatigue damage estimation, regardless of the shape of the broad-band input process.

Dirlik method is an empirical method which approximates the amplitude distribution of a process under the linear damage accumulation law. It is an improvement of the conventional narrow-band formula [36] by developing a model to estimate the cycle distribution $p_a(s)$, i.e. combining an Exponential and two Rayleigh densities for $p_a(s)$:

$$p^{DK}(s) = \frac{1}{(m_0)^{1/2}}[\frac{D_1}{Q}e^{-\frac{Z}{Q}} + \frac{D_2 Z}{R^2}e^{\frac{Z^2}{2R^2}} + D_3 Z e^{-\frac{Z^2}{2}}] \tag{4.77}$$

where the parameters are:

$$R = \frac{\alpha_2 - x_m - D_1^2}{1-\alpha_2 - D_1 + D_1^2}, \quad D_1 = \frac{2(x_m - \alpha_2^2)}{1+\alpha_2^2}; \quad D_2 = \frac{1-\alpha_2 - D_1 + D_1^2}{1-R},$$

$$D_3 = 1 - D_1 - D_2, \quad Q = \frac{1.25(\alpha_2 - D_3 - (D_2 R))}{D_1}, \quad x_m = \frac{m_1}{m_0}(\frac{m_2}{m_4})^{1/2} \tag{4.78}$$

$$\alpha_2 = \frac{m_2}{\sqrt{m_0 m_4}}$$

Depending on the linear cumulative damage rule, the expected fatigue damage intensity per time unit is calculated by:

$$E[D^{DK}] = \frac{\nu_p}{c} \int_0^{+\infty} s^b p^{DK}(s) ds \tag{4.79}$$

with $p^{DK}(s)$ substituted into the above equation, it gives:

$$E[D^{DK}] = \frac{\nu_p}{c} m_0^{b/2} [D_1 Q^b \Gamma(1+b) + (\sqrt{2})^b \Gamma(1+\frac{b}{2})(D_2 |R|^b) + D_3] \tag{4.80}$$

where ν_p denotes the expected rate of occurrence of peaks:

$$\nu_p = \frac{1}{2\pi}\sqrt{\frac{m_4}{m_2}} \tag{4.81}$$

and b, c are coefficients of the S-N relationship:

$$N(s)s^b = c \tag{4.82}$$

where N and s are cycle to failure and stress amplitude. b, c are positive constants estimated from material experimental test.

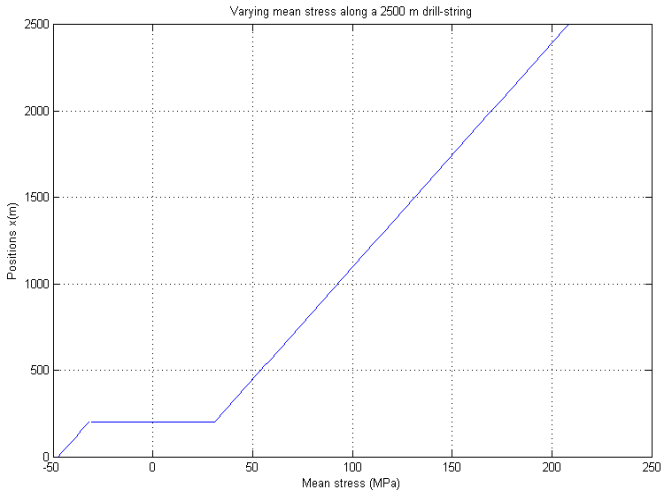

Figure 4.3: Varying mean stress along a 2500 m drill-string

4.2.4.3 S-N curves

In this thesis, S-N relationship from Grondin's experiments [18] is adopted. The experiments were carried out on API Grade E full-scale drill-pipe. Based on the test results, the S-N relationship model considering the effects of both stress range S_r and mean stress S_m is built by:

$$log_{10}\ N = 14.8 - 3.47\ log_{10} S_r - 1.65 \times 10^{-5} (S_m)^2 \tag{4.83}$$

in which mean stress S_m values vary along the drill-string, resulting from the static varying force. The following shows the calculation for the mean stress.

In drilling operation, the drill-string is lowered until the bit touches the bottom of the oil-well. Due to the drill-string's self-weight, hook load, weight on bit and mud hydrostatic force, a spatially varying force caused the initial static deformation of the drill-string. The static forces inside drill-pipe and drill-collar are governed by the

following two equations:

$$F_{pipe}(x) = F_h - \rho A_1 g(L_2 - x) \tag{4.84}$$

$$F_{collar}(x) = \rho A_2 g x - W_s - \rho_{mud} g L_2 A_2 \tag{4.85}$$

where F_h is the hook load, W_s is the static weight on bit. A_1, A_2 denote the cross-section area of drill-collar and drill-pipe respectively. ρ, ρ_{mud} are densities of steel and drilling mud. A diagram demonstrating the resulting static stress against the drill-string's length is depicted in Fig. 4.3. These static stress values are then substituted as mean stress in Eqn. 4.83 to form a group of S-N curves with coefficients b, c calculated, according to Eqn. 4.82. Fig. 4.4 highlights nine S-N curves with different mean stress values along the drill-string.

Finally, based on cumulative damage law that fatigue failure happens when expected damage $E[D^{DK}]$ exceeds 1, the estimated fatigue life T_F is given by:

$$T_F = \frac{1}{E[D^{DK}]} \tag{4.86}$$

4.3 Numerical results and discussions

From the analysis of static forcing equilibrium of the drill-string (Fig. 4.3), it can be seen that the neutral point is located at upper part of the drill-collar. That means the drill-pipe is subjected to tensile load while the drill-collar is in compression. Due to the fact that compressive stress has less contribution than tensile stress on crack growth, the drill-pipe section will be the focus of fatigue estimation.

Six sets of excitation listed in Table 4.1 are investigated in the following subsections.

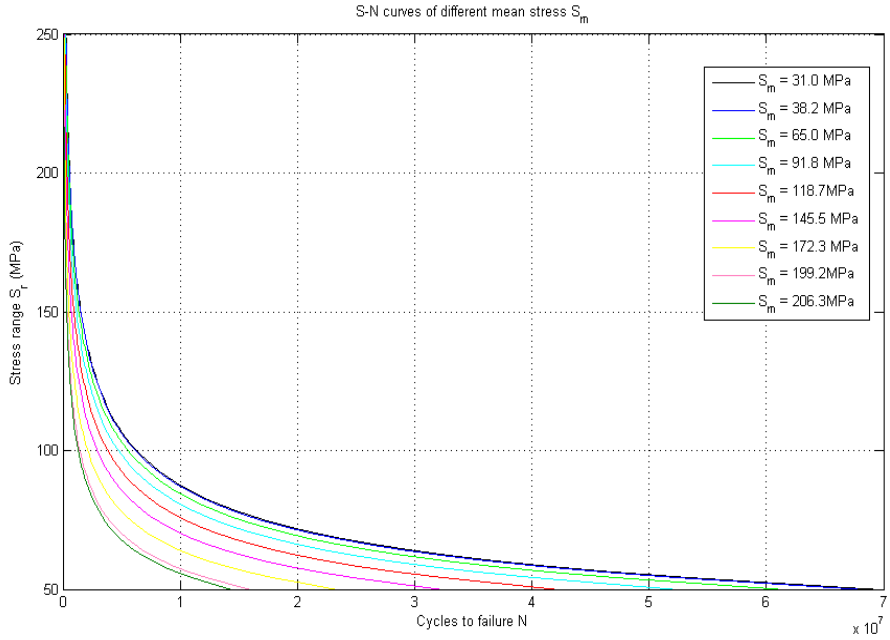

Figure 4.4: S-N curves with different mean stress

Table 4.1: Assumptions of acceleration amplitudes

Set Num.	No.1	No.2	No.3	No.4	No.5	No.6
A_d (axial) (G)	3	3	3	1.5	3	0
A_w (axial) (G)	0	0.3	0.6	0.15	0.3	0.3
A_d (torsional) (rad/s^2)	150	150	150	150	75	0
A_w (torsional) (rad/s^2)	0	15	30	15	7.5	15

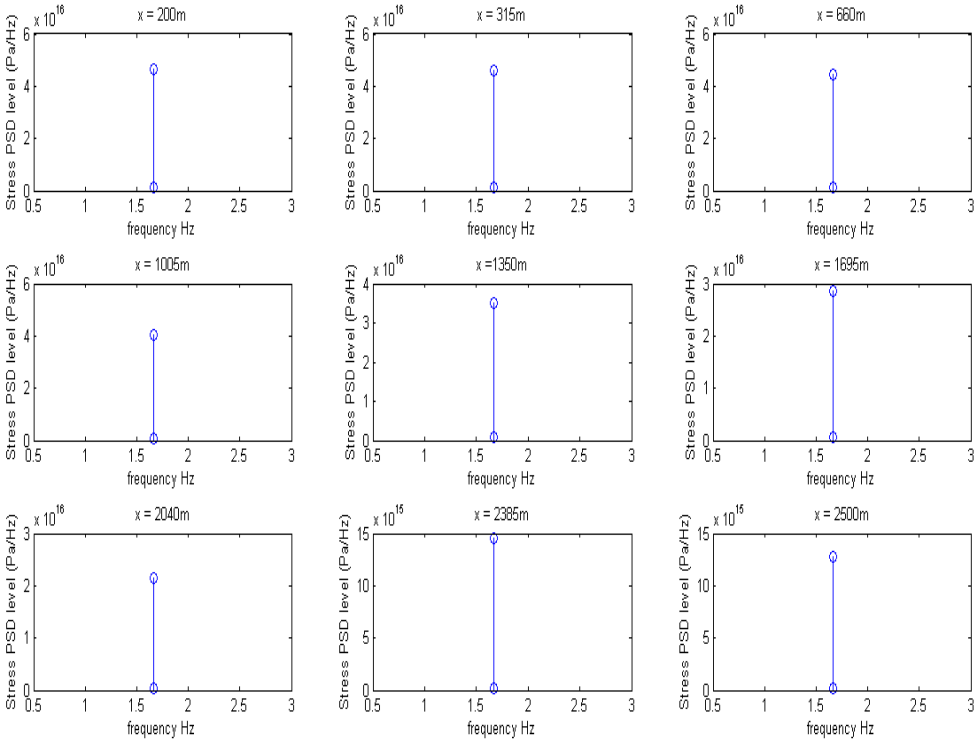

Figure 4.5: Equivalent stress PSD curve under deterministic excitation (Set No.1)

4.3.1 The most damaging position

Firstly, the resulting equivalent stress spectrum of excitation Set No.1, which has deterministic excitation only, is depicted in Fig. 4.5. The corresponding predicted life curve is shown in Fig. 4.6. The maximum peaks of the stress PSD have a monotonous decreasing variation from the bottom to the top of the drill-string. However, the mean stress along the drill-string has a monotonous increasing variation from the bottom to the top. As a result in Fig. 4.6, the predicted life curve is not monotonous, which indicates that fatigue damage is in affected by the combined effect of both its PSD and the mean stress level at a specific position. This explains why the most damaging position is located in the middle of the drill-string, not the bottom or the top.

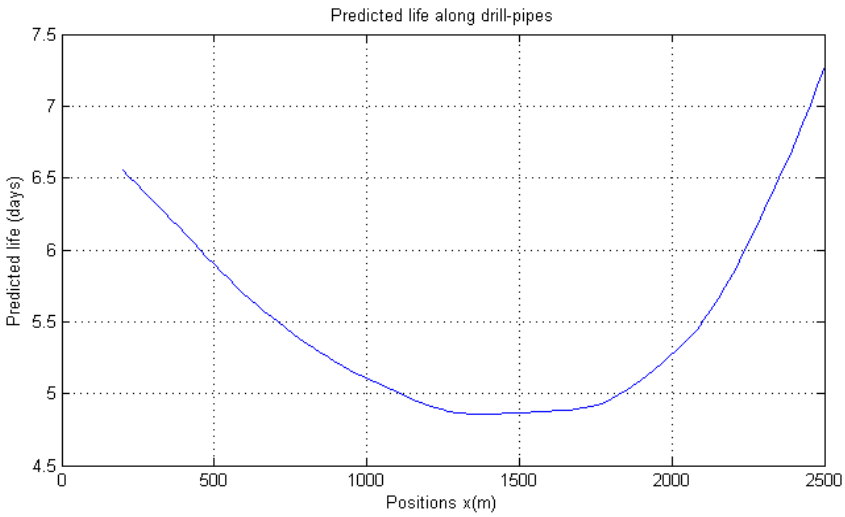

Figure 4.6: Predicted life curve under deterministic excitation (Set No.1)

Then, the resulting equivalent stress spectrum of Set No.6, which has only random excitation, is shown in Fig. 4.7. The corresponding predicted life curve is illustrated in Fig. 4.8. It is found that near the pipe-collar interface, random excitation affects the fatigue life most dramatically. One can refer to the stress PSD in Fig. 4.7, which indicates that near pipe-collar interface, equivalent stress PSD has the largest peaks, and stress PSD levels in high frequencies are more obvious than those at other positions.

Finally, the resulting predicted life curve from Set No.2, which includes both deterministic and random excitations, is illustrated in Fig. 4.9. Fluctuation along the drill-string is found and the most damaging position is spotted at the middle of the drill-string (near x= 1300m).

It can be concluded from the comparison among Fig. 4.6, 4.8 and 4.9 that the fatigue

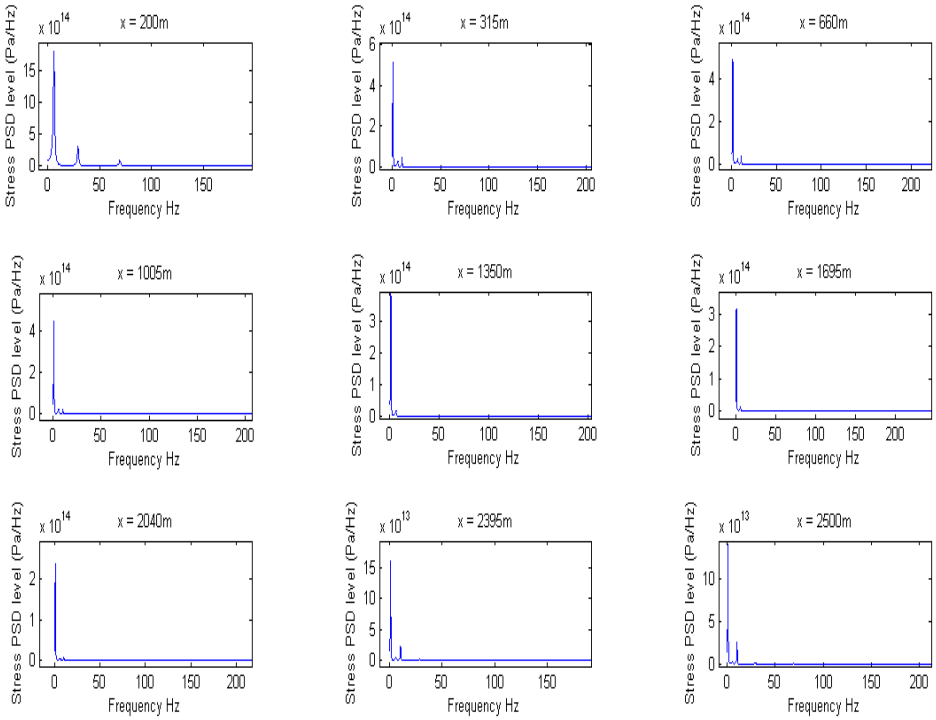

Figure 4.7: Equivalent stress PSD curve under random excitation (Set No.6)

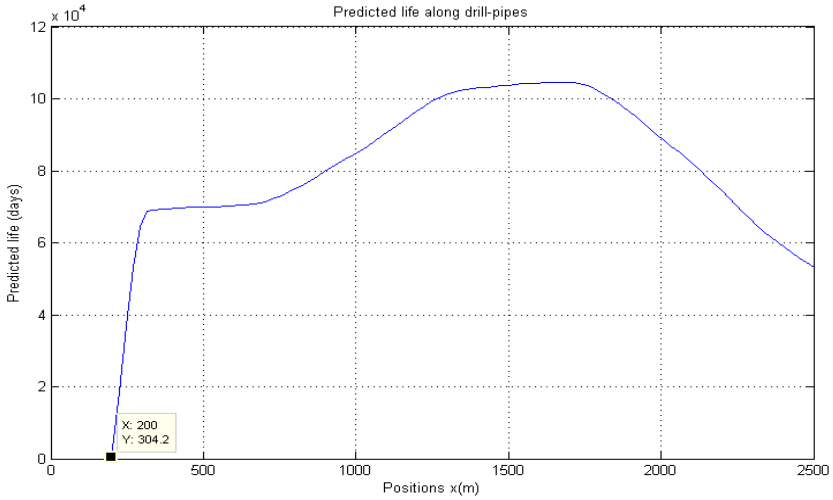

Figure 4.8: Predicted life curve under random excitation (Set No.6)

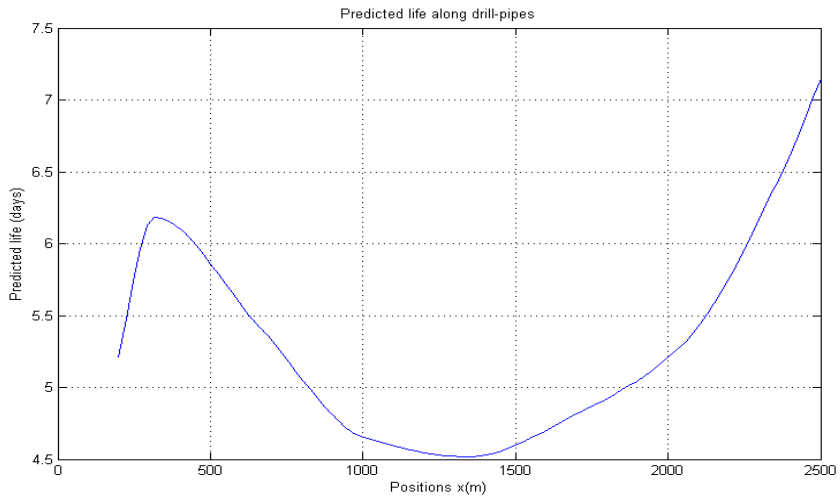

Figure 4.9: Predicted life curve under both deterministic and random excitation (Set No.2)

damage of each position is affected by combined effects of three factors: 1. The deterministic part of excitation; 2. The random part of the excitation; and 3. The mean stress level. The comparison also indicates that random excitation affects the fatigue damage near pipe-collar interface more than the other positions. And deterministic excitation dominates the influence of the whole drill-string's fatigue damage since the shapes of Fig. 4.6 and 4.9 are almost the same.

4.3.2 Effects of random excitation

The second comparison is among excitation Set No.1, No.2 and No.3, to figure out the effects from randomness. Set No.1 only contains deterministic excitation, while random excitation are added in both axial and torsional vibrations under Set No.2 and No.3. In Set No.2 the intensity of randomness is assumed as 10% of the amplitude of deterministic excitation, while in Set No.3 the intensity is assumed as 20%.

Life time prediction curves along the drill-pipe section under these three sets are depicted in Fig. 4.10. As can be seen in the figure, the shape of the curve changes with randomness included. This will be explained in the following section.

It can also be seen that shorter life time values are given with more intensive randomness added. When the intensity of randomness is 10% (Set No.2), the predicted life values decrease from results of Set No.1 by 0.5% to 6% at most positions. And at the position near collar-pipe interface, the largest decrease is witnessed by 26%.

Under the random intensity of 20% (Set No.3), the life predictions drop by 5% to 9% from the predictions under only deterministic excitation (Set No.1) for most positions. And the largest gap is again found near the collar-pipe interface, giving a 53% decrease of life time.

From the results above, it can be noted that randomness has a vital influence on fatigue damage, severer damage may occur with the same increase of random excitation. Hence, it is of importance to record more realistic PSD data from the down-hole, in order to reach a more reliable life prediction.

4.3.3 Effects from axial/ torsional excitation

The equivalent stress spectrum is a linear combination of stress components (Eqn. 4.63). It means that axial and shear stress spectra have different influences on the predicted fatigue life. To evaluate the effects from axial and torsional excitations, excitation Set No.2, No.4 and No.5 listed in Table 5.3 are investigated.

In Set No.4 the axial excitation are assumed as half of that in Set No.2, while in Set

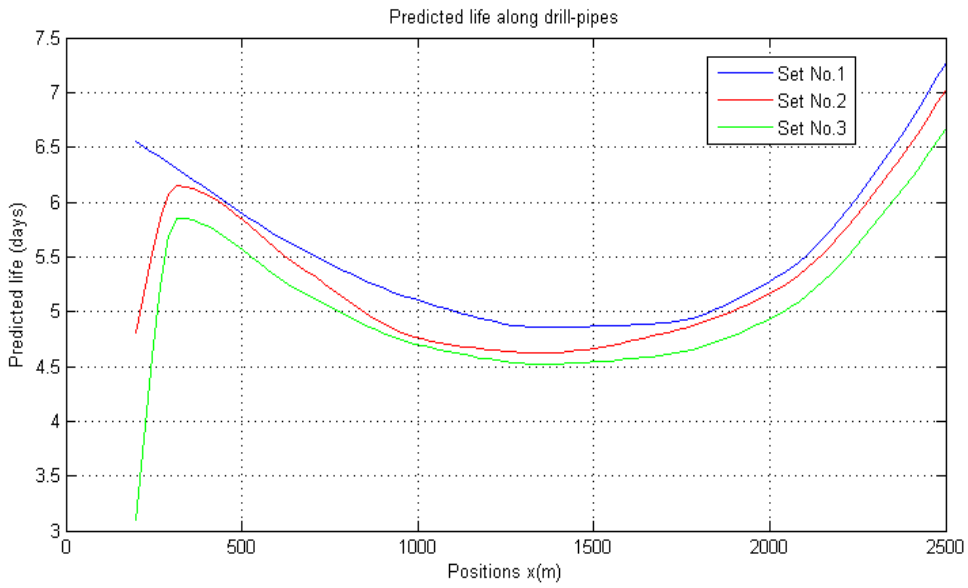

Figure 4.10: Predicted life for drill-pipe section (Under excitation Set No.1, No.2, No.3)

No.5 the torsional excitation are assumed as half of that in Set. No.2. The corresponding resulting life predictions are illustrated in Fig. 4.11.

With the decrease of either axial or torsional excitation, it is reasonable that corresponding life time prediction becomes longer, as all values from Set No.4 and No.5 are smaller than that of Set No.2.

It should be noted that torsional vibration affects the fatigue damage more than axial vibration, which can be seen from Fig. 4.11 that a maximum 27% of life time increase is witnessed when the axial input is reduced by half. While about 220% of life time increase is found at most positions when the torsional input is reduced by half. This is because the torsional stress PSD is the dominant part of the equivalent stress PSD, compared to axial stress PSD.

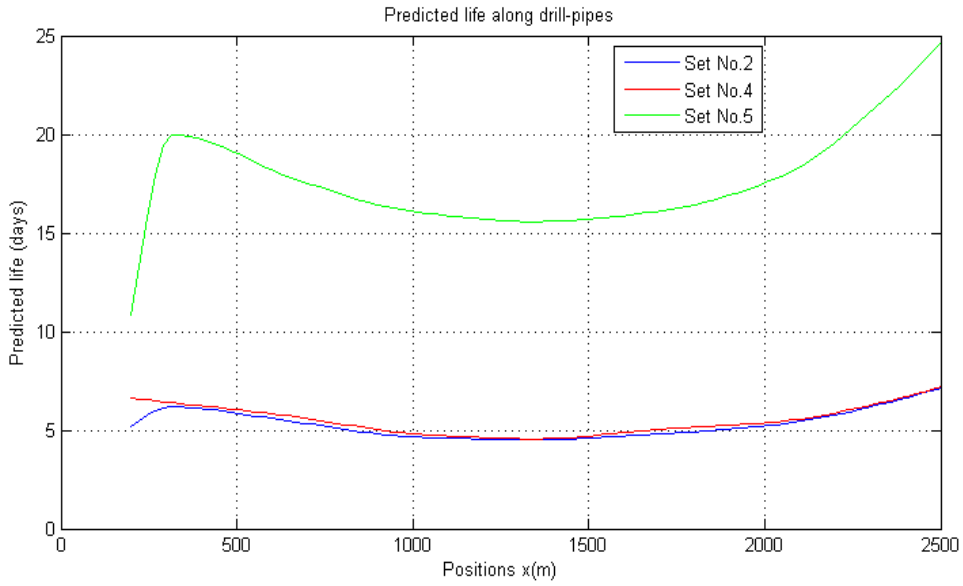

Figure 4.11: Predicted life for drill-pipe section (Under excitation Set No.2, No.4 and No.5)

Thus, torsional vibration should be paid more attention to during drilling operations.

4.4 Conclusion

A spectral method is proposed to estimate the fatigue life of a drill-string in frequency domain. One benefit of this method is that fatigue life can be obtained without solving the dynamic equations of the drill-string system. Another advantage is that this method is more applicable in cases including random loadings. It can significantly reduce the calculating time, compared with fatigue calculation methods by cycle counting method in time domain.

Further, the fatigue damage due to the combination of deterministic and random excitations is investigated. Results show random vibration has an intensive effect on

the fatigue life of the drill-string.

The predicted life of the drill-string is affected by the combined influence of three factors: 1. The deterministic part of excitation; 2. The random part of the excitation; and 3. The mean stress level. This fact results in a fluctuating life time prediction curve.

Chapter 5

Fatigue of Pipe Threaded Connection for Casing Drilling

Casing while drilling (CWD), as introduced in Chapter 1.2.2.3, is an emerging technology and a process for simultaneously drilling and casing a well. Pipe connections for casing drilling are weak points which must be carefully evaluated for any Casing Drilling program. This Chapter investigates the fatigue of threaded connections due to random vibrations in CWD.

5.1 Finite Element Model

In this chapter, the fatigue of the local structure of the drilling case - threaded connection, is investigated. Firstly, static stress analysis is conducted, which is to model the initial condition of the threaded connection when the drill-string is lowered into the oil-well before operating drilling. Finite element method via ANSYS is an effective way to model the threaded connection.

The following settings are included in the finite element model based on the actual

Table 5.1: Dimensions of pin, box and thread

Pin (in)	L1	L2	L3	L4	WT	r1 (°)	D	d
	0.844	1.300	4.000	1.734	0.125	6	4.500	4.070
Box (in)	NL	b	q	W	Q	r2 (°)		
	2.250	0.303	0.4920	5.200	4.594	36		
Thread (in)	p	H	$h_s = h_n$	$f_{rs} = f_{rm}$	$f_{cs} = f_{cm}$			
	1.250	0.1082	0.0950	0.0041	0.0091			

condition of threaded connection: 1. linear elastic material 2. thread large deformation on 3. interaction between the threads of pin and box.

As discussed in Chapter 1, 2-D axisymmetric finite element model is effective to model threaded connections, which can both give accurate results and reduce calculating time. In this thesis, a standard 4.5" API line pipe connection will be generated and analyzed to gain fatigue damage under random loading.

5.1.1 Geometry

According to reference [67], the material type of the threaded connection can be assumed as a linear elastic structural steel. Its Young's modulus is 208 GPa, and Poisson coefficient is 0.3.

The 2-D axisymmetric model contains three parts: pin 1, box and pin 2. Contact pairs exist between pin 1- box and pin 2 -box. The basic geometries of the pin and half of the box are depicted in Fig. 5.1 and 5.2 respectively. Details of the threads which will be constructed on the pitch lines of the pin and the box are shown in Fig. 5.3. According to API specification standard 5B and 5L [68, 67], the dimensions of the model are listed in Table 5.1.

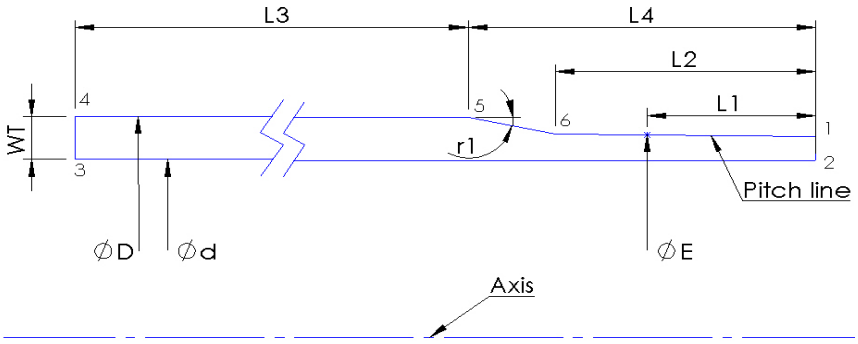

Figure 5.1: Pin geometry

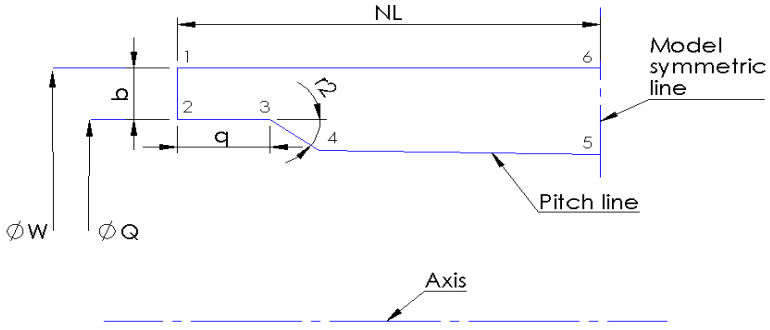

Figure 5.2: Box geometry

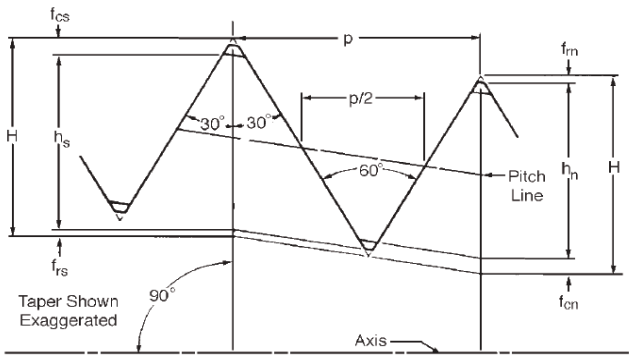

Figure 5.3: Thread geometry [68]

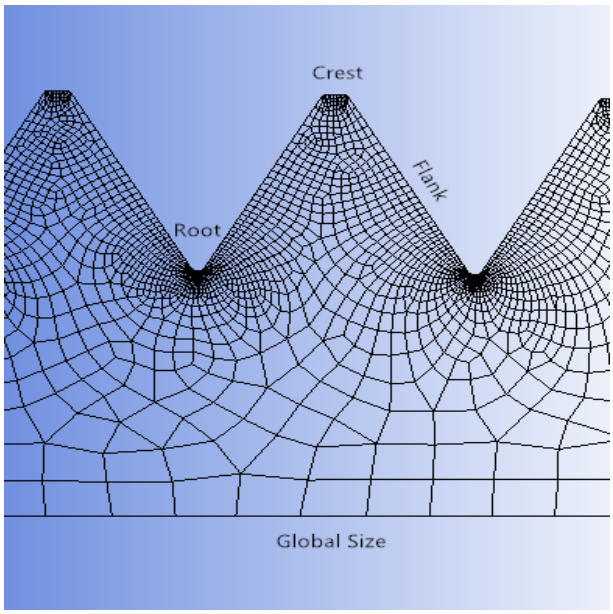

Figure 5.4: Thread mesh

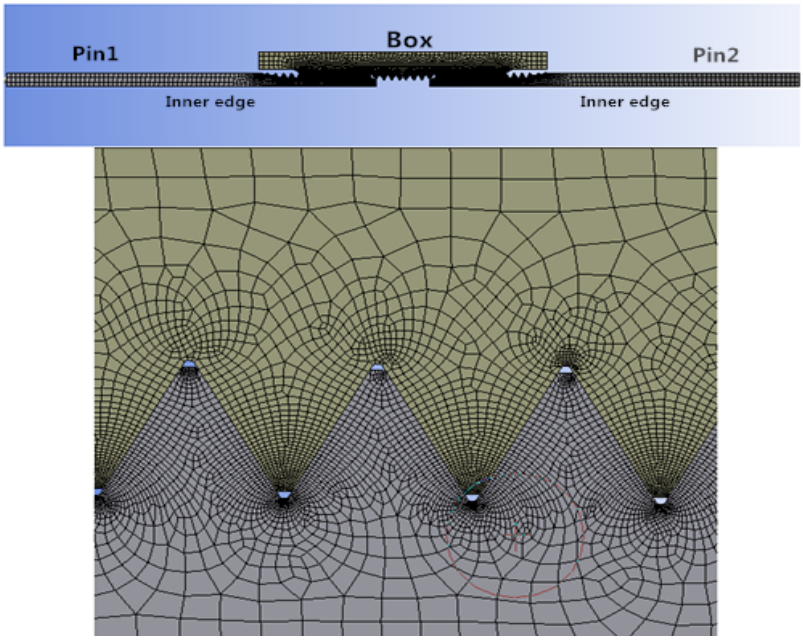

Figure 5.5: Mesh of the threaded connection

5.1.2 Mesh strategy

Rich literatures have been dealt with stress analysis on the threaded connection via both test and simulation [33, 34, 32]. One common finding of these researches is that the critical position of the threaded connection will be the root of the last engaged thread (LET) of the pin, which tends to suffer from highest stress level. In addition, the stress gradient at the root of the thread is relatively larger than the other positions of the threaded connection. Therefore, fine mesh should be applied to the roots of the threads, in order to obtain accurate results. In contrast, coarse mesh will be adequate in other regions where stress values have relatively low gradients.

Mesh optimization studies have been carried out by previous researchers. In this paper, meshing strategy is similar as the meshing method in [30]. Four parameters can

Table 5.2: Mesh sizes of the model

Pin (in)	Global	Root	Crest	Flank elements
	WT / 6 = 0.0358	0.00358	0.00179	35
Box (in)	Global	Root	Crest	Flank elements
	0.0358	0.0007	0.0035	35

sufficiently control the mesh of each of the three parts in the model. They are specified in Fig. 5.4. As discussed above, the element size at the roots is the finest, while the element size at the thread crests is coarser. And the thread flanks are divided by 35 elements with a biased sizing ratio equal to 5. This factor is related to the ratio between the crest size and root size. Besides, due to the fact that the pin serves as a master part and the box serves as a slave part of the contact pair, the box can have coarser mesh than the pins.

To avoid the convergent problem of ANSYS simulation, one suggestion is to generate the mesh in the contact regions with nearly identical element size.

With the above considerations and the mesh values listed in Table 5.2, the mesh diagram is generated in Fig. 5.5. As a result, the whole model contains 35920 elements.

5.2 Static stress analysis

5.2.1 Tensile stress

In drilling operations, the drill-string is lowered into the oil-well in order to reach the bottom, as shown in Fig. 5.6. Due to the drill-string's self-weight, hook load, hydrostatic force and weight on bit, ideally the drill-string is under a static stress state. It is assumed that these forces are only acting in the longitudinal direction, which

then cause the initial longitudinal deformation of the drill-string. Hence, the varying static stress inside drill-pipes and drill-collars can be calculated by the following two equations:

$$\sigma_{pipe}(x) = [F_h - \rho A_p g(L - x)]/A_p \tag{5.1}$$

$$\sigma_{collar}(x) = [\rho A_c g x - W_s - \rho_{mud} g L A_c]/A_c \tag{5.2}$$

where x represents the location in the drill-string, hook load F_h, static weight on bit W_s. A_c, A_p denote the cross-section area of drill-collar and drill-pipe respectively. ρ, ρ_{mud} represents densities of steel and drilling mud, respectively. These above two equations are similar to Eqn. 4.84 and 4.85, which give the axial load of the drill-string.

A diagram demonstrating this varying static force against the drill-string's length is depicted in Fig. 4.3. Due to the fact that the whole length of the threaded connection is relatively small compared to the whole drill-string, the forces at the two ends of the threaded connection are considered to have the same value, for each specific location.

As can be seen on Fig. 4.3, the drill-pipe section is in tension. In ANSYS workbench, these tensile forces are set as pre-loads of the springs attached to the two ends of the connection. Description of springs is in subsection: "boundary conditions".

5.2.2 Contact

Drill-strings are made up of numbers of drill-pipes which are linked together by threaded connections. Before being put into use, the pin and the box should be tightened via the threads, which is called "make-up" step. In the current study, the pin and the box geometries have been developed to be in the make-up state. The make-up turns can be simulated by a initial interference between the contact region

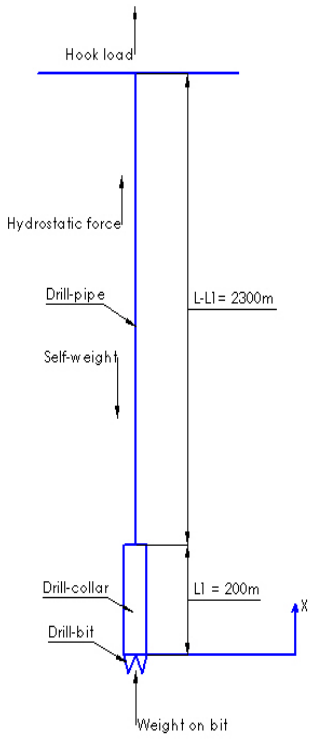

Figure 5.6: Static forces of a drill-string

of the pin and the box [54], which is to secure the tightness of the two parts. The initial interference δ is related to the make-up turns t, which is given by [30]:

$$\delta = t \cdot P \cdot tan(\alpha) \tag{5.3}$$

where P denotes the thread pitch and the taper angle α is set as 0.0625° [68]. The number of make-up turns can be in the range of 1 to 2 turns [68], here it is assumed as 2 turns, resulting in $\delta = 0.15625\ in.$

In addition, under tensile loads the pin and the box may experience friction between the threads. The current model accounts for friction by setting the contact type in ANSYS as "frictional". As for the setting of coefficient of friction (COF), different researchers have used various values ranging from 0.02- 0.20. In the current study, a 0.12 COF is set which lies in the ISO 10407-1 range of 0.06- 0.14.

5.2.3 Boundary conditions

In the current study, vibration effects will be considered as a contribution to fatigue. Therefore, the boundary conditions of the threaded connection are modeled by two equivalent springs, in representing of the drill-pipes linked to the two ends of the threaded connection in a specific location.

The stiffness value K of the equivalent spring in drill-pipe section depends on the length of the linked drill-pipes. Assuming the drill-string is in vertical position, then the upper and the lower equivalent springs attached to the threaded connection at a

Table 5.3: Stiffness values of equivalent springs linked to the threaded connection

Locations x (m)	300	700	1100	1500	1900	2300
Upper spring ($10^6 N/m$)	2.635	3.220	4.140	5.796	9.660	28.980
Lower spring ($10^6 N/m$)	14.567	7.264	4.839	3.627	2.901	2.417

specific location x can be calculated by:

$$K_{upper} = K_{pipe}|_{(L-x)} \tag{5.4}$$

$$K_{lower} = 1/(\frac{1}{K_{collar}} + \frac{1}{K_{pipe}|_{(x-L_1)}}) \tag{5.5}$$

where K_{collar} is a constant denoting the equivalent stiffness of the drill-collar section. And K_{pipe} is a function of x, where the thread connection locates. They are given by:

$$K_{collar} = \frac{A_c \cdot E}{L_1} \tag{5.6}$$

$$K_{pipe}|_x = \frac{A_p \cdot E}{x} \tag{5.7}$$

where x denotes the location of the threaded connection. Example for stiffness values of six different locations, are listed in Table 5.3.

In ANSYS workbench, this kind of boundary condition can be characterized as "connection-spring" at the two ends of the model. The spring attached to the lower end of the threaded connection links it with the ground, while the upper one links it with the top of the drill-string.

In addition, frictionless supports are assumed at the inner edges of the two pins (See Fig. 5.5). This constrains the model's motion to act only in the longitudinal direction, since the scope of the current study is only the axial motion.

5.2.4 Analysis on static stress analysis

The ANSYS simulation in the current study contains two loading steps: Step 1- make up, which sets the initial interference between the threads of pin and box; Step 2- tensile load, which simulates the internal static loadings added to the two ends of the threaded connection. Belows will show the static stress results for the threaded connection at the location of $x = 1500m$. The longitudinal stress, the radial stress as well as the hoop stress of the model for the two loading steps are shown in Fig. 5.7 and 5.8.

Stresses after Step 1 are shown in Fig. 5.7. Several phenomena are found:

1. Axial stress at the root of the LET of the two pins is the highest while the center part of the pin has compressive stresses. Different from previous research works, it is found that a high axial stress exists at the root of the pin's run-out region. This is the consequence of the pin's bending during make-up step.

2. Due to this bending, from outside the box's wall to the box's threads, stress changes from tensile to compressive.

3. Radial stress has relatively small value compared to axial and hoop stress, since no restrain is assumed to the right-hand side of the box.

4. Hoop stress in the pins is compressive while in the box it is tensile. This is because the pins serves as master part of the contact pair, which is forced to move toward the box. Thus, the pins are compressed while the box expands in the z direction.

5. Equivalent stress of the box are generally high mainly due to the large hoop stress.

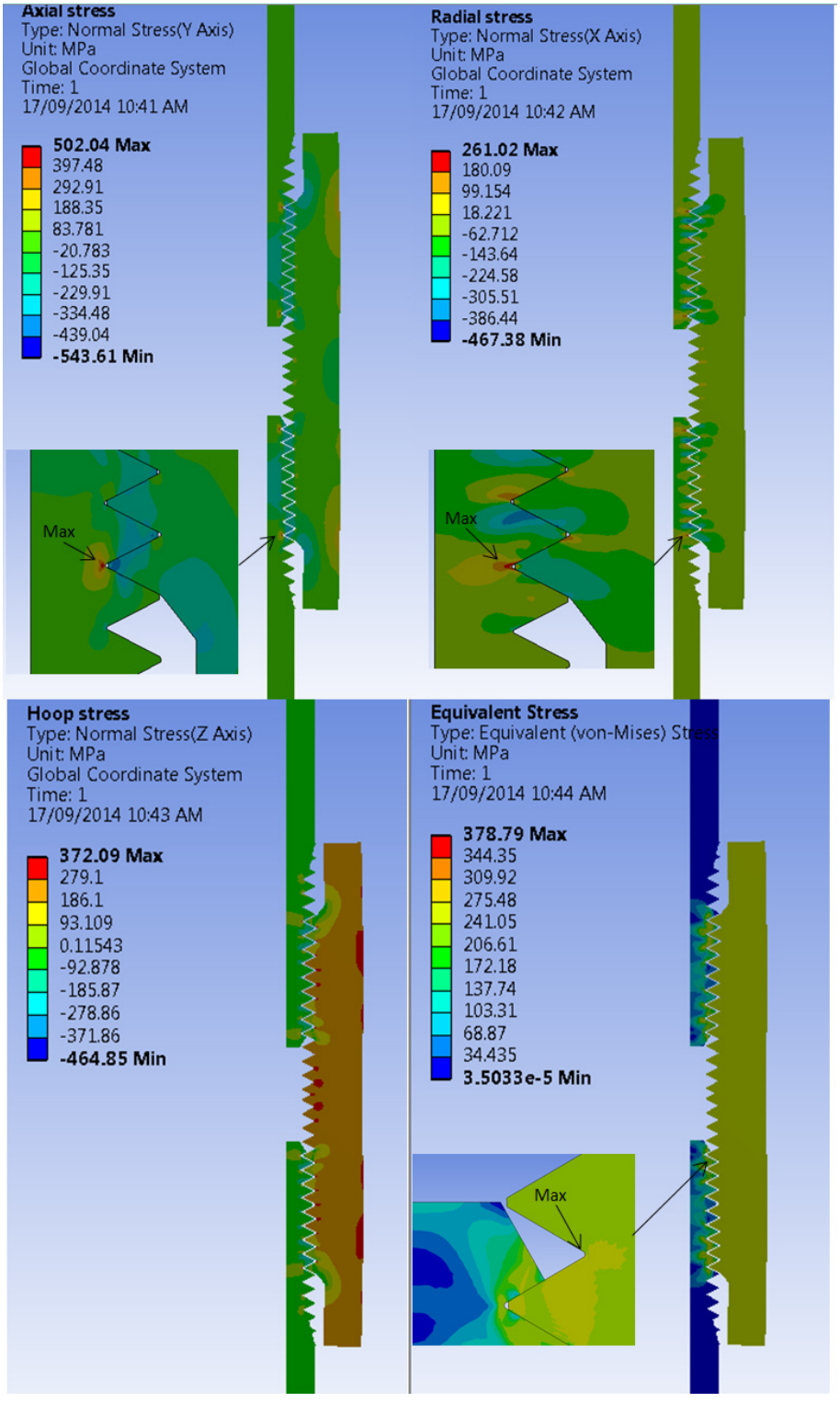

Figure 5.7: Stresses at location x = 1500m after loading step one

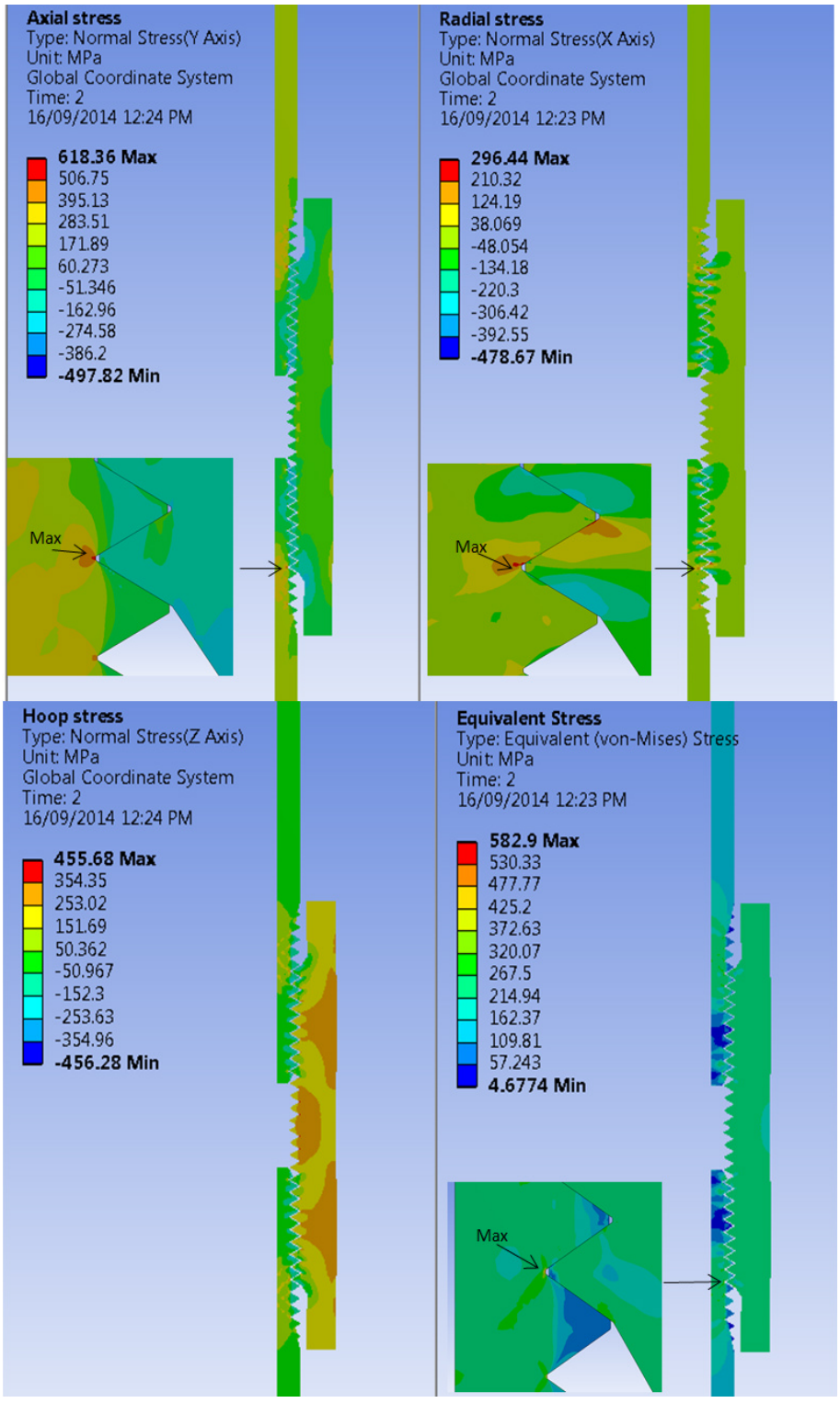

Figure 5.8: Stresses at location x = 1500m after loading step two

Stresses after Step 2 are depicted in Fig. 5.8. Several phenomena are witnessed:

1. Axial stress at the root of the LET of the two pins is higher than that of the make-up step. However, the axial stress at the run-out region of the pins is relieved to be smaller than that of the make-up step. This is the consequence of the tensile load.

2. Maximum stress is located in the lower pin. This is because of the asymmetric springs attached to the two ends. The lower spring is stiffer than the upper one which results in larger deformation inside the lower pin.

3. Hoop stress affects equivalent stress intensively in the aspect of stress level.

4. Critical position of the threaded connection is the LET of the lower pin since maximum equivalent stress is found.

The results of equivalent stress resulting from this static stress analysis will be used as mean stress correction for the fatigue calculation in the following sections.

5.3 Random vibration analysis

5.3.1 Modal analysis

After the static stress analysis, modal analysis will be conducted on the pre-stress model (the model after the two loading steps). Natural frequencies and mode shape functions will be obtained from modal analysis for the use of random vibration analysis in the following section. The structure's undamped equation of motion is given by:

$$[M]\left\{\ddot{u}\right\} + [K]\left\{u\right\} = \left\{0\right\} \tag{5.8}$$

Table 5.4: Stiffness values of equivalent springs linked to the threaded connection

Locations (m)	300	700	1100	1500	1900	2300
1st N.F (Hz)	225.63	176.28	163.16	167.14	192.9	304.26
2nd N.F (Hz)	5728.9	8637.1	8393.7	8230.3	8058.6	7849.2
3rd N.F (Hz)	12812	12693	12290	12002	11708	11348

where [M], [K] are mass matrix and stiffness matrix of the structure. For a linear system, it can be assumed that $\left\{u\right\} = \left\{\phi\right\} cos\omega t$, where $\left\{\phi\right\}$ is the mode shape vector and ω is the circular natural frequency. Thus, Eqn. 5.8 becomes:

$$(-\omega^2[M] + [K])\left\{\phi\right\} = \left\{0\right\} \tag{5.9}$$

Solution to the determinant: $|-\omega^2[M] + [K] = 0|$ gives the natural circular frequency ω of the threaded connection. Natrual frequency f with units of Hz is given by:

$$f = \frac{\omega}{2\pi} \tag{5.10}$$

For the threaded connections at the aforementioned specific 6 locations, the first three natural frequencies are listed in Table 5.4.

5.3.2 Random vibration method

During drilling operations, the unevenness of the rock formation at down-hole which the drill-string encounters is the source of random vibration. In ANSYS workbench this kind of random excitation can be characterized as "Base excitation". According to ANSYS theory document [69], for base excitation and nodal force excitation, the dynamic equations of motion of the threaded connection can be expressed as the free

and the restrained DOF as:

$$\begin{bmatrix}[M_{ff}] & [M_{fr}] \\ [M_{rf}] & [M_{rr}]\end{bmatrix}\begin{Bmatrix}\{\ddot{u}_f\} \\ \{\ddot{u}_r\}\end{Bmatrix}+\begin{bmatrix}[C_{ff}] & [C_{fr}] \\ [C_{rf}] & [C_{rr}]\end{bmatrix}\begin{Bmatrix}\{\dot{u}_f\} \\ \{\dot{u}_r\}\end{Bmatrix}+\begin{bmatrix}[K_{ff}] & [K_{fr}] \\ [K_{rf}] & [K_{rr}]\end{bmatrix}\begin{Bmatrix}\{u_f\} \\ \{u_r\}\end{Bmatrix}=\begin{Bmatrix}\{0\} \\ \{F\}\end{Bmatrix} \tag{5.11}$$

where $\{u_f\}$ are the free DOF and $\{u_r\}$ are the restrained DOF (excited by random loading). $\{F\}$ is the nodal force excitation which is not in the scope of the current study. The free displacements can be decomposed into pseudo-static and dynamic parts as:

$$\{u_f\} = \{u_s\} + \{u_d\} \tag{5.12}$$

The pseudo-static displacements can be obtained from Eqn. 5.11 by excluding the first two terms on the left-hand side of the equation and by replacing $\{u_f\}$ by $\{u_s\}$:

$$\{u_s\} = -[K_{ff}]^{-1}[K_{fr}]\{u_r\} = [A]\{u_r\} \tag{5.13}$$

where $[A] = -[K_{ff}]^{-1}[K_{fr}]$. Then substituting Eqn. 5.12 and 5.13 into Eqn. 5.11 and assuming light damping yields:

$$[M_{ff}]\{\ddot{u}_d\} + [C_{ff}]\{\dot{u}_d\} + [K_{ff}]\{u_d\} = -([M_{ff}][A] + [M_{fr}])\{\ddot{u}_r\} \tag{5.14}$$

where the right-hand side represents the equivalent force due to base excitations. Using mode superposition method, dynamic displacement can be written as:

$$\{u_d(t)\} = [\phi]\{y(t)\} \tag{5.15}$$

where $[\phi]$ is the mode shape vector obtained from modal analysis and $\{y(t)\}$ is the modal coordinate vector. Using the above equation, then Eqn. 5.14 is decoupled to

be:

$$\ddot{y}_j + 2\xi_j\omega_j\dot{y}_j + \omega_j^2 y_j = G_j, \qquad (j = 1, 2, 3, ..., n) \tag{5.16}$$

where n is the number of mode shapes chosen for evaluation. y_j is the generalized displacements, ω_j is natural circular frequencies and ξ_j is modal damping ratios. Also, modal loads G_j are defined as:

$$G_j = \{\Gamma_j\}^T \{\ddot{u}_r\} \tag{5.17}$$

where $\{\Gamma_j\}$ are modal participation factors given by:

$$\{\Gamma_j\} = -([M_{ff}][A] + [M_{fr}])^T \{\phi_j\} \tag{5.18}$$

By assuming PSD of the acceleration $\{\ddot{u}_r\}$ in the next subsection, response of random vibration can be evaluated.

5.3.3 Random vibration input

The PSDs of the acceleration of the axial base motion $u_r(t)$ should be assumed. It is applicable to assume the acceleration $\ddot{u}_b(t)$ as a combination of two parts: one related to the rotary speed as a cosine wave [53], the other considering the random effects. Thus, it can be expressed as:

$$\ddot{u}_b(t) = A_d cos(\omega t) + W(t); \qquad \omega = 2\pi f_c = 2\pi \frac{3N}{60} \tag{5.19}$$

where A_d is the amplitude of cosine wave. $W(t)$ is the random part of the acceleration assumed as a white noise. f_c represents the rotary table critical frequency. According

to this, its one-sided PSD can be obtained as:

$$G_{\ddot{u}_b}(f) = \frac{A_d^2}{2}\delta(f - f_c) + \frac{A_w^2}{2}; \qquad f \in [0, +\infty] \tag{5.20}$$

where A_w is a constant representing the maximum amplitude of random acceleration. f denotes the frequency in unit Hz.

In ANSYS, it is applicable to set acceleration PSD as input of the model. According to the downhole measurement [63], the amplitude of dynamic acceleration can range from 0 - 4 G, where G means the gravity acceleration. In other words, A_d can be assumed as a value ranging from 0 - 4 G. Then the PSD level of the cosine wave will be $\frac{A_d^2}{2}$, which ranges from 0 - 8 G^2/Hz. For the white noise, it can be assumed A_w as 10 percent of the cosine wave amplitude A_d, as 0 - 0.4 G, which results in PSD level $\frac{A_w^2}{2}$ as 0 - 0.08 G^2/Hz.

5.4 Fatigue damage calculation

5.4.1 Damage evolution law

Damage evolution law (DEL) is an accurate method to calculate fatigue damage because it accounts for the multiaxial stresses at the thread roots, rather than treat the load as uni-axial only. It was proposed by Abdel Wahab et al. [70], based on an energy criterion. In Van Wittenberghe's work [30], the material parameters of the DEL were determined using the experimental data from the standard API Line Pipe connection.

Table 5.5: Stress concentration factor for 6 positions in this study

Locations (m)	300	700	1100	1500	1900	2300
SCF	5.964	4.246	3.323	3.573	5.268	6.583

The resulting DEL is expressed by:

$$N = 2.95 \times 10^6 \cdot \Delta\sigma_{eq}^{-1.26} \cdot R_V^{4.12} \tag{5.21}$$

$$R_V = \frac{2}{3}(1+\nu) + 3(1-2\nu)[\frac{\sigma_H}{\sigma_{eq}}]^2 \tag{5.22}$$

In the above equation, $\Delta\sigma_{eq}$ is the nominal equivalent stress satisfying: $\Delta\sigma_{eq} = \Delta\sigma/SCF$.

Here, the SCF is the stress concentration factor and $\Delta\sigma$ is the equivalent stress obtained from ANSYS. The SCF is calculated by the ratio between the maximum axial stress value and the applied tensile load. They are calculated for 6 positions in Table 5.5 and all fall in the range of 1.8 to 6.5, which is concluded by Van Wittenberghe's work [30]. ν denotes the Poisson's ratio and σ_H is the hydrostatic stress obtained from ANSYS.

5.4.2 Mean stress correction

Mean stress effect should be included by using Goodman correction equation:

$$(\frac{S_a}{S_n}) + (\frac{S_m}{S_u}) = 1 \tag{5.23}$$

where S_a denotes the nominal equivalent stress amplitude, mean stress S_m is the mean stress obtained in static stress analysis section, S_u is the material's ultimate

strength, which is 521 MPa, and S_n is the corrected fatigue stress amplitude. Hence, the corrected stress range: $2S_n$ will be substitude into Eqn. 5.21 to calculate fatigue life.

5.4.3 Random fatigue

The three-band technique is a widely used method for evaluating random vibration fatigue [71]. It is based on the assumption that the input acceleration follows the Gaussian distribution. In other words, the resulting 1σ equivalent stress (E.S) is assumed to act at the 1σ level 68.3% of the time. The 2σ E.S is assumed to act at the 2σ level 27.1% of the time. And the 3σ E.S is assumed to act at the 3σ level 4.33% of the time. ANSYS workbench's random vibration analysis can give the 1σ, 2σ and 3σ maximum E.S values under specific PSD input.

Then, the number of cycles to cause failure (N_i) is calculated by the DEL in Eqn. 5.21. By substituting the 1σ, 2σ and 3σ corrected equivalent stress ranges.

According to damage accumulative law, the fatigue damage ratio is given as:

$$D = \sum_{i=1}^{3} \frac{n_i}{N_i} \tag{5.24}$$

where $i = 1, 2, 3$ relates to 1σ, 2σ and 3σ stresses. n_i is the actual number of fatigue cycles generated in specific exciting time T (in sec):

$$n_1 = \nu_{eq} \cdot T \cdot 0.683 \tag{5.25}$$

$$n_2 = \nu_{eq} \cdot T \cdot 0.271 \tag{5.26}$$

$$n_3 = \nu_{eq} \cdot T \cdot 0.0433 \tag{5.27}$$

where ν_{eq} is the stochastic stress cycling number within unit time, namely the equiv-

alent frequency. It is calculated by:

$$\nu_{eq} = \frac{1}{2\pi}\sqrt{\frac{m_2}{m_0}} \tag{5.28}$$

where m_2 and m_0 are spectral moments of the stress PSD $G(\omega)$:

$$m_2 = \int_0^\infty G(\omega)d\omega \tag{5.29}$$

$$m_0 = \int_0^\infty \omega^2 G(\omega)d\omega \tag{5.30}$$

The stress PSD $G(\omega)$ can be obtained from ANSYS. In this thesis, it is found that the resulting stress PSDs in high frequency modes larger than mode 1 are neglectable, ν_{eq} can be approximated as the first natural frequency of the threaded connection, which is directly given by ANSYS.

5.5 Results analysis

First of all, all the simulation results show the critical position in a threaded connection is at the LET of the lower pin. Hence, the results analyzed in this section are all from this position.

Secondly, it is found in the simulations that the fatigue damage including the cosine wave (the first term of Eqn. 5.20) has only a maximum 0.2% difference from the fatigue damage excluding the cosine wave. This is because the natural frequencies of a threaded connection are large (Table 5.4), compared to the cosine wave, which only has a vital PSD level at small frequency f_c. Hence, it is adequate to consider only the white noise (the second term of Eqn. 5.20) as input in the following simulations.

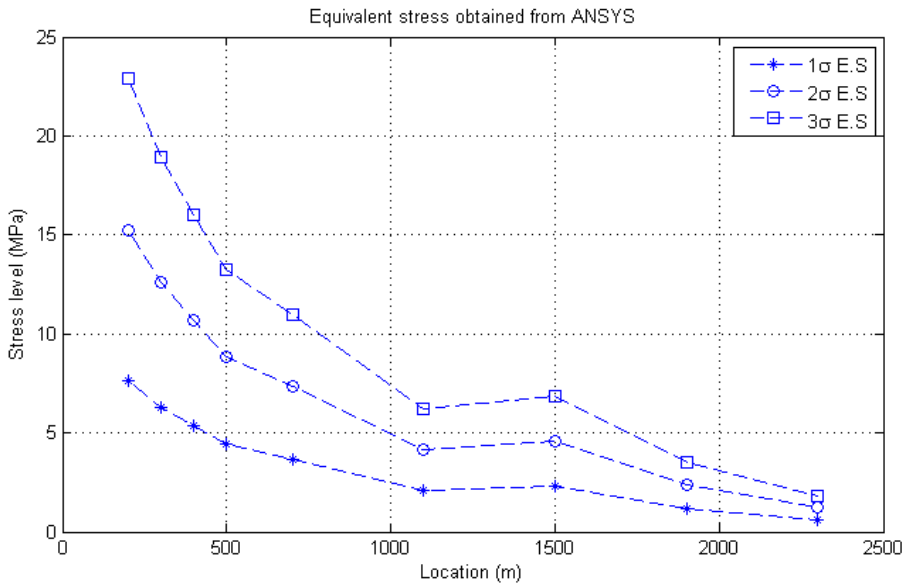

Figure 5.9: Equivalent stress obtained from ANSYS under random input

Effects from random input intensity, static tensile load and location of the threaded connection are discussed below.

5.5.1 Random vibration effects

Three levels of white noise intensity are assigned in this paper as: $0.04, 0.06\ and\ 0.08 G^2/Hz$. The exciting time T in this paper is chosen as 10 days, which equals to: $T = 3600 \times 24 \times 10$ seconds.

For threaded connection located at different positions, the 1σ, 2σ, 3σ E.S levels under input $0.08 G^2/Hz$ are depicted in Fig. 5.9. Fatigue damage ratio results calculated by Eqn. 5.24 under the three input levels are shown in Fig. 5.10. From the figures, it can be recognized that:

1. The maximum equivalent stress occurs at the threaded connection located near the bottom, while stress fluctuation is observed at the area around the location

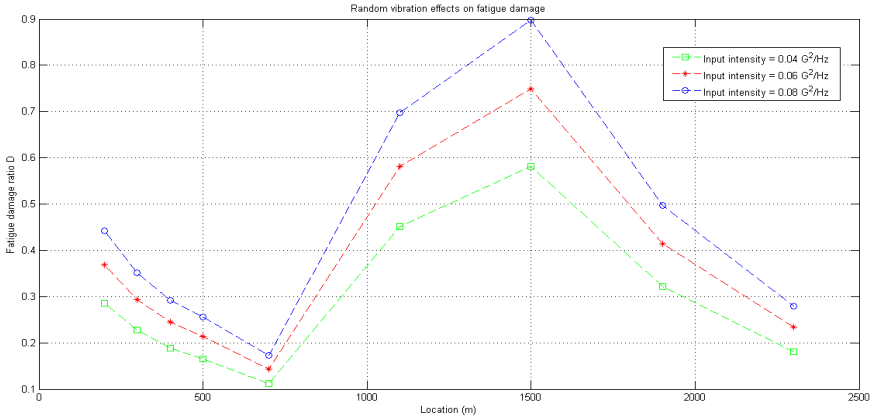

Figure 5.10: Random vibration effects on threaded connection located at different positions

$x = 1500m$. This is caused by the combined effect of tensile load and the threaded connection's location, which will be given in next subsection.

2. The threaded connection's fatigue damage has a more severe varying pattern from the bottom to the top. The critical position lies in the area near $x = 1500m$, which gives the largest damage ratio after the exciting time period T. It seems to be a common sense that larger stress level will cause larger fatigue damage. However, the S-N curve used in this paper accounts for the tri-axial effect R_v by Eqn. 5.22, which has different values at different positions. The fatigue damage is a combined effect of both stress level and tri-axiality function R_v, resulting in a fluctuating damage curve.

3. The threaded connections are sensitive to the random input intensity, especially near the critical position. An increase of 2 times to the input intensity can result in an maximum increase of 1.9 times to the fatigue damage in this area.

5.5.2 Tensile load effect and location effect

At different locations, three factors are considered to affect the threaded connection's fatigue damage. They are the static tensile stress, the location of the threaded connection (i.e. the equivalent springs' stiffness), and the tri-axiality function R_v. Since R_v can be obtained directly from ANSYS' results, here only the effects from the first two factors are discussed.

The threaded connection at location $x = 700m$ is analyzed by parametric study. Its tri-axiality function value remains the same, and the random input is set as $0.08G^2/Hz$ for the following simulations.

Firstly, it is assumed that the stiffnesses of the upper spring and lower spring remain the same, as the value calculated in Table 5.3, at $x = 700m$. Five different tensile loads (56.3, 84.15, 112.6, 140.75, 168.9 MPa) are assigned to the model to conduct individual simulation respectively. The corresponding results of fatigue damage are illustrated in Fig. 5.11.

It can be found that under the same input intensity and the same location, with the increase of tensile load the fatigue damage increases monotonously.

Secondly, It is assumed that the static tensile load of the threaded connection remains a constant as 112.6 MPa, while it is assumed that its location varies (i.e. the stiffness pair of the upper spring and lower spring changes). Stiffness pair values calculated at $x = 300, 700, 1100, 1500, 1900, 2300m$ using Eqn. 5.4 to 5.7 are examined. They are listed in Table 5.6. The corresponding results of fatigue damage ratio are given in Fig. 5.12.

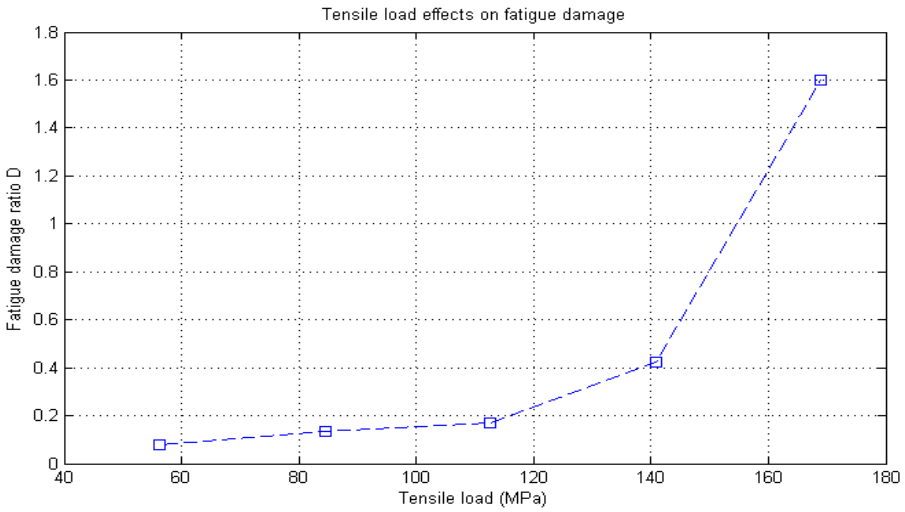

Figure 5.11: Tensile load effects on threaded connection at the same location x= 700 m

Table 5.6: Examined stiffness pair values

Locations (m)	300	700	1100	1500	1900	2300
Upper spring ($10^6 N/m$)	2.635	3.220	4.140	5.796	9.660	28.980
Lower spring ($10^6 N/m$)	14.567	7.264	4.839	3.627	2.901	2.417

It can be found that under the same input intensity and the same tensile load, the fatigue damage decreases monotouously with the location changes from the bottom to the top.

5.6 Conclusion

A theoretical method is proposed and simulations are conducted to estimate the fatigue damage of threaded connection. It accounts for random input effects on the threaded connection, which is not covered by previous researches. The followings are

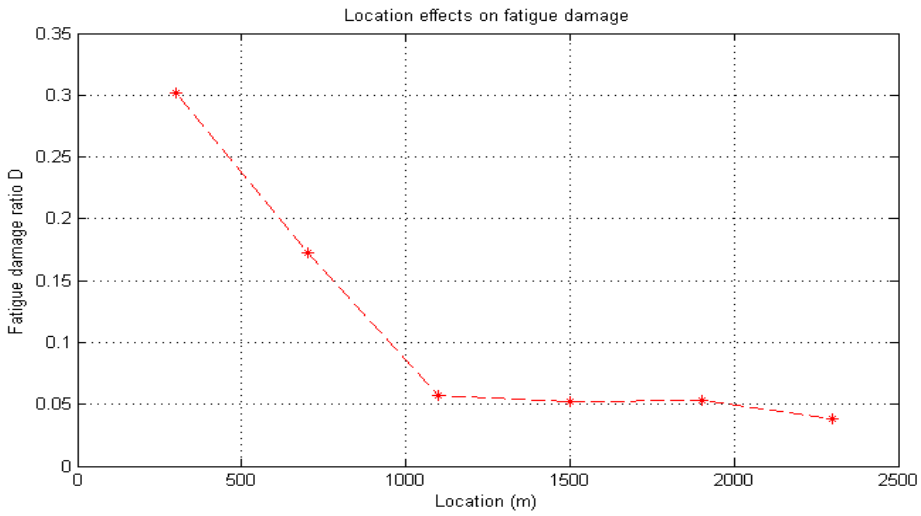

Figure 5.12: Location effects on threaded connection under the same tensile load 112.6 MPa

several conclusions drawn from the results:

1. The threaded connection's critical position lies in LET of the lower pin under random loading. This lives up to the previous researches of static stress analysis on threaded connections.

2. Threaded connection's fatigue damage is affected by the complex combined effects from tensile load, its location and its tri-axiality.

3. Tensile stress added to the threaded connection affects its fatigue damage monotonously. The more tensile stress added, the more fatigue damage it will suffer from.

4. Threaded connection's location also has a vital effect on its fatigue damage. It is the equivalent springs pair that affects the thread connection's natural frequencies, stress level, and then the fatigue damage. Generally, the threaded connection located near the bottom tends to suffer from large fatigue damage, regardless of other factors.

Improvements of this study will be done by gathering realistic field data of power spectral density. Also, test verification for the simulation results will be the focus of future researches.

Chapter 6

Conclusions and Recommendations

6.1 Research findings

Chapter 3 introduced a time domain method to predict fatigue life of a drill-string. Under deterministic loadings, stick-slip phenomenon has severe negative effect on the fatigue life of drill-string, therefore it should be avoided in drilling operation. Besides, the predicted fatigue life increases with the increase of rotary speed. This is mainly because the drill-string tends to operate more smoothly at a larger rotary speed, while stick-slip phenomenon tend to occur at lower rotary speed. An appropriate rotary speed has to be adjusted during drilling operations. Additionally, the different life predictions at different positions of the drill-string are found to be affected by two factors: mean stress and stress range. Depending on different operational conditions, different weakest point of the drill-string may be found. Further, the random excitations have obvious effect on the fatigue life of drill-string. The amount of the effect depends on the intensity and the characteristic of the random excitations.

Chapter 4 introduced a frequency domain method to predict fatigue life of a drill-string. Results show random vibration has an intensive effect on the fatigue life of

the drill-string. And the predicted life of the drill-string is affected by the combined influence of three factors: 1. The deterministic part of excitation; 2. The random part of the excitation; and 3. The mean stress level. This fact results in a fluctuating life time prediction curve as given in Chapter 4.

Chapter 5 introduced a method to predict fatigue life of a threaded connection. The threaded connection's weakest point lies in LET of the lower pin under random loading. This lives up to the previous researches of static stress analysis on threaded connections. And the threaded connection's fatigue damage is affected by the complex combined effects from tensile load, its location and its tri-axiality.

6.2 Achievements

1. This thesis develops two different methods to assess fatigue damage of the drill-string under random vibration.

2. Finite element method is used as modeling method for time domain fatigue calculation. Rainflow counting method is the main tool to address stress time history so that fatigue calculation can be conducted.

3. In frequency domain, a spectral method is proposed to estimate the fatigue life of a drill-string in frequency domain. One benefit of this method is that fatigue life can be obtained without solving the dynamic equations of the drill-string system. Another advantage is that this method is more applicable in cases including random loadings. It can significantly reduce the calculating time, compared with fatigue calculation methods by cycle counting method in time domain.

4. Furthermore, the fatigue damage of the complex structure - threaded pipe connection is also investigated with the help of ANSYS.

6.3 Recommendations

1. Random excitations are assumed as white noise, which is a common consent in simulation researches. However, to assess more realistic fatigue damage and life predictions, reliable field data should be measured in the future research.

2. Experimental tests of the threaded connections should be the focus of future research work, which can be the validation of simulations conducted in the current thesis.

3. Lateral vibration direction is not included in the current study of random fatigue calculation. It is of importance to consider lateral vibration of the drill-string in the future works.

Bibliography

[1] B. S. Aadnoy and U. S. of Petroleum Engineers, *Advanced drilling and well technology*. SPE, 2009.

[2] Wikipedia, "Drilling rig," *In WIKIPEDIA*, retrieved on Oct, 11, 2014. *http://en.wikipedia.org/wiki/Drillingrig*.

[3] D. W. Dareing, *Drillstring Mechanics*. ASME Press, 2012.

[4] Wikipedia, "A tricone bit," *In WIKIPEDIA*, retrieved on Oct, 11, 2014. *http://en.wikipedia.org/wiki/Drillbit(well)*

[5] Wikipedia, "A PDC bit," *In WIKIPEDIA*, retrieved on Oct, 11, 2014. *http://en.wikipedia.org/wiki/Drillbit(well)*

[6] J. Van Wittenberghe, J. De Pauw, P. De Baets, W. De Waele, W. Ost, G. De Roeck, and T. Bui, "Fatigue investigation of threaded pipe connections," *Sustainable Construction and Design*, vol. 1, no. 1, p. 182, 2010.

[7] Wikipedia, "Anatomy of a land based drilling rig - hoisting system," *In WIKIPEDIA*, retrieved on Oct, 11, 2014.

[8] J. J. Azar and G. R. Samuel, *Drilling engineering*. PennWell Books, 2007.

[9] M. Joosten, R. Ferguson, and J. Shute, "New study shows how to predict accumulated drill pipe fatigue," *World Oil;(United States)*, vol. 201, no. 5, 1985.

[10] T. Hill, P. Seshadri, K. Durham, "A unified approach to drillstem-failure prevention (includes associated papers 26205 and 26213)," *SPE drilling engineering*, vol. 7, no. 04, pp. 254–260, 1992.

[11] M. Patel and M. Vaz, "Comparisons of drill string cyclic loading due to vibration and dog-legs," *Proceedings of the Institution of Mechanical Engineers, Part E: Journal of Process Mechanical Engineering*, vol. 209, no. 1, pp. 17–25, 1995.

[12] B. Extending, "Spe/iadc 67696," 2001.

[13] A. Chevallier, *'Nonlinear Stochastic Drilling Vibrations.* PhD thesis, Ph. D. thesis, Rice University, Department of Mechanical Engineering, Houston, Texas, 2001.

[14] E. Skaugen, "The effects of quasi-random drill bit vibrations upon drillstring dynamic behavior," in *SPE Annual Technical Conference and Exhibition*, Society of Petroleum Engineers, 1987.

[15] Shepard, SF and Reiley, RH and Warren, TM and others, "Casing drilling: An emerging technology," in *SPE drilling & completion* , Society of Petroleum Engineers, 2002

[16] W. C. Chin, *Wave propagation in petroleum engineering: modern applications to drillstring vibrations, measurement-while-drilling, swab-surge, and geophysics.* Gulf Publishing Company, 1994.

[17] O. Vaisberg, O. Vincke, G. Perrin, J. Sarda, and J. Fay, "Fatigue of drillstring: state of the art," *Oil & Gas Science and Technology*, vol. 57, no. 1, pp. 7–37, 2002.

[18] G. Y. Grondin and Kulak, GL, *Fatigue of drill pipe*. Department of Civil Engineering, University of Alberta, 1991.

[19] T. Hill, R. Money, C. Palmer, "Qualifying drillstring components for deep drilling," *Journal of Petroleum Technology*, vol. 37, no. 08, pp. 1–511, 1985.

[20] P. Weiner and M. True, "A means of increasing drill collar connection life," *Journal of Manufacturing Science and Engineering*, vol. 95, no. 1, pp. 243–246, 1973.

[21] W. Bachman, "Fatigue testing and development of drill pipe to tool joint connection," *World Oil*, vol. 132, p. 104, 1951.

[22] R. P. Morgan and M. J. Robin, "A method for the investigation of fatigue strength in seamless drillpipe," 1969.

[23] K. Sobczyk and B. Spencer Jr, *Random fatigue: from data to theory*. Academic Press, 1992.

[24] A. Lubinski, "Maximum permissible dog-legs in rotary boreholes," *Journal of Petroleum Technology*, vol. 13, no. 2, pp. 175–194, 1961.

[25] J. E. Hansford and A. Lubinski, "Cumulative fatigue damage of drill pipe in dog-legs," *Journal of Petroleum Technology*, vol. 18, no. 3, pp. 359–363, 1966.

[26] J. Wu, "Drill-pipe bending and fatigue in rotary drilling of horizontal wells," in *SPE Eastern Regional Meeting*, 1996.

[27] J. Van Wittenberghe, P. De Baets, W. De Waele, and J. De Pauw, "The influence of connection geometry on the fatigue life of national pipe thread threaded pipe couplings," *Journal of Pressure Vessel Technology*, vol. 135, no. 1, p. 011201, 2013.

[28] F. P. Brennan, *Fatigue and fracture mechanics analysis of threaded connections*. PhD thesis, University of London, 1992.

[29] M. I. Lourenco and T. A. Netto, "Low cycle fatigue of corroded pipes under cyclic bending and internal pressure," in *2010 8th International Pipeline Conference*, pp. 41–50, American Society of Mechanical Engineers, 2010.

[30] J. Van Wittenberghe, *Experimental analysis and modelling of the fatigue behaviour of threaded pipe connections*. PhD thesis, Ghent University, 2011.

[31] E. N. Dvorkin and R. G. Toscano, "Finite element models in the steel industry: Part ii: Analyses of tubular products performance," *Computers & structures*, vol. 81, no. 8, pp. 575–594, 2003.

[32] Y. Guangjie, Y. Zhenqiang, W. Qinghua, and T. Zhentong, "Numerical and experimental distribution of temperature and stress fields in api round threaded connection," *Engineering Failure Analysis*, vol. 13, no. 8, pp. 1275–1284, 2006.

[33] K. Macdonald and W. Deans, "Stress analysis of drillstring threaded connections using the finite element method," *Engineering Failure Analysis*, vol. 2, no. 1, pp. 1–30, 1995.

[34] A. Tafreshi and W. Dover, "Stress analysis of drillstring threaded connections using the finite element method," *International journal of fatigue*, vol. 15, no. 5, pp. 429–438, 1993.

[35] P. A. Brodtkorb, P. Johannesson, G. Lindgren, I. Rychlik, J. Rydén, and E. Sjö, "Wafo–a matlab toolbox for analysis of random waves and loads," in *Proceedings of the 10th international offshore and polar engineering conference*, vol. 3, pp. 343–350, 2000.

[36] J. W. Miles, "On structural fatigue under random loading," *Journal of the Aeronautical Sciences (Institute of the Aeronautical Sciences)*, vol. 21, no. 11, 2012.

[37] D. Benasciutti, "Fatigue analysis of random loadings," *PhD thesis, University of Ferrara, Italy*, 2004.

[38] T. Dirlik, *Application of computers in fatigue analysis*. PhD thesis, University of Warwick, 1985.

[39] D. Benasciutti and R. Tovo, "Spectral methods for lifetime prediction under wide-band stationary random processes," *International Journal of fatigue*, vol. 27, no. 8, pp. 867–877, 2005.

[40] W. Zhao and M. J. Baker, "On the probability density function of rainflow stress range for stationary gaussian processes," *International journal of fatigue*, vol. 14, no. 2, pp. 121–135, 1992.

[41] Y. Khulief, F. Al-Sulaiman, and S. Bashmal, "Vibration analysis of drillstrings with self-excited stick–slip oscillations," *Journal of Sound and Vibration*, vol. 299, no. 3, pp. 540–558, 2007.

[42] S. C. Ritto, T. G. and R. Sampaio, "Non-linear dynamics of a drill-string with uncertain model of the bit¨crock interaction," *International Journal of Non-Linear Mechanics*, vol. 44, no. 8, pp. 865–876, 2009.

[43] P. M. T. Sampaio, R. and G. Venero Lozano, "Coupled axial/torsional vibrations of drill-strings by means of non-linear model," *Mechanics Research Communications*, vol. 34, no. 5, pp. 497–502, 2007.

[44] A. Christoforou and A. Yigit, "Fully coupled vibrations of actively controlled drillstrings," *Journal of Sound and Vibration*, vol. 267, no. 5, pp. 1029–1045, 2003.

[45] C. A. P. Yigit, A. S., "Stick-slip and bit-bounce interaction in oil-well drillstrings," *Journal of Energy Resources Technology*, vol. 128, pp. 268–274, May 2006.

[46] D. W. Dareing, *Mechanics of Drillstrings and Marine Risers*. ASME Press, 2012.

[47] K. Z. Khan, *Longitudinal and torsional vibration of drill strings*. PhD thesis, Massachusetts Institute of Technology, 1986.

[48] C. Li, "An analytical study of drill string vibrations," Society of Petroleum Engineers, 1986.

[49] M. A. Trindade, C. Wolter, and R. Sampaio, "Karhunen–loève decomposition of coupled axial/bending vibrations of beams subject to impacts," *Journal of Sound and Vibration*, vol. 279, no. 3, pp. 1015–1036, 2005.

[50] A.-N. H. Khulief, Y. A., "Finite element dynamic analysis of drillstrings," *Finite elements in analysis and design*, vol. 41, no. 13, pp. 1270–1288, 2005.

[51] M. T. Piovan and R. Sampaio, "Non linear model for coupled axial/torsional/flexural vibrations of drill-strings.," in *III European Conference on Computational Mechanics*, pp. 620–620, Springer, 2006.

[52] A. K. Sengupta, *Numerical simulation of the roller cone drill bit lift-off phenomenon*. PhD thesis, Masters Thesis, Rice University. http://hdl. handle. net/1911/13894, 1994.

[53] D. Dareing and B. J. Livesay, "Longitudinal and angular drill-string vibrations with damping," *Journal of Manufacturing Science and Engineering*, vol. 90, no. 4, pp. 671–679, 1968.

[54] A. Zhong, "Thread connection response to critical pressures," in *Abaqus Users' Conference, Paris, France*, pp. 690–706, 2007.

[55] G. Gazetas, "Analysis of machine foundation vibrations: state of the art," *International Journal of Soil Dynamics and Earthquake Engineering*, vol. 2, pp. 2–42, May 1983.

[56] C. Bucher, *Computational Analysis of Randomness in Structural Mechanics: Structures and Infrastructures Book Series*. CRC Press, 2009.

[57] C. To and M. Liu, "Large nonstationary random responses of shell structures with geometrical and material nonlinearities," *Finite elements in analysis and design*, vol. 35, no. 1, pp. 59–77, 2000.

[58] P. Johannesson, *Rainflow analysis of switching Markov loads*, vol. 1999. No.4. Lund University, 1999.

[59] I. Rychlik, "Simulation of load sequences from rainflow matrices: Markov method," *International journal of fatigue*, vol. 18, no. 7, pp. 429–438, 1996.

[60] S. S. Rao, *Vibration of continuous systems*. John Wiley & Sons, 2007.

[61] M. Vaz and M. Patel, "Analysis of drill strings in vertical and deviated holes using the galerkin technique," *Engineering structures*, vol. 17, no. 6, pp. 437–442, 1995.

[62] L. D. Lutes and S. Sarkani, *Random vibrations: analysis of structural and mechanical systems*. Butterworth-Heinemann, 2004.

[63] F. Deily, D. Dareing, G. Paff, J. Ortloff, and R. Lynn, "Downhole measurements of drill string forces and motions," *Journal of Manufacturing Science and Engineering*, vol. 90, no. 2, pp. 217–225, 1968.

[64] A. Nieslony and E. Macha, *Spectral method in multiaxial random fatigue*, vol. 33. Springer, 2007.

[65] A. Karolczuk and E. Macha, "A review of critical plane orientations in multiaxial fatigue failure criteria of metallic materials," *International Journal of Fracture*, vol. 134, no. 3-4, pp. 267–304, 2005.

[66] J. Grzelak, T. Lagoda, and E. Macha, "Spectral analysis of the criteria for multiaxial random fatigue," *Materialwissenschaft und Werkstofftechnik*, vol. 22, no. 3, pp. 85–98, 1991.

[67] A.P.I. Specifications, "5l (2007) specifications for line pipe."

[68] A.P.I. Specifications, "5b specification for threading," *Gauging and Thread Inspection of Casing, Tubing, and Line Pipe Threads*, 2008.

[69] P. Kohnke, *ANSYS Mechanical APDL theory reference*. Ansys, 2003.

[70] M. A. Wahab, I. Ashcroft, A. Crocombe, and S. Shaw, "Prediction of fatigue thresholds in adhesively bonded joints using damage mechanics and fracture mechanics," *Journal of adhesion science and technology*, vol. 15, no. 7, pp. 763–781, 2001.

[71] D. S. Steinberg, "Vibration analysis for electronic equipment," *New York, Wiley-Interscience, 1988, 460 p. No individual items are abstracted in this volume.*, vol. 1, 1988.

Appendix A

Data used in Section 4

(a) Common data

Collar O.D. = 0.1651 m, Collar I.D. = 0.0572 m, Pipe O.D. = 0.114 m, Pipe I.D. = 0.0972 m,

$A_1 = 0.0188\ m^2$, $A_2 = 0.0028 m^2$, $L_1 = 200\ m$, $L = 2500\ m$, $\rho = 7.89 \times 10^3\ kg/m^3$, $N = 100\ rpm$,

$F_h = 7{\times}10^5\ N$, $W_s = 1{\times}10^5\ N$, $\rho_{mud} = 1.5{\times}10^3\ kg/m^3$, $g = 9.81\ m/s^2$, $\omega_+ = 1000 Hz$

(b) Axial vibration data

$E = 2.07 \times 10^{10} N/m^2$, $\gamma_1 = 239.4\ Ns/m^2$, $\gamma_2 = 33.5\ Ns/m^2$, $K_d = 9.34 \times 10^6\ N/m$.

$M_d = 9070\ kg$

(c) Torsional vibration data

1) Torsional dynamic vibration equation of motion

$$GI_{pi}\frac{\partial^2\theta_i(x,t)}{\partial x} - \gamma_{Ti}\frac{\partial\theta_i(x,t)}{\partial t} - \rho I_{pi}\frac{\partial^2\theta_i(x,t)}{\partial t^2} = -\gamma_{Ti}\frac{\partial\theta_b}{\partial t} - GI_{pi}\frac{\partial^2\theta_b}{\partial t^2} \tag{6.1}$$

in the above eqution θ is the relative torsional displacement to the base, θ_b is the torsional base displacement, and shear modulus of steel $G = 8.28 \times 10^{10}\ N/m^2$, and torsional damping: $\gamma_{T1} = 2.22\ Ns$, $\gamma_{T2} = 0.311\ Ns$

2) Torsional boundary conditions

$$Top: \qquad GI_{p2}\frac{\partial\theta_2}{\partial x}(L,t) + K_T\theta_2(L,t) + I_k\frac{\partial^2\theta_2}{\partial t^2}(L,t) = 0 \tag{6.2}$$

$$Interface: \qquad \begin{cases} GI_{p1}\frac{\partial\theta_1}{\partial x}(L_1,t) = GI_{p2}\frac{\partial\theta_2}{\partial x}(L_1,t) \\ \theta_1(L_1,t) = \theta_2(L_1,t) \end{cases} \tag{6.3}$$

$$Bottom: \qquad \theta_1(0,t) = 0 \tag{6.4}$$

in the above eqution:

Torsional stiffness of derrick: $K_T = 678\ Nm$; Polar moment of inertia of kelly: $I_k = 210.7\ kg\ m^2$; Polar moment of cross-setional area: $I_{p1} = 7.189 \times 10^{-5} m^4$, $I_{p2} = 7.818 \times 10^{-6} m^4$.